Molecular Basis of Motor Switch Complex from *Helicobacter pylori*

LAM, Kwok Ho

A Thesis Submitted in Partial Fulfillment
of the Requirements for the Degree of
Doctor of Philosophy
in
Molecular Biotechnology

The Chinese University of Hong Kong
September 2011

ProQuest LLC.
789 East Eisenhower Parkway
P.O. Box 1346
Ann Arbor, MI 48106 - 1346

Thesis / Assessment Committee

Professor Shaw Pang-Chui (Chair)

Professor Au Wing-Ngor, Shannon (Thesis Supervisor)

Professor Tsui Kwok-Wing, Stephen (Committee Member)

Acknowledgements

I would like to express my sincere thanks to my supervisor Prof. Au Wing Ngor, Shannon for her trust, valuable advice and endless support that help to expand my horizon and enjoy the wonder and discovery in this field. I would like to express my special thanks to Prof. Shaw Pang-Chui, Prof. Tsui Kwok-Wing, Stephen, Prof. Lau Kwok-Fai, Prof. Leung Yun-Chung, Thomas and Prof. Ling Kin-Wah, Thomas for their advice and support to this project.

I would also like to thank all the people in Prof. Au's group, especially Miss Wendy, Wai Ling LAM, Miss Jenny, Ching Yi HON and Miss Levina, Suk Mi LAM, for all their support and contribution to this project.

I am grateful to Prof. Ottemann Karen and people in her group, especially Dr. Susan Williams, Miss Pam Lertsethtakarn, Miss Lisa Collison, Dr. Khalid Mehmood for their advice and discussion in the microbiology works of *H. pylori*.

Most importantly, I would like to express my deepest thanks to my parents. Your encouragement and support give me enough strength and confidence to go forward and finish this dissertation.

Publication

Lam KH, Ling TK, & Au SW (2010) Crystal structure of activated CheY1 from *Helicobacter pylori*. ***J Bacteriol*** 192:2324-2334.

Table of Contents

Abstract

Bacterial chemotaxis is the directional movement of bacterium towards favourable environment. In flagellated bacteria, chemotaxis is achieved by controlling the frequency of alternating clockwise-counterclockwise switching. Center of this control is the interaction between signaling molecule CheY and switch protein complex (SPC) located at the cytosolic part of flagellum. SPC is a ring-shaped macromolecular complex composed of ~ 26 copies of FliG, ~34 copies of FliM, and over 100 copies of FliN in *E. coli*. Each component plays distinctive roles in flagellar assembly, export, torque generation and flagella switching. The structures and functions of chemotaxis and switch proteins have been extensively studied in *E. coli* and *S. typhimurium*, however, the molecular basis governing their assembly and the switching process remains controversial.

All gastric *Helicobacter* species possess a prominent feature of flagella-driven motility that is essential for colonization and infection. Interestingly, the chemotactic system of *H. pylori* is marked by the presence of multiple response regulators: CheY1, one CheY-like-containing CheA protein (CheAY2), and three CheV proteins. Besides, *H. pylori* harbors an additional SPC member FliY which bears a CheC-phosphatase-like domain fused with a FliN-like domain. Deletions of FliG, FliM, FliN and FliY and FliN/FliY led to non-flagellate, suggesting that all four switch proteins are required for flagellation and FliY is a structural component of SPC.

The organization and functions of SPC in *H. pylori* are not well understood. This study aims to characterize the structures and functions of chemotaxis protein CheY1 and switch

proteins from *H. pylori*. Here we report the crystal structures of CheY1, FliM middle domain ($FliM_M$) and FliG middle and C-terminal domain ($FliG_{MC}$). These proteins share high structural homology to their counterpart in *E. coli* or *T. maritima*. The interactions among the switch proteins, specifically CheY-FliM, FliM-FliG, FliG-FliF were verified, suggest they function similarly as in other bacteria.

Structural comparison of CheY1 with BeF_3^--bound CheY and fluorescence quenching experiments reveal the importance of Thr84 in the phosphotransfer reaction. Complementation assays using various nonchemotactic *E. coli* mutants demonstrated that CheY1 displays differential association with the flagellar motor in *E. coli*. Structural rearrangement of helix 5 and the C-terminal loop in CheY1 provide a different interaction surface for FliM. On the other hand, interaction of the CheA-P2 domain with CheY1, but not with CheY2/CheV proteins, underlines the preferential recognition of CheY1 by CheA in the phosphotransfer reaction.

Structure of $FliM_M$ shows the position of a flexible loop close to the FliG binding site that was previously unresolved in *T. maritima* $FliM_M$ ($TmFliM_M$). Mutagenesis studies supported that residues $_{139}YDQ_{141}$ on the loop are important for FliG interaction.

Two crystal structures of $FliG_{MC}$ were resolved each showing distinct domain orientations from previously-solved structures. Structural comparisons highlight the flexibility of a conserved $_{245}MFXF_{248}$ motif connecting the three helices ARM and the charged-ridge-bearing subdomains of FliG C-terminal domain. Remarkably, rotational freedom of M245 psi and F246 phi prompted a ~180° rotation of the charge ridge. We identified a highly conserved Asn216 that is in close proximity to the backbone of $_{245}MF_{246}$. Studies of swarming and swimming behavior of *E. coli* showed that mutation of Asn216 to Asp, Ala

and Val leads to CW bias while mutation to His did not affect switching. Furthermore, conformational flexibility of the FliG C-terminal subdomains coordindated by the MFXF loop in solution was verified by intramolecular cysteine crosslinking. We hypothesized that the 180° rotation of charge ridge prompted by intrinsic flexibility of MFXF motif explained the symmetrical rotation during motor switching event.

FliY contains two discrete domains and likely carries unique function in motility. Here, we demonstrated that FliY C-terminal domain ($FliY_C$) complemented flagellation of *ΔfliY* mutant but showed impairment in motility. $FliY_C$ binds to FliN and the complex interacts with FliH, suggesting that $FliY_C$ is the minimal domain required for protein export. On the other hand, $FliY_N$ is necessary to full motility function, although the specific role of $FliY_N$ remains to be elucidated.

In summary, the structural and functional data obtained will provide insights to dissect the mechanistic details of the coupling between chemotaxis and SPC in flagellar rotation and switching in *H. pylori*.

摘要

細菌趨化性是細菌游向良好環境的向性運動。部份細菌長有鞭毛，並通過控制鞭毛的順時針及逆時針切換達成向性運動。信號分子 CheY 與位於細胞質的開關蛋白複合物（SPC）負責控制鞭毛的順 – 逆旋轉。 SPC 是由一個環狀的複合大分子所構成 。在大腸桿菌中, SPC 的組成蛋白包括~26 FliG，～34 FliM 以及超過 100 個 FliN 份子。每個組件都起著獨特的功用，其中包括協調鞭毛的組裝和出口以及產生扭矩並控制鞭毛切換。雖然科學家已廣泛於大腸桿菌和鼠傷寒沙門氏菌中研究 SPC 和趨化蛋白的結構及功能，但 SPC 組成的基礎及和它控制切換過程的分子基理仍存在著爭議。

所有胃幽門物種都長有鞭毛。要細菌成功感染人類，這種由鞭毛所驅動的運動是不可或缺的。幽門螺旋桿菌的 SPC 和趨化系統存有多個特點: 1. 除了典型的信號分子 CheY (CheY1) ，螺旋桿菌有其他的多功能趨化蛋白含有信號分子蛋白的結構，包括 CheAY2，和三個 CheV 蛋白質。此外，螺旋桿菌的 SPC 較其他細菌多了一個成員 FliY。FliY 的結構可分爲 CheC -磷酸酶結構域及 類 FliN 結構域兩個部份。在螺旋桿菌破壞 FliG，FliM，FliN 和 FliY 和 FliN / FliY 的基因會導致細菌不能成功長出鞭毛。這表明鞭毛的組成需要這四個開關蛋白質。

直到現在，我們對於幽門螺旋桿菌的 SPC 的結構和職能的了解仍所知甚少。本研究的目標是描繪趨化蛋白 CheY1 和各個開關蛋白的結構特性並研究該結構與蛋白功能之間的聯繫。我們成功取得 CheY1， FliM 中間域（$FliM_M$）和 FliG 中間和 C-端結構域（$FliG_{MC}$）的晶體結構。這些蛋白質的結構與存在大腸桿菌中或嗜熱細菌

T. maritma 中的同源蛋白有一定的相似性。我們爲驗證了 CheY-FliM，FliM - FliG 及 FliG - FliF 的相互作用，結果表明它們的功能與其他細菌類似。

從比較 CheY1 與大腸桿菌 BeF_3^- 激活 CheY 的結構分別中，我們找到 Thr84 在磷酸鹽傳遞反應中起著重要作用，並使用熒光猝滅驗證之。我們利用互補實驗在各種缺失趨化功能的大腸桿菌中表達 CheY1 並發現 CheY1 與開關蛋白複合物之間的相互作用有別於大腸桿菌。從 CheY1 結構中可見 CheY1 的 Helix 5 和 C -末端迴路(Loop) 提供了不同的互動表面給 FliM 由此解釋相互作用的差別。另一方面，CheA - P2 域能與 CheY1 的相互結合，但不能與 CheY2/CheV 蛋白質相互結，協助解釋 CheA 會優先 把磷酸鹽傳遞及 CheY1。

從 $FliM_M$ 的結構中我們觀察到幾個住在於高度靈活性的迴路結構的氨基酸的位置。這些氨基酸的位置在 *T. maritma* $FliM_M$（$TmFliM_M$）的結構中沒有被看到的。突變實驗支持改變 $_{139}YDQ_{141}$ 爲 $_{139}AAA_{141}$ 會破壞 FliM 與 FliG 間的互動，由此證明這個迴路對 $FliM_M$ 功能的重要性。

我們獲得了兩個 $FliG_{MC}$ 的晶體結構。比較其他結構，我們發現 FliGMC 的各個域呈現不同的三維結構聯繫。仔細比較 FliG C -端結構域可見由三個 Helix 組成的 ARM 結構與的帶電脊子軸的 $FliG_{C\alpha 1\text{-}6}$ 結構間是以靈活的 $_{245}MFXF_{248}$ 所連技。值得注意的是，M245 psi 和 F246 phi 的彈性給予帶電脊子軸～180° 旋轉自由度。我們確定了一個高度保守的 Asn216 是在靠近 $_{245}MF_{246}$ 的骨幹並影響其彈性。研究的細菌的游泳行爲表明，在大腸桿菌的 FliG 中突變 Asn216 到 Asp，Ala 或 Val 會引起鞭毛偏好順時針旋轉但突變 Asn216 到 His 並沒有做成影響。此外，我們利用內交聯半胱氨酸連結 (cysteine crosslinking) 的實驗再次證實 MFXF 存在彈性。我們推

測，由 MFXF 帶動電脊子軸的 180 度旋轉充可解釋鞭毛順時針及逆時針旋轉運動的對稱性。

FliY 包含兩個獨立的域並各自可能對細菌游泳有不同的功用。在這裡，我們證明了 FliY C -端結構域（$FliY_C$）在合成鞭毛的功用中，可補充 *ΔfliY* 突變菌珠。但這引致菌珠的游泳運動出現偏差。再者 $FliY_C$ 可與 FliN 結合並且 $FliY_C$/FliN 複合物的可作用於 FliH，$FliY_C$ 最小的域填補 FliY 在鞭毛合成上的功用。另一方面，這實驗也表明了 $FliY_N$ 對細菌游泳運動的重要性，雖然其具體的作用 $FliY_N$ 仍有待闡明。

綜上所述，綜合我們對 SPC 蛋白的組成結構及功能分析，我們對幽門螺旋桿菌中趨化蛋白和 SPC 蛋白之間的聯繫進行了剖析，及爲其在鞭毛旋轉和切換的基理上提供了重要見解。

List of abbreviations

Å	angstrom
Ala / A	alanine
ATP	Adenosine triphosphate
Arg / R	Arginine
Asn / N	Asparagine
Asp / D	Aspartic acid
bp	Base pair
BeF_3^-	Beryllofluoride
B. subtilus	*Bacillus subtilus*
C. jejuni	*Campylobacter jejuni*
°C	Degree Celsius
CW	Clockwise
CCW	Counter-clockwise
CCP4	Collaborative Computational Project Number4
CH_3	methyl group
Che	Chemotaxis protein
Cys / C	Cysteine
DALI	Distance matrix alignment
DTT	dithiothreitol
E. coli	*Escherichia coli*
EcCheY	Escherichia coli CheY protein
EDTA	Ethylenediaminetetraacetic acid
Fli	Flagella protein
Glu / E	Glutamic acid
Gln / Q	Glutamine
Gly / G	Glycine
GST	Glutathione S-transferase
h	Hour / hours
H. pylori / Hp	*Helicobacter pylori*
His / H	Histidine
6×His / His_6	Six histidine tag
Hz	Hertz
Ile / I	Isoleucine
IPTG	Isopropyl b-D-thiogalactoside
kb	Kilobase pair
kDa	Kilo Dalton
KEGG	Kyoto Encyclopedia of Genes and Genomes
L. pneumophila	*Legionella pneumophila*
LB	Luria Broth
Lys / K	Lysine
Leu / L	Leucine
Met / M	Methionine
mg	milligram
Mg^{2+}	Magnesium ion

min	Minute / minutes
ml	Millimeter
Mot	motility
NaCl	Sodium chloride
Ni-NTA	Nickel-nitrilotriacetic acid
OD	Optical density
P	phosphoryl group
PCR	Polymerase chain reaction
PEG	Poly (ethylene glycol)
Phe / F	Phenylalanine
PMSF	Phenylmethanesulfonyl fluoride
Pro / P	Proline
rmsd	Root mean square deviation
R. sphaeroides	*Rhodobacter sphaeroides*
S. typhimurium	*Salmonella typhimurium*
SAM	S-adenosylmethionine
SDS-PAGE	Sodium dodecyl sulphate polyacrylamide gel electrophoresis
s	Second / seconds
Ser / S	Serine
SPC	Switch protein complex
T. maritima / Tm	*Thermotoga maritima*
Thr	Threonine
Trp / W	Tryptophan
Tyr / Y	Tyrosine
µg	microgram
µl	microliter
Val / V	Valine

List of figures

List of tables

Chapter 1 Introduction

1.1 Motility, flagella and chemotaxis

Bacteria move to favorable environments and away from drastic conditions by a process called chemotaxis. Microbe evolved various strategies to move in different environments, including gliding, twisting, swarming and swimming (Bardy SL et al., 2003). Most of the previous researches focused on the mechanism of flagellum-based motility, using enteric bacterium *E. coli* and *S. typhimurium* as model organisms. Flagellum is a macromolecular assembly of protein molecules extending out of the bacterial cell body. In *E. coli*, the flagellum is about 10 μm in length and 20 nm in wide (Berry RM and Armitage JP, 1999). The rotation of flagella is powered by electrochemical gradient of hydrogen or sodium ion gradient across the cell membrane. The rotation rate of a proton-driven motor in *E. coli* is about 100 Hz , but can be up to over 1500 Hz for Na^+-driven motor in *Vibrio* species with swimming speed of hundreds micrometer per second (McCarter LL, 2001). The energy conversion efficiency of the motor under low load approaches 100% (Derosier D, 1998). Synthesis of flagellum is a highly dynamic process that involves hierarchy of transcriptional events and association-dissociation of protein molecules. These distinctive features make flagellum a fascinated model to study the basis of self-assembly and the logical design of nanomachine (Erhardt M et al., 2010).

Chemotaxis is regulated by unique bidirectional movement of bacterial flagellar motor. When the motor turns counter-clockwise (CCW), the flagellar filaments coalesce into a bundle and bacterium runs smoothly. While the motor switches to clockwise rotation (CW), the filaments fly apart and bacterium tumbles to re-orient its cell body (Terashima H et al., 2009; Berg HC, 2008). Chemotaxis is achieved by controlling the frequency of tumbles. Different regulation on flagellar behavior has been demonstrated, for examples, *Sinorhizobium meliloti*, a

nitrogen-fixing plant symbiont, respond to tactic stimuli by slowing the rotary speed; *Rhodobacter sphaeroides*, a photosynthetic bacteria, rotate exclusively in one direction with tandem stops (Armitage JP and Schmitt R, 1997).

Motility is a virulence factors to several pathogens, including *S. typhimurium, L. pneumophila, C. jejuni, H. pylori*, etc. It plays various roles from initial phases of infection, for example, flagellum-assisted adherence of bacterial cells on the epithelial surface of host by tethering, to maintenance and persistence of infection in the host during adverse conditions, for example, during starvation (Josenhans C and Suerbaun S, 2002).

1.2 Architecture of flagellum

Flagellum is extended from the cytoplasm, periplasmic space, peptidoglycan layer to outside the cell body. It can be divided into 3 parts, basal body, hook and filament. Filament is the outermost region mainly composed of flagellins (FliC in *S. typhimurium*) (Samatey FA et al., 2001). It is a rigid helical-shaped mechanical portion for propelling the bacterium. Hook is a universal joint connecting filament to basal body allowing the two parts to rotate about different axis. Flagellar hook and filament are exported by Type III secretion export machinery. Basal body plays critical roles in flagellar biogenesis, torque generation for rotation and control the frequency of rotational switching (DeRosier DJ et al., 1998). It is composed of rings of protein oligomers, from outer membrane to inner membrane, includes L ring (outer membrane), P ring (peptidoglycan layer), MS ring (inner membrane) and C ring (cytoplasm) (Fig. 1.1). L and P rings are believed to act as bushing that allows central rotating rod to pass through. MS ring consists of membrane protein FliF which acts as an anchor for the assembly of cytoplasmic proteins. C ring contains the switch protein complex. MS ring and C ring contribute to the rotor part. Torque is generated by membrane-bound stator which converts electrochemical potential to mechanical force acting on the rotor.

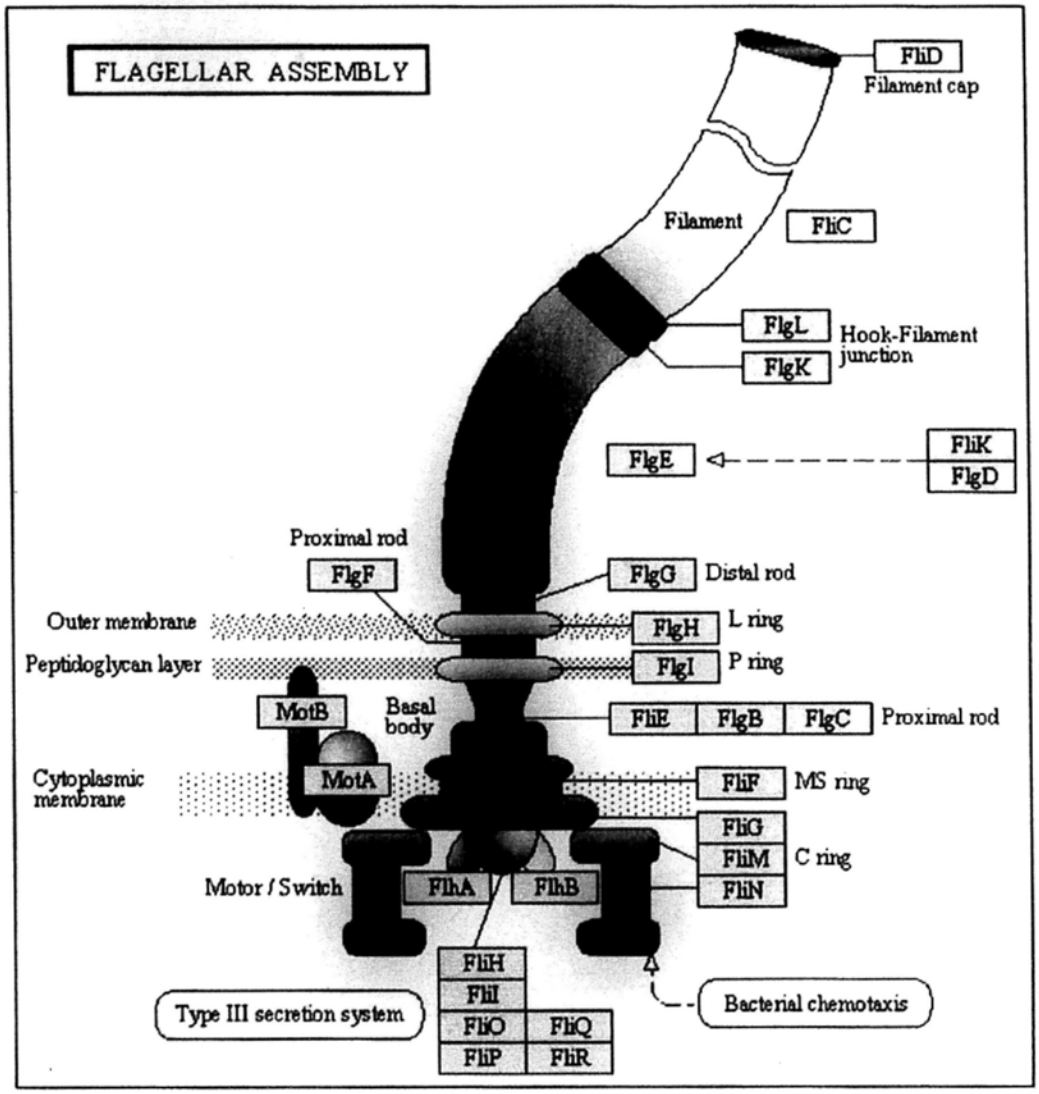

Fig. 1.1. Schematic diagram illustrates the organization of flagellum.

The figure is adapted from the website of KEGG Pathway (http://www.genome.jp/kegg/pathway/ko/ko02040.html). Genes involved in the synthesis of flagellum are boxed.

1.2.1 Switch protein complex

Switch Protein complex (SPC) is essential to torque generation and bidirectional rotation of the flagellum. It is assembled into the cytoplasmic side of flagellum during early phase of self-assembly (Macnab RM, 2003). SPC is composed of three proteins in *E. coli*, including FliG, FliM and FliN. These switch proteins, each having a distinct role, contribute interactively for the function of the motor. All three proteins are important to switching. Besides, FliG directly interacting with the stator is the start site of rotation. FliM provides the binding surface for response regulator CheY. It may also contribute to flagellar export by interacting with putative charperone FliJ, although the mechanism is not clear yet. FliN also takes part in flagellar assembly by assisting the localization of flagellar export regulatory protein FliH (González-Pedrajo B et al., 2006).

Two key biological questions concerning the function of the motor is the molecular bases of self-assembly and bidirectional switching. The C-ring is formed by dynamically interaction of ~26 copies of FliG, ~34 copies of FliM and over 100 copies FliN. By combining of the ~20Å low resolution EM map of CW-biased basal body from *S. typhimurium*, results from protein-protein interaction studies and atomic structures of individual switch proteins, the orientations of FliG, FliM and FliN in the ring has been proposed (Fig. 1.2A) (Lloyd SA et al., 1999; Brown PN et al., 2002, 2005; Lowder BJ et al., 2005; Paul K et al., 2006; Park SY et al., 2006; Thomas DR et al., 2006; Lee LK et al., 2010; Sarkar MK et al., 2010; Minamino T et al., 2011). The structure of the C-ring is organized by FliG positioning at the top, FliM in the middle, and FliN at the bottom. FliG contains three domains each interacts with different proteins. The N-terminal globule ($FliG_N$) interacts with FliF on MS-ring, middle domain ($FliG_M$) binds to FliM and the C-terminal domain ($FliG_C$) interacts with stator $MotA_4B_2$ and possibly with FliM. For FliM, its N-terminal

helix ($FliM_{N\alpha}$) is the docking site for activated CheY while the middle domain of FliM ($FliM_M$) interacts with FliG and C-terminal domain binds to FliN ($FliM_C$). FliN forms a ring structure by forming dimer of FliN dimer, consistent with the observation from EM map (Fig. 1.2A, 1.3).

Flagellum rotates by 26 discrete but identical steps per revolution in CCW direction, suggesting torque generation involves association-dissociation of FliG with MotA (Sowa Y et al., 2005). However, EM map of C ring showed a 26-fold symmetry in the inner ring and a 34-fold symmetry in the outer ring. Since it is believed that MotA interact with $FliG_C$ in the outer ring, it remains unclear how ~26 copies of FliG give a 34-fold symmetry in the outer ring, and how ~34 copies of FliM assemble with FliG (Fig. 1.2B).

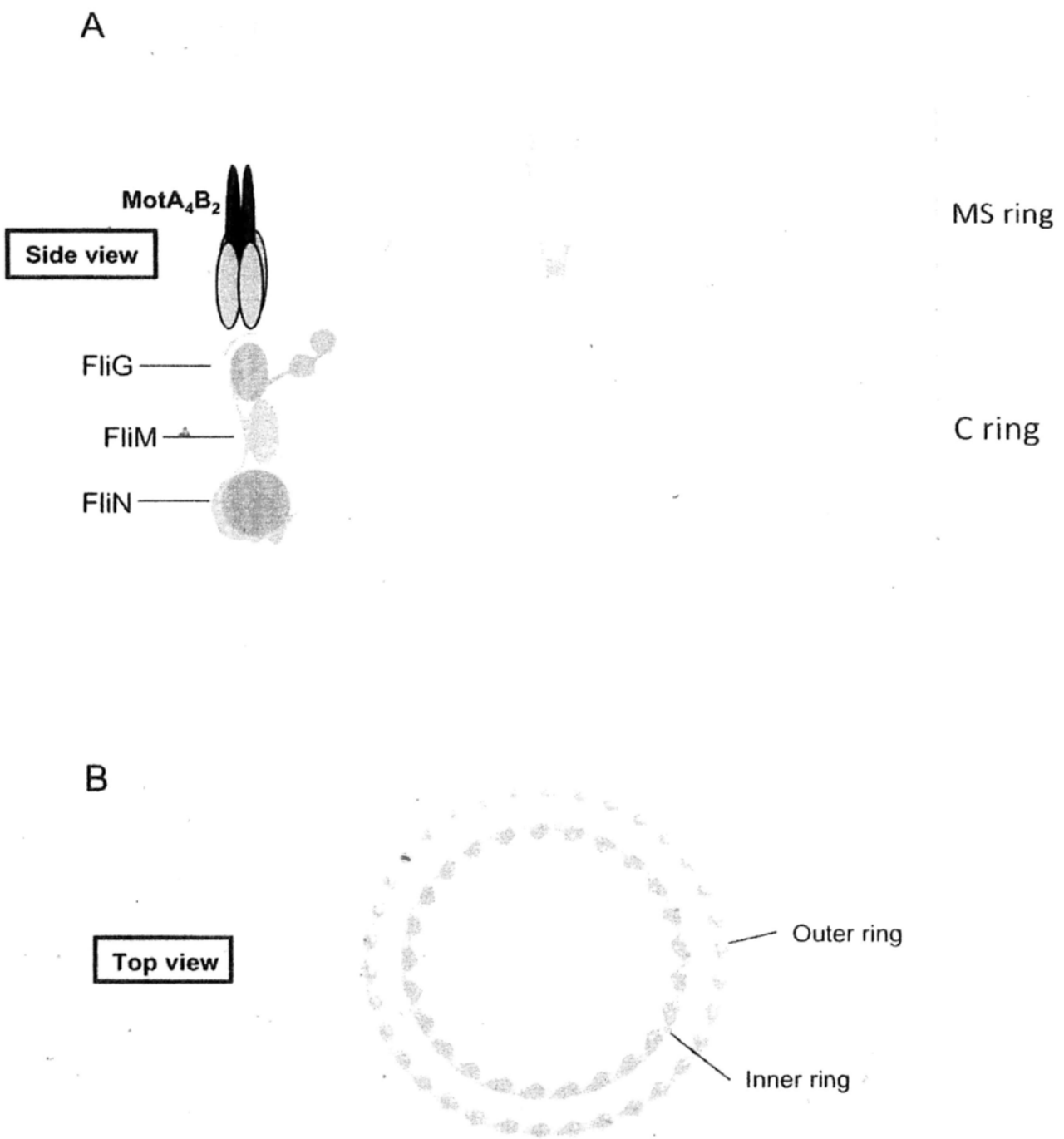

Fig. 1.2. EM map of the C ring and MS ring from CW biased motor in *S. typhimurium* (kindly provided by DeRosier JD) (Thomas DR et al., 2006). The map is drawn as surface using Pymol. **(A)** Cross section of the rotor showing the positions of FliG, FliM, FliN and $MotA_4B_2$ complex. **(B)** Top view of C-ring. Note the differential symmetry of the outer and inner rings.

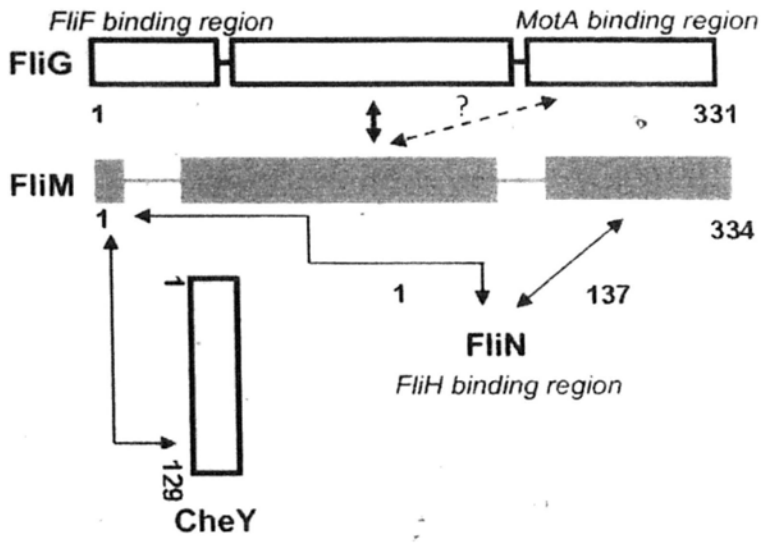

Fig. 1.3. Interactions between switch proteins in *E. coli*. Domains of the switch proteins and chemotaxis protein CheY are represented by boxes. Protein-protein interactions are presented as arrows. The drawing is not on scale.

1.2.2 FliG

Torque is generated by coupling proton flow through stator $MotA_4B_2$ which forces the movement of rotor through FliG interacting surface. $FliG_C$ contains conserved oppositely charged residues that associate complementarily to charged residues of MotA cytoplasmic domain. Structure of FliG middle and C-terminal domain ($FliG_{MC}$) from *T. maritima* is featured by two compact globular domain connected by a helix and flexible loop that contains well-conserved GlyGly motif (Brown PN et al., 2002). It is believed that motor switching involves modulating the relative movement between these domains and the MotA-FliG interacting face (Lloyd SA et al., 1999; Brown PN et al., 2007). FliG contains two FliM binding sites, including the conserved EHPQR motif and the hydrophobic patch at two globular domains (Brown PN et al., 2002). The significance of containing two discrete FliM binding sites remains to be

elucidated. Despite FliG structures has been resolved, assembly of FliG to form torque ring as well as the basis of conformation change of FliG during motor switching remains controversial (Brown PN et al., 2002; Lee LK et al., 2010) (Fig. 1.4).

1.2.3 FliM

Sequence analysis of FliM by alignment of 50 microbial species from different genus showed that the CheY binding site at $FliM_{N\alpha}$ is well-conserved. Besides, residues around GGXG motif important for FliG interaction are moderately conserved while the C-terminal part is less conserved. The interacting surface between *E. coli* $FliM_{N\alpha}$ and activated CheY has been mapped from the structures of FliM-CheY complexes (Dyer CM et al., 2004, 2006; Lee SY et al., 2001). Despite extensive molecular genetic and biochemical analyses of FliM-FliG interaction in *E. coli* or *S. typhimurium* had been performed (Toker AS et al., 1996; Toker AS and Macnab RM 1997; Sockett H et al., 1992; Brown PN et al., 2007; Passmore SE et al., 2008), the interacting surface between FliG-FliM is still not well defined due to the lack of FliG-FliM complex structure. Structure of FliM middle domain resolved from *T. maritima* is ellipsoidal shaped and the GGXG motif is located at an exposed surface on the top of the globular structure, consistently showing that this region is important to FliG interactions (Park S et al., 2006). Besides crosslinking study of FliM provides insight into the organization of ~ 34 molecules of FliM in C-ring (Park SY et al., 2006). The structure of FliM C-terminal domain is not known. Interestingly, cysteine crosslinking showed that FliM-FliN interacting surface is different in CW and CCW rotational bias, suggesting a relative movement between FliM and FliN is occurred during rotational switching (Sarkar MK et al., 2010). Recent studies demonstrated that bacterial motor is a dynamic, both FliN and FliM exhibit turnover. There are two populations of FliM, which one is

tightly associated with the motor while the other undergoes stochastic turnover depends on the presence of activated CheY, indicating that turnover may be related to switching mechanism (Fig. 1.5) (Delalez NJ et al., 2010; Fukuoka H et. al. 2010).

1.2.4 FliN

FliN is organized as tetrameric doughnut-like structure formed by dimer-dimer interaction. The hydrophobic character of residues at the monomer-monomer and dimer-dimer interface is well-conserved (Brown PN et al., 2005; Paul K & Blair DF 2006). Besides, the conserved hydrophobic surface patch of FliN is the docking site of FliH and the interaction may be important for targeting FliH-containing export complexes close to the vicinity of the export apparatus to facilitate protein export (Paul K et al., 2006; Minamino T et al., 2009). FliN is assembled into the switch complex by binding to $FliM_C$ in stoichiometry 4:1. Crosslinking studies showed the relative movement between FliN-$FliM_C$ interfaces during motor switching (Sarkar MK et al., 2010). Interestingly, CheY-bound-$FliM_{N\alpha}$ also binds to FliN and mutation on this binding surface causes rotational bias (Sarkar MK et al., 2010). The multiple roles of how FliN is in motor switching remains to be elucidated (Fig. 1.6).

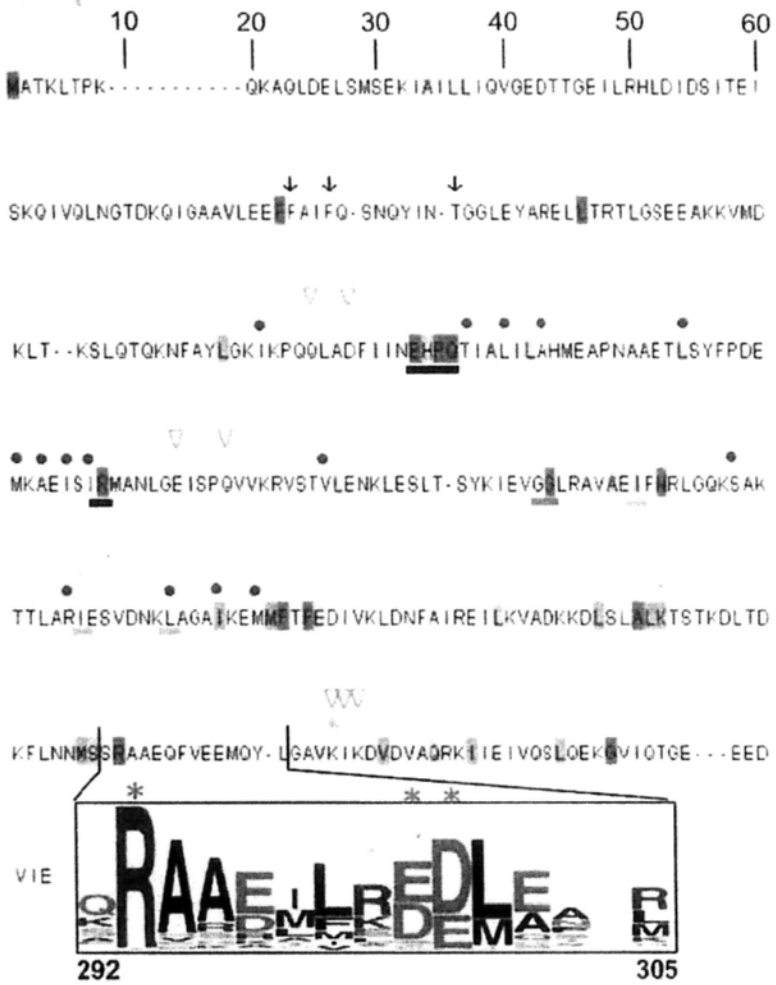

Residues important for:

FliF interaction in *C. crescentus*.

FliM interactions shown by pull down experiment, by yeast two hybrid assay.

MotA interactions that are of primary importance, secondary importance

FliG – FliG binding probed by *in vivo* crosslinking studies.

conserved GG motif.

conserved EHPQ motif.

conserved hydrophobic patch.

Fig. 1.4. Amino acid sequence of *H. pylori* FliG highlighting conservation of the regions important for FliF, FliM and MotA interactions (Grünenfelder B et al., 2003; Brown PN et al., 2007; Marykwas DL & Berg HC 1996; Lloyd SA & Blair DF 1997; Lowder BJ et al., 2005). Alignment was generated from 50 microbial species obtained from KEGG Pathway using T-Coffee. Aligned sequences were exported and analyzed in Jalview. Only amino acid sequence of *H. pylori* is shown and gap is represented by " – ". Sequence is blue colored according to conservation score with deeper color represent higher conservation. The region important for MotA interaction is represented by Weblogo (Inbox).

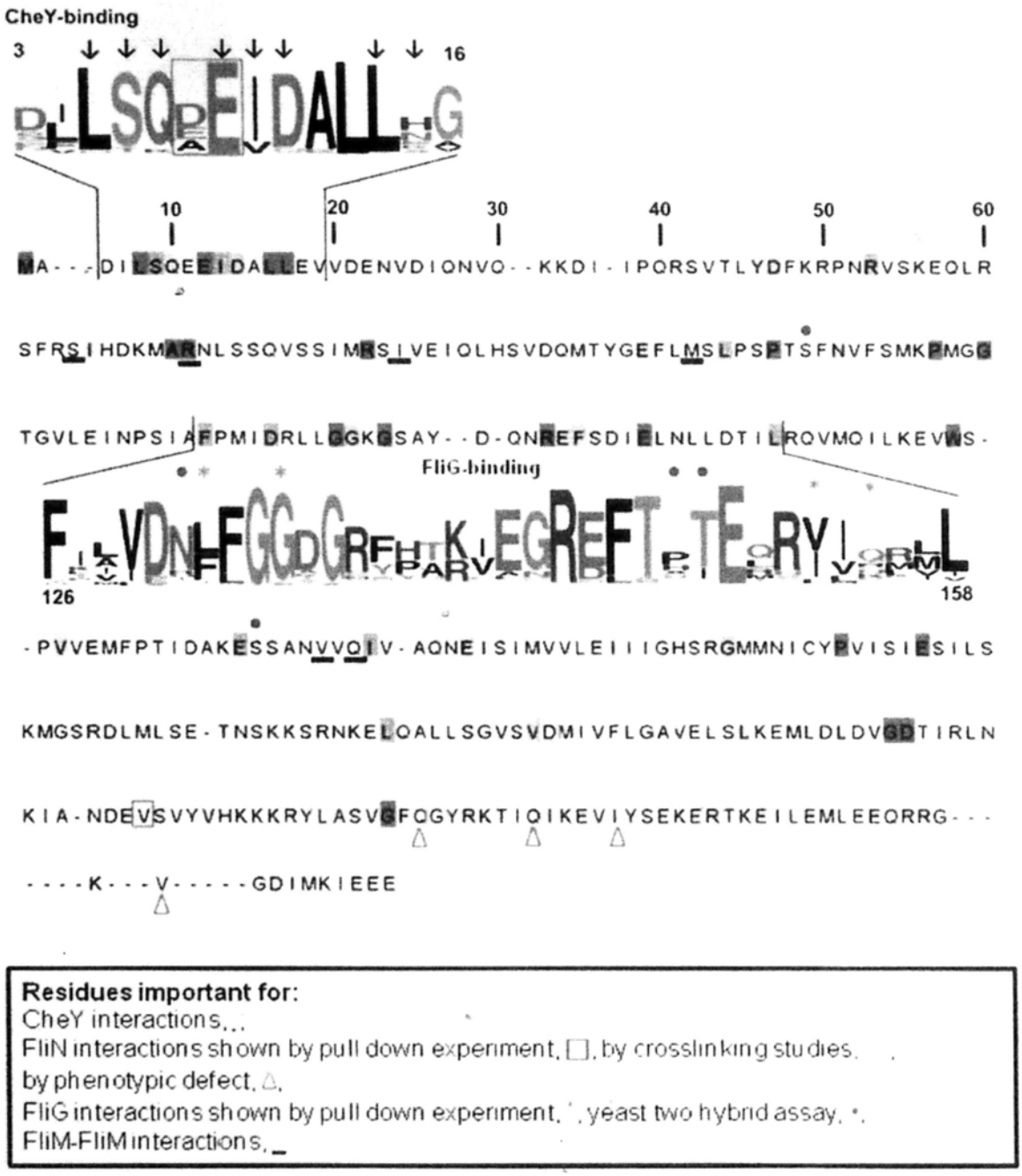

Fig. 1.5. Amino acid sequence of *H. pylori* FliM showing conservation of different regions for the interactions with CheY, FliG and FliN (Lee SY et al., 2001; Passmore SE et al., 2008; Sarkar MK et al., 2009, 2010; Paul K et al., 2010). Alignment was generated as described in Fig. 1.4. Inset sequence in logo format shows the CheY-binding region (residues 3 – 16) and the FliG binding region (residues 126 - 158) (Weblogo).

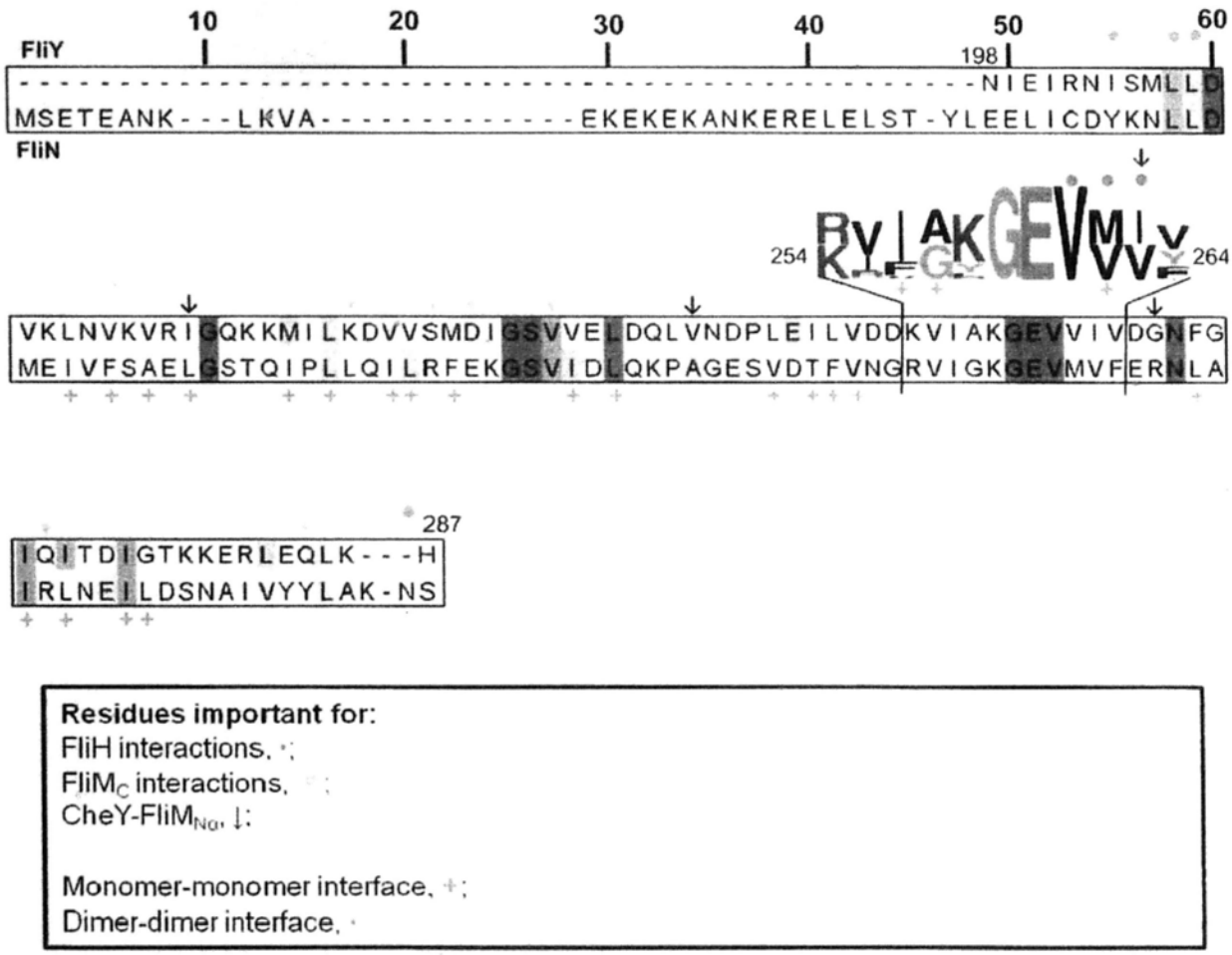

Fig. 1.6 Alignment of FliN and FliN-like domain of FliY showing the regions important for FliH and FliM interactions (Paul K et al., 2006; Lowenthal AC et al., 2009; Sarkar MK et al., 2010). Inset sequence logo format shows sequence close to FliH binding region.

1.3 Chemotaxis system

Bacterial chemotaxis is regulated by a two-component system composed of a histidine autokinase CheA and a response regulator CheY (Che – chemotaxis). CheA is coupled to chemoreceptor [(methyl-accepting chemotaxis protein (MCP)] through an adaptor protein CheW. Chemoreceptors are localized in the inner membrane and organized as a cluster at the cell pole (Briegel A et al., 2009). CheY conveys the signal by binding to the motor. The default direction

of flagellar rotation in many Gram negative bacteria is CCW. Repellent sensed by chemoreceptor (for example, L-leucine) enhances the autokinase activity of CheA and catalyzes the phosphoryl-transfer to CheY (CheY-P). The effect is to increase the affinity of CheY to the motor and turn the motor from CCW to CW direction. Then, the tumbling frequency increases and bacteria choose the path away from repellent (Szurmant H and Ordal GW, 2004). On the other hand, attractant decreases the kinase activity of CheA and the association of CheY to the motor. The phosphoryl group of CheY can be removed by either autodephosphorylation or dephosphorylation by phosphatase CheZ which also enhances the autodephosphorylation reaction (Eisenbach M 1996). Recent studies suggested an additional level for the regulation of CheY that involves acetylation-deacetylation of CheY (Liarzi O et al., 2010; Li R et al., 2010; Yan J et al., 2008).

Bacteria evolved diverse pathways in regulating chemotaxis. Some bacteria contain multiple CheYs and CheAs, (e.g. *R. sphaeroides* contains six CheY homologues and four CheA homologues), and some developed alternative adaptation (e.g. CheV in *B. subtilus*) and signal termination mechanisms (e.g. FliY and CheC in *B. subtilus*) (Hamblin PA et al., 1997; Szurmant H et al., 2004; Rao CV et al., 2008)

Bacteria sense the ligand gradients in the surrounding environment by performing temporal comparisons of ligand concentrations. This adaptation process is mediated by methylation-demethylation of chemoreceptors, for example, CheR methyltransferase and CheB methylesterase in *E. coli*. The activity of CheR is increased and the activity of CheB is inhibited when attractant binds to chemoreceptors. The net effect is the transfer of methyl groups to conserved glutamate residues of the chemoreceptors that subsequently augments the kinase activity of CheA (Rao CV and Ordal GW 2009) (Fig. 1.7).

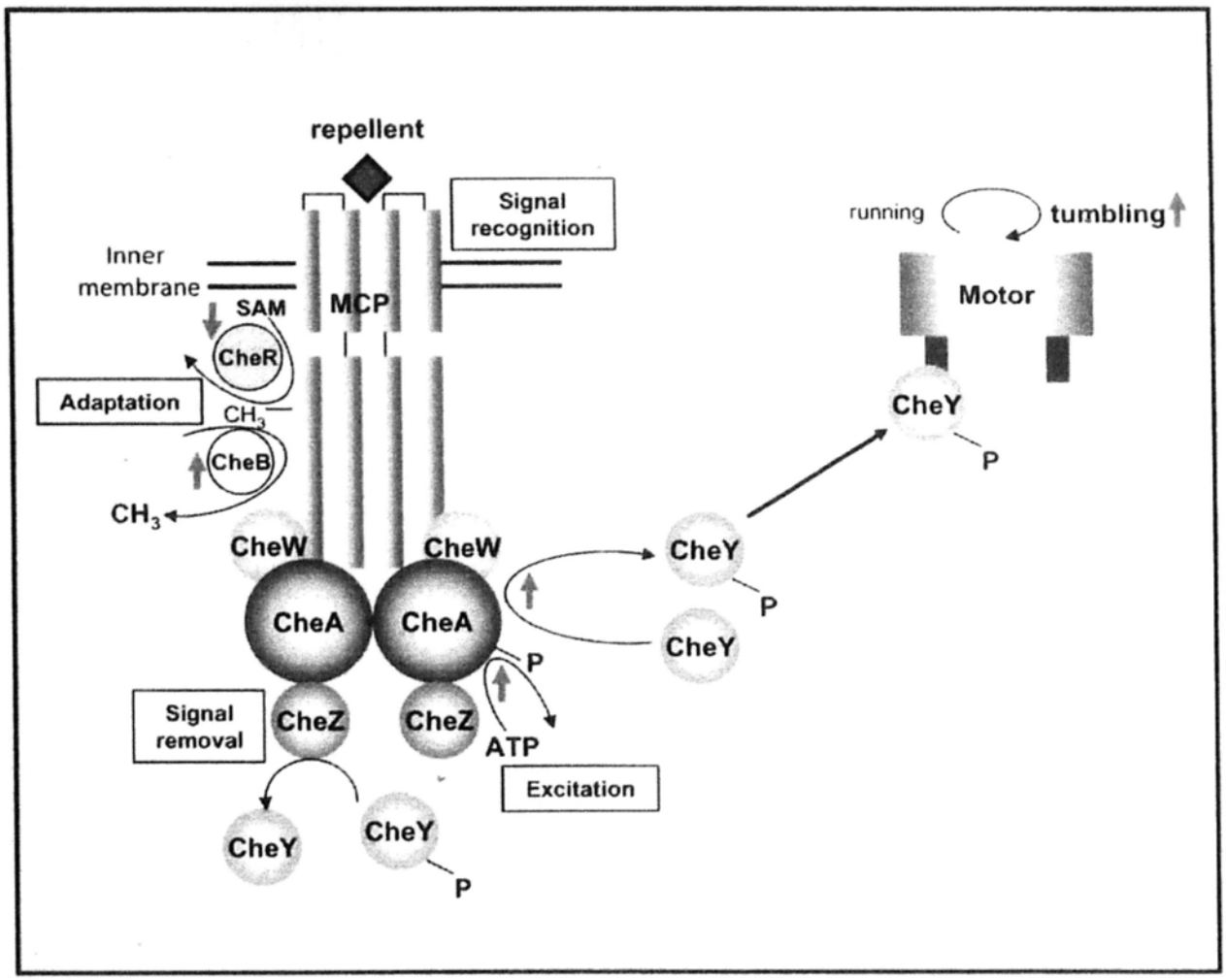

Fig. 1.7. Schematic diagram illustrates the chemotactic events in response to chemorepellent in *E. coli*. Effects on the enzyme activity are indicated by red arrows: Upper arrow: enhanced; Lower arrow, reduced. SAM, S-adenosylmethionine; CH_3, methyl group; P, phosphoryl group.

1.3.1 CheY

CheY is a single domain protein with autophosphorylation (by acetyl phosphate) and autodephosphorylaion activity (Lukat GS et al., 1992). Phosphorylated-CheY (CheY-P) as an activated form enhances the binding affinity to FliM. Structural studies on inactive and active *E. coli* CheYs and their complexes with FliM have revealed the molecular mechanisms of CheY phosphorylation and activation (Dyer CM and Dahlquist FW 2006; Lee SY et al., 2001). Phosphorylation is initiated by nucleophilic attack of Asp57 by phosphoryl phosphorus. Bound phosphate that is hydrogen bonded with Thr87 and Lys109 causes a displacement of the β4/α4 and β5/α5 loops and restricted the inward positioning of Tyr106. The activation of EcCheY requires a divalent metal ion (Mg^{2+}/Mn^{2+}), which is coordinated by Asp13, Asp57, the backbone carbonyl of Asn59, the phosphoryl oxygen and two water molecules in the active site pocket. Activated EcCheY binds the N-terminal fragment of FliM through its α4/β5/α5 interface. Recent NMR study suggests that the transient interaction between the surface residues around the active site pocket of *T. maritima* CheY and the middle FliM domain causes a displacement of $FliG_C$, suggest a possible correlation between CheY binding and motor switching (Dyer CM et al., 2009) (Fig. 1.8).

1.3.2 Proposed model of rotational switching

Recent observation on the stepping motion of the flagellum also reviewed 26 steps per revolution in CW direction (Nakamura S et al., 2010), indicating the mechanism of torque generation is symmetrical in both directions. However, the molecular basis of this symmetric rotation remains elusive. Switching process is initiated when activated CheY binds to N-terminal helix of FliM ($FliM_{N\alpha}$). Subsequently, CheY- $FliM_{N\alpha}$ complex docks to a second site on FliN

(Sarkar MK et al., 2010). It is believed that the reorientation of FliM causes a conformational change of FliG that favors CW rotation. The mechanistic details of rotational switching are unclear.

The regulation of switching is complicated by recent findings that CheA-CheY two-component system is not the sole route controlling motor switching. It has been found that H-NS (Ko M, 2000), FRD (fumarate reductase) (Cohen-Ben-Lulu GN et al., 2008), YcgR (a cyclic di-GMP binding protein) (Paul K et al., 2010), and EpsE (Blair KM et al., 2008) bind to motor and regulate switching event. These findings imply that the switching event is an integrated signaling output from environmental information and metabolic state of the cells.

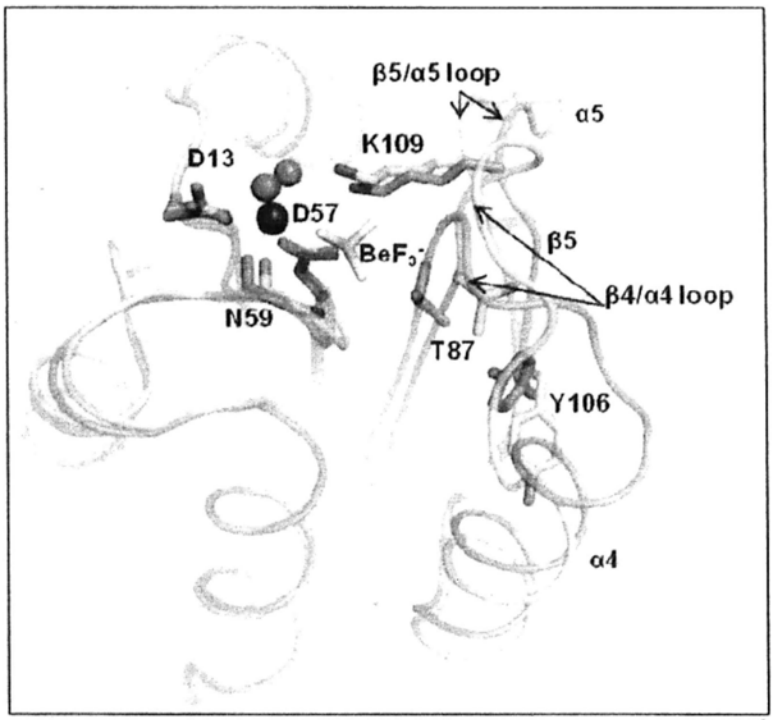

Fig. 1.8. Structural differences between inactive (PDB-ID: 1CHN, yellow) and active (PDB-ID: 1FQW, green) *E. coli* CheY. Beryllofluoride (BeF_3^-, a phosphate analog) in active CheY is shown as stick. Magnesium ion (blue) and two water molecules (red) in the active site pocket are represented as sphere.

1.4 *Helicobacter pylori*

Helicobacter pylori is spiral-shaped, gram negative anaerobic bacterium that colonizes human gastric epithelial cells and mucus layer. Around 50% of the world population is infected with *H. pylori*, with infection being more prevalent in developing countries. Host infected with *H. pylori* are usually asymptomatic, but up to 20% of individuals developed severe diseases, ranging from peptic ulcer, gastric adenocarcinoma to gastric MALT (mucous-associated lymphoid tissue) lymphoma. *H. pylori* is the first bacterium classified as class I carcinogen by WHO (Marshall BJ and Warren JR 1984; Parsonnet J et al., 1991; Correa P and Houghton J, 2007).

H. pylori share a long history and co-evolution with human. It is believed that the bacterium is transmitted by oral-oral route from person to person or fecal-oral route through contaminated water (Sachs G et al., 2003; Brown LM, 2002). One important feature of this bacterium to adapt to the human host is its heterogeneous genome. *H. pylori* can uptake DNA from their environment and insert it into its genome to cause genomic diversification (Basso D et al., 2010). *H. pylori* grow best around neutral pH but fail to grow under pH 4 unless urea is present. To survive in the final destination at the epithelial cells of stomach, *H. pylori* need to pass though the acidic gastric media, the gastric mucus layer and then adhere on the epithelial cells. The bacteria have developed mechanisms for acid resistance in stomach. Large quantities of urease are constitutively expressed in bacterial cytosol with optimal enzyme activity at neutral pH (Stingl K et al., 2002). Urea from gastric juice is imported into the bacterial cytosol through acid activated channel UreI and is broken down by urease into ammonia and carbon dioxide. NH_3 can either diffuse or be exported to periplasmic to neutralize the acidic pH. Besides motility is important for *H. pylori* to move to a specific niche in the stomach for long term infection, it is

likely necessary for the movement across the gastric mucus barrier. Interestingly, urease activity can reduce mucin viscoelasticity and allow *H. pylori* to move across mucin (Celli JP et al., 2009). *H. pylori* adheres to the surface of epithelial cells by adhesion-like proteins such that it is not removed during gastric emptying into stomach (Sachs G et al., 2003).

Currently, triple therapy, including antibiotics clarithromycin, amoxicillin or metronidazole and omeprazole (a proton pump inhibitor), is applied for the treatment of *H. pylori* infection. Increasing cases of clarithromycin resistant strains have been reported (Graham DY et al., 2011). It is surged to develop alternative therapeutic strategies to combat against antibiotics resistance strain of *H. pylori* (Duckworth MJ et al., 2009).

1.5 Role of motility and chemotaxis on *H. pylori* infection

Motility has been suggested as an virulence factor for successful colonization and infection. *H. pylori* colonize the mucus layer covering the gastric epithelial cell surface, and this colonization step is indispensible to establish a long-term infection. It is becoming convincing that motility and chemotaxis is crucial in *H. pylori* infection and long-term colonization as supported by a number of *in vivo* mutagenesis studies. Eaton KA et al., showed that depletion of components of flagellar filament, flagellin A and B, affected full colonization in gnotobiotic piglets (Eaton KA et al., 1996). Kavermann H et al., used large scale screening approach to identify genes important in colonization in Mongolian gerbil stomach, and they isolated several flagellar genes that are involved in the flagellar assembly (e.g. fliF, fliI, fliP, fliS) as well as chemotaxis (e.g. CheA, CheV3) (Kavermann H et al., 2003). Study of the roles of chemotaxis in colonization and its capacity to trigger inflammation has further showed that *cheY* mutant completely failed to colonize gerbil and *cheY* or *cheW* mutant displayed attenuated phenotype and altered distribution in the stomach with less intimate association with the gastric cells.

Nonchemotactic mutants are less competitive than wild type and showed reduced inflammatory response in mice. Besides, mutants lacking chemoreceptors TlpA and TlpB altered host's inflammation severity (McGee DJ 2005; Terry K et al., 2005; Williams SM et al., 2007). These findings implicate the association of chemotaxis and motility in initial colonization, achieving high-level of infection, persistence for infection with competing *H. pylori*, proper gastic distribution and host inflammatory responses.

H. pylori migrate to a very narrow zone close to the gastric epithelial surface and away from the lumen. The living environment of *H. pylori* is a highly dynamic, mucus being continuously secreted in the glands and by surface epithelial cells, and is degraded at the luminal surface (Schreiber S and Scheid P, 1997). Thus, the motility and chemotactic capability is important to prevent the bacterium from being carried to acidic gastric lumen that would inhibit bacterial growth. Schreiber S et al., reported that *H. pylori* detects gastric mucus pH gradient for proper orientation (Schreiber S et al., 2004). TlpB and TlpD are identified that monitor energy-related parameters in *H. pylori*. (Croxen MA et al., 2006; Schweinitzer T et al., 2008)

1.6 Flagella and chemotaxis system in *H. pylori*.

H. pylori possesses 2 – 6 sheathed unipolar flagella that allows proper motility in the viscous environment of gastric mucosa. Sheathed flagellum is a unique feature that the flagella filament is covered by extension of outer membrane and displays a bulb-like structure at the distal end of filament. The sheath is thought to protect flagella structure from exposure to acidic environment (Geis G et al., 1993). *H. pylori* showed positive chemotaxis towards bicarbonate, mucin (Foynes S et al., 2000), urea (Mizote T et al., 1997), urea analogs (fluorfamide) (Nakamura H et al., 1998) and amino acids (Cerda O et al., 2003); and negative chemotaxis towards quorum sensing molecule autoinducer-2 (AI-2) and acidic pH (Rader BA et al., 2011).

Genomic sequences from five *H. pylori* strains have been elucidated, including 26695 (Tomb JF et al., 1997), J99 (Alm RA et al., 1999), HPAG1 (Oh JD et al., 2006), G27 (Baltrus DA 2009) and Shi470 (Kersulyte D et al., 2010). Homologs of chemotaxis and switch proteins in *E. coli* have been identified including CheY (HP1067) (denotes as CheY1 in the following text), CheA (HP0392), CheW (HP0391), a remote CheZ homolog (HP0170), FliG (HP0352), FliM (HP1031) and FliN (HP0584). However, *H. pylori* differs from *E. coli* in that no homolog of adaptation proteins CheR and CheB are found. Besides, *H. pylori* harbors genes encoding multiple CheY-like proteins – a bifunctional CheA with a CheY-like domain (this domain is denoted as CheY2 in the following text) (CheAY2) (HP0392) fused to the C-terminus and three CheV (CheV1-HP0019, CheV3-HP0393, CheV2-HP0616) genes each consisting of an N-terminal CheW-like domain and a C-terminal CheY-like domain. *H. pylori* also possess an additional putative switch protein FliY (Valenzuela M et al., 2003).

1.6.1 Switch protein complex of *H. pylori*

FliG, FliM, FliN and FliY are necessary for normal flagellation in *H. pylori*. Deletion of FliG or FliM was completely non-flagellate, while deletion of FliN or FliY was partially flagellated but immotile, consistent with the phenotype of switch gene deletion mutants observed in *E. coli*. The interactions among these proteins and their regions important for the switching function in *H. pylori* are not understood. Based on the sequence alignment results, the residues important for protein-protein interactions among the proteins (FliG, FliM and FliN) are fairly conserved (Fig. 1.4 – 1.6). Besides, substitution of Arg54 by Cys in FliM led to smooth swimming bias. Taken together the result that FliM interacts with CheY1, these proteins likely performs similar functions as in other organisms (Lowenthal AC et al., 2009).

H. pylori is featured by carrying two FliN-containing proteins, FliY and FliN. FliY was firstly characterized in *B. subtilus* (BsFliY) with domain organization resembles to that of FliM, which composed of CheY-binding site at N-terminus, CheC/FliY/CheX-like domain at the middle and FliN-like domain at the C-terminus, respectively (Bischoff DS & Ordal GW 1992). The middle domain exhibits phosphatase activity towards phosphorylated CheY *in vitro*. Deletion of CheY-binding site on BsfliY showed opposite phenotypic effect to *cheY* deletion mutant, consistent with a role in signal termination (Szurmant H et al., 2003). Expression of FliY in wild-type *Salmonella* severely inhibits chemotaxis while expression in a non-motile *FliN* mutant restores motility but not chemotaxis, suggesting FliY assembles into the switch complex (Bischoff DS et al., 1992). Distinct from *H. pylori*, no discrete FliN homolog was identified in *B. subtilis* and it is believed that FliY replaces the role of FliN in the complex. Sequence of *H. pylori* FliY and FliN has been analyzed by Lowenthal AC et al., by comparing 768 genomes, to search for microbes that possess both proteins. They suggest that the presence of both proteins is universal among epsilonproteobacteria and is scattered in a few species in phylogenetically diverse taxa, including members of *Clostridia*, *Spirochaetales*, firmicutes (Lowenthal AC et al., 2009). The FliN-like domain of FliY and FliN share 30% and 39% sequence identity to *E. coli* FliN respectively. The character of residues involving in flagellar protein export and homodimerization of FliN are significantly conserved, although it was noted that the exact amino acid was often not the same (Lowenthal AC et al., 2009) (Fig. 1.6). Interestingly, CheY-binding peptide in BsFliY is missing in *H. pylori* FliY. Besides the conserved active site for phosphatase activity, EXXN, in CheC/ FliY/CheX family (CYX family) is replaced with conserved EXXXN motif in *H. pylori* FliY while the corresponding phosphatase motif is DXXXQ in CheZ (Zhao R et al., 2002) (Fig. 1.9). By comparing structures of CheX-CheY, CheZ-CheY complexes, it has

been suggested that they share an identical dephosphorylation mechanism, although the active site helices do not aligned, and are almost perpendicular to each other (Pazy Y et al., 2010). The amino acid properties of the catalytic motif are conserved in *H. pylori* suggesting that FliY may carry phosphatase activity. Since deletion of the CheY-binding region of BsFliY impairs its phosphatase activity, *H. pylori* likely establishes a novel mechanism to display CheY to the active site (Szurmant H et al., 2004). Individual FliY and FliN knockdown causes impairment in flagellar formation, while deletion of both proteins is non-flagellate, these data support that both proteins are switch proteins and the functions of FliY and FliN are redundant (Lowenthal AC et al., 2009). However, how FliY is incorporated into the switch protein complex, and whether their C-terminal domain have distinct functions and whether the N-terminal domain possesses phosphatase activity towards CheY remains to be understood.

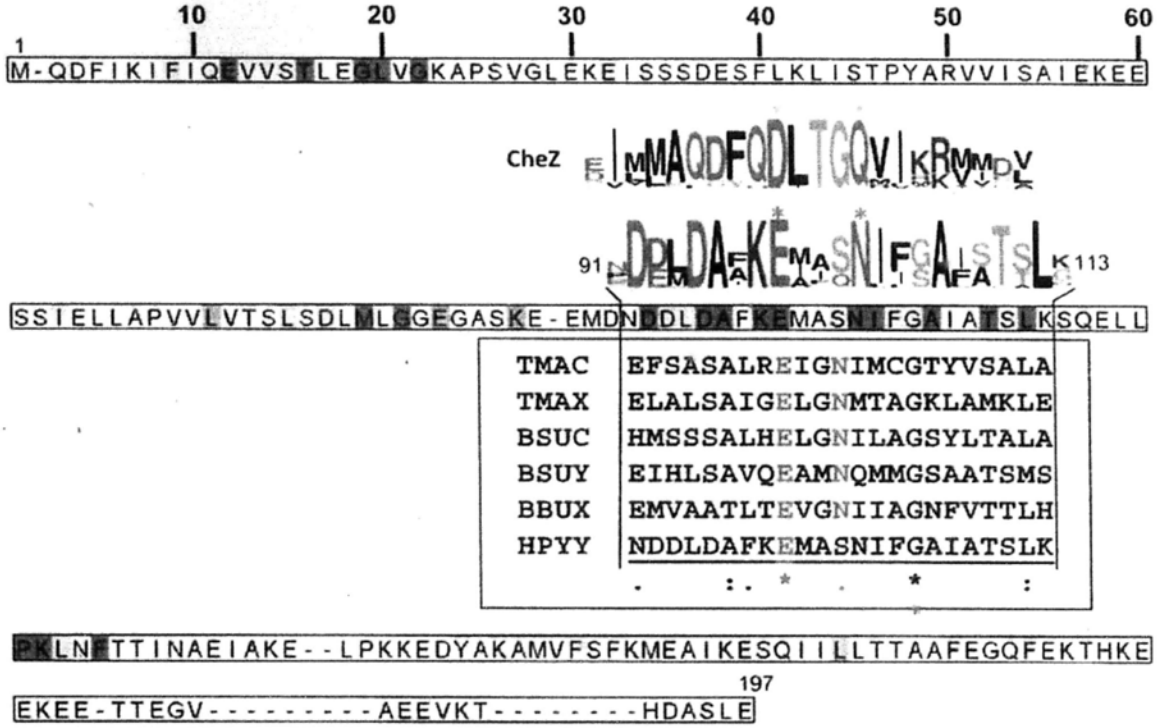

Fig. 1.9. Amino acid sequence of *H. pylori* FliY N-terminal domain showing conservation among FliY orthologues in epsilonproteobacterium (Lowenthal AC et al., 2009). Inset sequence logo format shows sequences of a predicted helix (residues 92 – 112) containing putative active site residues (JNET). Inbox: Alignment of FliY with sequences from CYX family, note that the conserved EXXN motif (Red) is replaced by EXXXN in *H. pylori* FliY (Red asterisks) (Silversmith RE 2010). Active site region of CheZ (aligned from 20 randomly selected species) is also displayed as sequence logo format with conserved DXXXQ motif are indicated by blue asterisks (Zhao R et al., 2002). TMAC and TMAX denotes CheC and CheX from *T. maritima*, respectively; BSUC and BSUY denotes CheC and FliY from *B. subtilus*, respectively; BBUX denotes CheX from *B. burgdorferi*, HPYY denotes *H. pylori* FliY.

1.6.2 Chemotaxis system of *H. pylori*

CheY1 shares 46% amino acid sequence identity with *E. coli* CheY (EcCheY) (ClustalW2) and both of these proteins exhibit a dephosphorylation rate of about 0.035 s^{-1} (Jiménez-Pearson MA et al., 2005; Silversmith RE et al., 2001). Residues involved in

phosphorylation and activation of EcCheY are conserved in CheY1, suggesting that CheY1 shares a similar activation mechanism (Fig. 1.10). However, deletion of CheY1 showed contradictory results from two independent studies. Foynes S et al., reported rapid tumbling phenotype of *cheY1* mutant and smooth swimming phenotype of *cheY2* mutant, suggesting that CheY2 rather than CheY1 interacts with flagellar motor switch (Foynes S et al., 2000). On the other hand, a recent study on chemotaxis by fixed time diffusion analysis showed that *cheY1* mutant was smooth-swimming biased, that the result is in line with the *E. coli* model. *In vitro* experiments showed that CheY1 was phosphorylated by CheA and interacted with FliM upon activation by acetyl phosphate (Lowenthal AC et al., 2009). It appears more likely that the biological function of CheY1 is comparable to that of EcCheY.

The chemotactic regulatory mechanisms of *H. pylori* are featured with multiple response regulators. All response regulators can be phosphorylated by CheA which preferentially acts on CheY1 (Jiménez-Pearson MA et al., 2005). Interestingly, CheY1-P is able to transfer the phosphate back to CheA, and the phosphate moiety is then transferred to CheY2, suggesting that *H. pylori* may exhibit retrophosphorylation, although this observation is not yet supported by *in vivo* evidence. CheV is proposed to be involved in adaptation mechanisms of *Bacillus subtilis* (Rao CV et al., 2008), while the biological significance of CheVs in *H. pylori* is not as well understood. Only the CheV1 mutant is nonchemotactic, while heterologous overexpression of CheV2 and CheV3 in *E. coli* inhibits swarming of the wild type bacteria (Pittman MS et al., 2001), suggesting that all three CheVs are associated with chemotaxis. In addition, CheV1 and CheV2 mutants are smooth swimming biased, while CheV3 is tumbling biased. Given that CheVs can be phosphorylated *in vitro* to different levels by CheA and that CheV mutants show various extents of deficiency in colonizing mouse stomachs (Jiménez-Pearson MA et al., 2005; Lowenthal AC et al., 2009), it is probably that CheVs have distinct and important roles in *H. pylori*. Furthermore, these proteins may display distinctive structural characteristics.

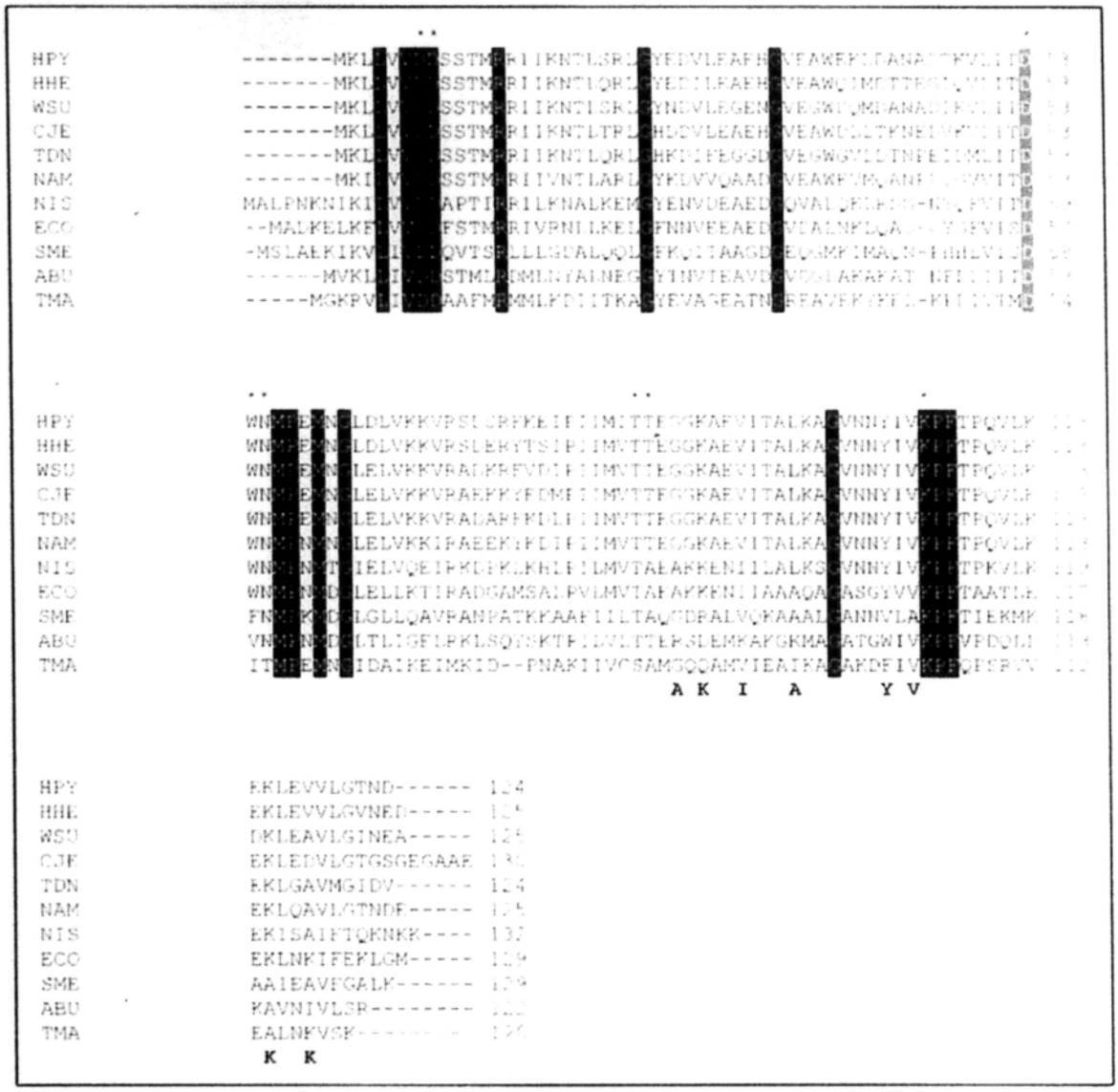

Fig. 1.10. Multiple sequence alignments of CheY1 from *Helicobacter pylori* 26695 (HPY), *Helicobacter hepaticus* (HHE), *Wolinella succinogenes* (WSU), *Campylobacter jejuni* NCTC11168 (CJE), *Sulfurimonas denitrificans* (TDN), *Nautilia profundicola* (NAM), *Nitratiruptor sp.* SB155-2 (NIS), *Arcobacter butzleri* (ABU), *Escherichia coli* K-12 MG1655 (ECO), *Sinorhizobium meliloti* (SME) and *Thermotoga maritime* (TMA) (ClustalW). Totally conserved residues are shaded. Phosphorylation site Asp53 is shaded in grey. Asterisks (*) - residues of the active site pocket; Residues of *E. coli* involved in FliM binding are marked below the alignment (Lee SY et al., 2001).

1.7 Objectives

Switch protein complex is a macromolecular assembly of protein oligomers critical for flagellar biosynthesis, torque generation and motor switching. Interestingly, genomic sequence suggests diverse organizations and functions of the motor. The chemotaxis and flagellar systems have been extensively studied in enteric bacteria *E. coli* and the structures of switch proteins have been elucidated from thermophilic bacterium. However, the molecular basis of flagellar assembly and switching of the motor remains controversial. Besides, the regulatory mechanism in other microbial species remains not explored. *H. pylori* carries multiple response regulators and a putative switch protein FliY, potentially implying a distinct organization and function of the flagellar system in epsilonproteobacteria. In this study, we take the initiative to characterize the structure and function of chemotactic proteins and switch proteins from *Helicobacter pylori*. We applied multidisciplinary approaches in molecular and structural biology to characterize the chemotactic response regulator CheY1, the structural architecture of the switch complex and the biological significance of FliY in *H. pylori*. The molecular interactions among the switch proteins were studied by pull down experiments and gel filtration analysis. Purified individual switch protein or their complexes were subjected to crystallization screening and the structures of successful candidates were solved by X-ray crystallography. Knowledge gained from the structural comparisons with their respective counterparts from *T. maritima* and *E. coli* was further verified by mutagenesis studies and various biochemical or phenotypic assays. Besides, the biological role of FliY was investigated by functional complementation of *H. pylori* G27 Δ *fliY* mutant. Taken together, a model of switch protein assembly and rotational switching is proposed.

Chapter 2

Crystal structure of activated CheY1

2.1 Introduction

The chemotactic system of *H. pylori* is marked by the presence of multiple response regulators: CheY1, one CheY-like-containing CheA (CheAY2) and three CheV proteins. These molecules are shown to play unique roles in the chemotactic signal transduction mechanisms of *H. pylori*. *CheV1*, *cheV2* and *cheY2* mutants are smooth swimming biased, while *cheV3* mutant is tumbling biased. The biological function of CheY1 is still ambiguous, since both smooth and tumbling swimming phenotypes of *cheY1* mutant have been reported (Foynes S et al., 2000; Lowenthal AC et al., 2009). Despite the fact that the chemotactic system in *H. pylori* carries unique features and is crucial for bacterial infection, structural characterization of any of these chemotactic proteins in *H. pylori* have not been reported.

In the present study, we studied the structures of active and inactive CheY1 by X-ray crystallography. Structural comparisons of activated CheY1 with EcCheY identified Thr84 possibly involved in the phosphotransfer reaction. The effect of Thr84 mutation on CheY phosphorylation was investigated by fluorescence quenching experiments. To address whether CheY1 possesses similar biological function as EcCheY, complementation assays of various nonchemotactic *E. coli* mutants by CheY1 were performed. Besides, interactions of CheY1 to FliM and CheA were investigated by *in vitro* pull down experiment.

2.2. Materials and methods

2.2.1 Cloning, expression and purification

Genes encoding CheY1 (HP1067), CheY2 (HP0392; residues 677 – 803, designed according to previous study) (Jiménez-Pearson MA et al., 2005), CheV1 (HP0019), CheV2 (HP0616), CheV3 (HP0393), CheA-P2 domain (HP0392; residues 110-261) and C-terminal truncated FliM (HP1031; residues 1 – 237, $FliM_{NM}$) were amplified from *H. pylori* strain 26695 genomic DNA using DNA polymerase (Expand). The primers are designed using software OligoPerfect™ Designer tools (Invitrogen) (Table 2.1). Amplified genes were cloned into various expression vectors in order to obtain optimal expression level and solubility. CheY1, CheV1 and CheV2 were cloned into pGEX-6P-1 expression vector (Appendix 1). CheY2 and CheV3 were cloned into pET28m-sumo1 vector (Appendix 1). CheA-P2 and $FliM_{NM}$ were cloned into pT7-7 vector with a C-terminal 8×His tag (Appendix 1). Mutants CheY1/D53A and CheY1/T84A were generated using the QuikChange Site-Directed Mutagenesis kit (Stratagene) and verified by commercial sequencing service (1st BASE).

Recombinant proteins were expressed in *Escherichia coli* strain BL21. After transformation, cells were grown at 37°C until OD_{600} reached 0.4 – 0.6. Protein expression was induced by the addition of 0.3 mM isopropyl-β-D-thiogalactopyranoside (IPTG) and the cells were further grown at 16°C or 25°C for 16 h.

Proteins were purified by two steps, affinity and size exclusion chromatography. GST-tagged and 6×His-tagged proteins were purified by glutathione-S transferase (GST) sepharose (GE Healthcare) and Nickel-NTA agarose (Qiagen), respectively. In general, cell pellet was resuspended in lysis buffer (Table S2.1) and lysed by sonication. Buffer

with the addition of 0.5 mM EDTA and 4 mM DTT was used for the purification of GST-tagged proteins and 20 mM imidazole was included in His-tagged proteins. Cell lysate was clarified by centrifugation (40,000 x g, 1 h and 4°C) and the supernatant was filtered by 0.22 µm filter and incubated with pre-equilibrated affinity resin at 4°C with gentle shaking. The lysate was incubated with GST-resin for 2 h and Ni-NTA resin for 1 h. After washing the beads with the lysis buffer, the GST tag was cleaved by prescission protease when necessary, by incubation at 4°C for 16 h with gentle shaking. For His-sumo1 fusion protein, the tag was removed by incubation with sumo protease SENP1 catalytic domain in a mass ratio of 1:100 at 37°C for 30 min with shaking (Xu Z and Au SW, 2005). The eluted proteins were then concentrated to 2 ml in volume, and injected into a size exclusion chromatography column Superdex 75 or Superdex 200 equilibrated with buffer (Table S2.1).

2.2.2 Nickel pull down assay

2.2.2.1 CheAP2-CheY interaction assay

An aliquot of 25 µl nickel NTA resin (Qiagen) was pipetted into a 1.5 ml eppendorf and centrifuged (3300 x g, 10 s, 4°C). The beads were washed 3 times with binding buffer containing 20 mM imidazole pH 7.0, 150 mM NaCl and 2 mM $MgCl_2$. It was followed by the addition of 1 ml purified CheA-P2-8xHis protein solution in a concentration of 0.1 mg/ml. The mixture was incubated at 4°C for 1 h with gentle shaking. The beads were washed three times with the binding buffer followed by the addition of purified CheY1, CheY2, CheV1, CheV2 and CheV3 in a molar ratio of 1:1. The mixture was incubated for another 1 h at 4°C. The beads were washed three times with the buffer

and then resuspended in 25 µl of 2x SDS-PAGE gel loading buffer and heated to 90°C for 8 min. The samples were subjected to SDS-PAGE analysis and Coomassie blue staining.

Table 2.1 Primers used for the cloning of the genes encoding chemotaxis proteins and FliM.

Primer Name	Primer Sequence (5' – 3')	Restriction Site
CheY1 – F	cgggatccatgaaactactggtagtagatgatagctca	BamHI
CheY1 – R	catatggtcgactcaatcgtttgtccctaaaacaac	SalI
CheY2 – F	catgacggatccatgattgtcttagcgattgatgacagcagcacggata	BamHI
CheY2 – R	catgacgtcgactcacgattggtctccttctaatttaatgctgcgcttc	SalI
CheV1 – F	gggggggggatccatggctgatagtttagcgggcattgatcaagttacgag	BamHI
CheV1 – R	gggggggcggccgctcatgctaattccaaaaattgcttaaccactcgctggatgtc	NotI
CheV2 – F	gggggggggatccatggtaagagatattgacaaaacgacttcgttgcacttaaacaacg	BamHI
CheV2 – R	gggggggtcgacttatgaaagcgtttttttaagcatttcatggatttcaagaatg	SalI
CheV3 – F	tccattggatccatggcagaaaaaacagctaaggatt	BamHI
CheV3 – R	tccattgcggccgcttacgcattcttgtctaaaatcttagaaa	NotI
CheAP2 – F	gggggggggatccatggatactaataacggcaaggaaaacgagattga	BamHI
CheAP2 – R	gggggggtcgactcaatggtgatggtgatggtgatggtgctccacgccaatagaggggcttat	SalI
$FliM_{NM}$ – F	catatgcatatgatggctgatattttaagccaagaa	NdeI
$FliM_{NM}$ – R	gggggggtcgactcaatggtgatggtgatggtgatggtgaagcatcaaatccctactcccc	SalI
CheYD53A-F	actaaggtgcttatcacagcttggaacatgcctgaaatg	-
CheYD53A-R	catttcaggcatgttccaagctgtgataagcaccttagt	-
CheYT84A-F	cctattattatgatcaccgcagagggcggtaaagctg	-
CheYT84A-R	cagctttaccgccctctgcggtgatcataataatagg	-

2.2.2.2 FliM-CheY interaction assay

Pull down experiment was performed as described previously with modifications (Lowenthal AC et al., 2009). All experimental steps were performed at 25°C. $FliM_{NM}$ was immobilized onto nickel NTA resin pre-equilibrated with buffer containing 10 mM Hepes pH7.6, 5 mM $MgCl_2$, 250 mM KCl, 0.15% Tween20 and 20 mM imidazole. After incubation for 1 hour, the beads were washed for 3 times. To activate CheY1, beryllofluoride was incubated with CheY1 during the pull down experiment. CheY1 and CheY1/D53A were pre-incubated with 0.75 mM $BeCl_2$ and 18 mM NaF for 10 min before incubated with the immobilized $FliM_{NM}$ for 15 min. The beads were washed twice, boiled with gel loading buffer and subjected to SDS-PAGE analysis.

2.2.3 Size exclusion column chromatography

Purified CheY1 and CheV3 were individually mixed with CheA-P2-8xHis (in 1:2 molar ratio) in a buffer containing 10 mM Hepes pH 7.4, 150 mM NaCl and 2 mM $MgCl_2$. The mixture was incubated on ice for 30 min. Individual proteins or mixtures were applied to a Superdex 200 HR 10/30 gel filtration column (GE Healthcare) and eluted at 0.6 ml/min with the same buffer. Eluted proteins were subjected to SDS-PAGE analysis and Coomassie blue staining.

2.2.4 Fluorescence spectroscopy

Fluorescence measurement was carried out using Perkin Elmer 50B spectrofluorimeter. Fluorescence was measured at an excitation wavelength of 293 nm and an emission wavelength of 341 nm with slit widths of 3 nm and 6 nm for excitation and emission, respectively. All reactions were carried out at 25°C. Equilibrium titration of CheY1, CheY1/D53A or CheY1/T84A by acetyl phosphate were carried out in a buffer containing 20 mM sodium phosphate pH 7.5, 50 mM NaCl and 2 mM $MgCl_2$. The final concentrations were 1 μM for CheY1s and 0.3-10 mM for acetyl phosphate. Titration of CheY1 or CheY1/D53A with BeF_3^- was performed by sequential addition of NaF to the protein solution containing 10 μM $BeCl_2$. The final concentration of NaF was set to 0 – 5 mM. Fluorescence changes upon addition of small molecules were monitored until the fluorescence signal stabilized. The fluorescence values were corrected for dilution. *Km* was determined as described (Lukat GS et al., 1992; Pittman MS et al., 2001; Silversmith RE et al., 1997). Acetyl phosphate concentration was plotted versus $(Io - I) / (I - I_{inf})$, where Io is initial fluorescence intensity; I is the intensity at the corresponding acetyl

phosphate concentration and I_{inf} is the intensity at saturating concentration. From the plot, the reciprocal of the slope of the line corresponds to the *Km* value. According to proposed reaction scheme (Lukat GS et al., 1992) shown as follow, $Km=K_s k_3/k_2$

$$\text{CheY1} + \text{Ac}\sim\text{P} \overset{K_s}{\rightleftharpoons} \text{CheY1}\bullet\text{AcP} \overset{k_2}{\rightarrow} \text{CheY1}\bullet\text{P} \overset{k_3}{\rightarrow} \text{CheY1} + \text{P}_i$$

where K_s is the equilibrium dissociation constant between CheY1 and acetyl phosphate, k_2 and k_3 is the phosphorylation and dephosphorylation rate constants respectively.

2.2.5 Swarming assay

E. coli motility wild type strain RP437 and chemotaxis mutant strains RP1616 (*ΔcheZ*), RP5232 (*ΔcheY*) were gifts from Parkinson JS (Parkinson JS, 1978). Complementation assay was performed by individual transformation of pTrc99a, pTrc99a-CheY1 and pTrc99a-CheY1/D53A in strain RP437 and chemotaxis mutants RP1616 (*ΔcheZ*) and RP5232 (*ΔcheY*). An aliquot of 1 μl overnight culture was spotted onto 0.4% TB soft agar (1% tryptone, 0.5% NaCl and 0.5% glycerol, 0.4% agar). Ampicillin (100 μg/ml) and IPTG (final concentration of 0.05, 0.1, or 0.5 mM) were added when necessary. The diameter of the chemotactic rings was measured after incubation at 30°C for 7 h.

2.2.6 Immunoblotting

An aliquot of 1 μl overnight culture of *E.coli* strains RP437 and RP1616 (*ΔcheZ*), RP9535 (*ΔcheA*), RP5232 (*ΔcheY*) transformed with the recombinant plasmids were added to 3 ml of TB medium with 0, 0.05, 0.1 and 0.5 mM IPTG when necessary. Cells

were grown overnight at 30°C with vigorous shaking. The cells were harvested and washed with a buffer containing 10 mM Hepes pH 7.4 and 150 mM NaCl. The samples were subjected to SDS-PAGE analysis followed by immunoblotting with polyclonal anti-CheY1 antibody (Invitrogen).

2.2.7 Crystallization condition of CheY1

Initial crystallization trials were performed by Crystal Screens I & II from Hampton Research (Hampton Research) using sitting drop vapour diffusion method. Diffraction-quality crystals of CheY1 grown at 16°C were obtained from an optimized screening condition containing 0.1 M sodium acetate, pH 5.0, 0.2 M ammonium sulfate, 35% MPEG2000 and 1 mM $MgCl_2$. Crystals of CheY1/D53A and T84A were grown under similar condition. For BeF_3-bound CheY1, the crystals were grown in crystallization buffer containing 0.1 M sodium acetate, pH 5.0, 0.05 M ammonium sulfate, 1.6 mM $BeCl_2$ ([CheY1] : $BeCl_2$ = 1 : 10) and 16 mM NaF.

2.2.8 Data collection and processing

1.8 Å X-ray data set for CheY1 crystal, 2.2 Å X-ray data set for BeF3-bound CheY1 crystal, 2.2 Å X-ray data set for CheY1/D53A crystal and 1.7 Å X-ray data set for CheY1/T84A crystal were collected at 100 K using a Rigaku MicroMax 007 X-ray generator at the Centre for Protein Science and Crystallography, The Chinese University of Hong Kong, and recorded on a RAXIS IV++ image plate. For each crystal, crystallization buffer containing 15% glycerol was used as a cryoprotectant. Images were processed using *Mosflm* (Leslie A, 1995) and scaled and reduced with *SCALA* from the

CCP4 suite (Collaborative Computational Project, 1994). Coordinates have been deposited in the Protein Data Bank (PDB-ID: 3GWG, 3H1E, 3H1F, and 3H1G).

2.2.9 Structure determination and refinement

The CheY1 structure was solved by molecular replacement using a molecule of EcCheY (PDB-ID: 3CHY) as a search model. Molecular replacement program *PHASER* (McCoy AJ et al., 2007) in CCP4 suite was performed with data in the resolution range 15–3.0 Å. For the other three structures, the refined structure of CheY1 was used as a search model. The randomly selected 5% of data was reserved for the R_{free} calculation for all the three structures. Rounds of refinements and manual rebuilding were performed by using the programs *REFMAC* and *COOT* (Collaborative Computational Project, 1994; Emsley P and Cowtan K, 2004), respectively. The electron density maps from *2Fo–Fc* and *Fo–Fc* calculations were used for model building, and for all the structures, strong electron density was found close to the active site Asp 53. We modeled them as sulfate molecule for CheY1, CheY1/D53A and CheY1/T84A structures. For the CheY1 crystal grown in the presence of beryllium and sodium, a beryllium fluoride molecule was modeled in the active site. The Ramachandran plots drawn by the program PROCHECK (Laskowski RA et al., 1998) showed that over 90% of all residues in the four CheY1 structures fall within the most favored region (Appendix 2.1).

2.3 Results

2.3.1 CheY1 is activated by beryllofluoride

CheY1-P has a short half-life (20 s) therefore precludes structural analysis of the activated form (Jiménez-Pearson MA et al., 2005). BeF_3^- is known to form a persistent complex with response regulators by mimicking an acyl phosphate (Cho HS et al., 2000; Lee SY 2001). In prior to our structure-function analysis, the binding of BeF_3^- to CheY1 was examined by steady-state fluorescence quenching. CheY1 contains two tryptophan residues (Trp38 and Trp54). Equivalent conserved residue Trp54 in EcCheY has been targeted to monitor the binding of small molecules to the active site pocket (Lukat GS et al., 1992). The fluorescence of Trp38 is not affected by this binding because it is located at helix 2, and no conformational change in helix 2 was reported upon phosphorylation (Lee SY et al., 2001). A reaction mixture containing 1 μM CheY1 and 10 μM $BeCl_2$ was titrated by sequential addition of 0.5 M NaF to a final concentration of 0 – 5 mM. As shown in Figure 2.1A, the tryptophan fluorescence of CheY1 decreased upon addition of increasing amounts of NaF and was almost saturated at 4 mM of NaF. The CheY1-D53A mutant, a non-phosphorylatable analog, showed no decrease in fluorescence, suggesting that CheY1 binds BeF_3^- and that an aspartic residue is necessary for the binding. As a control, phosphorylation of CheY1 by acetyl phosphate was monitored, and a comparable decrease in fluorescence was observed for the wild type and D53A mutant (Fig. 2.1B).

Activated CheY has an enhanced affinity for FliM (Yan D et al., 1999) and a recent study demonstrated the binding of CheY1-P to FliM upon activation by acetyl phosphate (Lowenthal AC et al., 2009). To further verify that CheY1-BeF_3^- mimics CheY1-P, the interaction of CheY1-BeF_3^- with FliM was examined by *in vitro* pull-down

assay. CheY1 and $FliM_{NM}$ (consisting of the N-terminal and middle domains fused to a C-terminal His_8 tag) were purified to greater than 95% purity. $FliM_{NM}$ was immobilized on Ni-NTA resin, followed by incubation with wild-type CheY1 or the D53A mutant with or without BeF_3^-. As shown in Figure 2.1C, only wild-type CheY1 complexed with BeF_3^- showed a stable interaction with $FliM_{NM}$, suggesting that CheY1- BeF_3^- mimics the activated form of CheY1 in the interaction with $FliM_{NM}$.

A

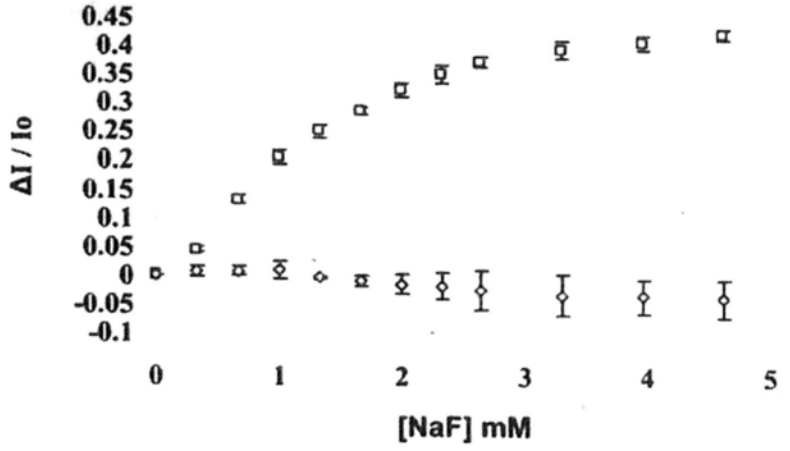
0.45
0.4
0.35
0.3
0.25
0.2
0.15
0.1
0.05
0
-0.05
-0.1
ΔI / Io
0
1
2
3
4
5
[NaF] mM

B

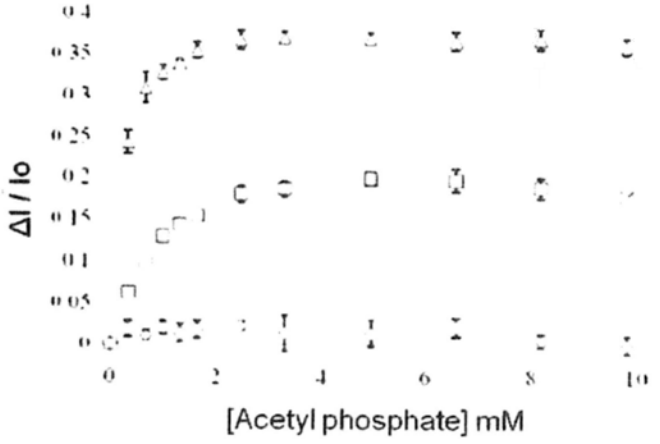
ΔI / Io
[Acetyl phosphate] mM

C

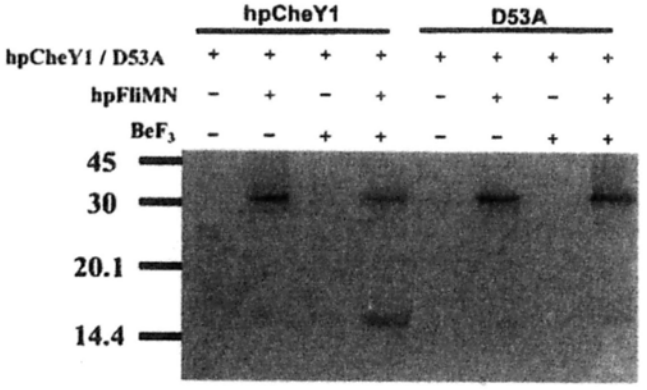
hpCheY1
D53A
hpCheY1 / D53A
hpFliMN
BeF3
45
30
20.1
14.4

Fig. 2.1. Activation of CheY1 by beryllofluoride. Fluorescence spectroscopy analysis of CheY1 (□), CheY1/D53A (◇) and CheY1/T84A (△) upon addition of sodium fluoride **(A)** and acetyl phosphate **(B)** are plotted. Fluorescence changes were plotted as △I/Io against concentration, where △I is the cumulative changes in fluorescence intensity at the corresponding small molecule concentrations; Io is fluorescence intensity without addition of small molecules. **(C)** Pull down study of CheY1 with FliM. Purified $FliM_{NM}$ in 0.1 mg/ml was immobilized on pre-washed resin. CheY1 or D53A mutant in 2:1 molar ratio to $FliM_{NM}$ was incubated with immobilized $HpFliM_{NM}$ with or without BeF_3^- at 25°C for 15 min.

2.3.2 Description of the CheY1 structures

2.3.2.1 Beryllofluoride-bound CheY1

Polygonal-shaped crystal of CheY1-$BeF3^-$ was obtained under condition 0.1 M sodium acetate, pH 5.0, 0.05 M ammonium sulfate (Fig. 2.2). The crystal structure of CheY1-BeF_3^- was solved at a resolution of 2.4 Å, with R=15.14% and R_{free}=22.01%. All the four protein structures were in spacegroup C2, and unit cell parameters and statistics for the data collected are summarized in Table 2. The overall structure retained a $(\beta/\alpha)_5$ fold typical of response regulators. From a *DALI* search (Holm L et al., 2008), CheY1 showed high structural homology to EcCheY/D13K/Y106W (PDB-ID: 1U8T) (Dyer CM et al., 2004) and to BeF_3^--bound EcCheY/F14E/N59M/E89L (PDB-ID: 3F7N) (Pazy Y et al., 2009) with $RMSD_{C\alpha}$ values of 0.776 Å and 0.684 Å, respectively. Alignment of the amino acid sequences of CheY1 proteins from different *H. pylori* strains revealed four variable residues: Asp42 positioned at α2 (Asn in Shi470), Lys66 at α3 (Ile in Shi470), Ser70 at α3 (Ala in P12 / J99 / Shi470) and Ser72 at the α3-β4 loop (Asn in J99 and Glu in Shi470). These residues are located on the distal side of the active site, which may not be directly involved in activation or FliM binding (Fig. 1.10).

Table 2.2. Diffraction data and refinement statistics of CheY1

Parameter	Result for[a]:			
	CheY1	CheY1-BeF_3^-	CheY1-D53A	CheY1-T84A
X-ray data statistics				
Spacegroup	C2	C2	C2	C2
Unit cell				
a, b, c (Å)	70.3, 38.5, 38.9	70.3, 38.4, 38.7	70.3, 38.1, 38.6	70.4, 38.1, 39.0
α, β, γ (Å)	90.0, 107.0, 90.0	90.0, 107.0, 90.0	90.0, 107.4, 90.0	90.0, 107.6, 90.0
Resolution range (Å)	37.2 – 1.8 (1.9 – 1.8)	33.3 – 2.2 (2.28 – 2.2)	36.9 – 2.2 (2.28 – 2.2)	23.08 – 1.7 (1.76 – 1.70)
No. of observations	33,157	20,879	18,875	38,199
No. of unique reflections	9,175	4,888	4,993	10,972
Redundancy	3.6 (3.6)	4.3 (4.4)	3.8 (3.8)	3.5 (3.3)
Completeness (%)	98.1 (96.1)	95.3 (91.8)	98.5 (97.0)	99.9 (100.0)
R_{merge}	0.031 (0.072)	0.019 (0.029)	0.082 (0.240)	0.033 (0.199)
Mean I/σI	30.3 (15.4)	55.1 (39.0)	10.6 (4.5)	14.2 (5.2)
Refinement statistics				
Resolution	37.16 – 1.8	33.46 – 2.4	36.89 – 2.2	23.08 – 1.7
R value	14.67	15.14	17.78	17.35
R_{free} (5% of data)	18.61	22.01	23.11	20.28
No. of atoms refined				
Protein	966	966	963	964
Water/SO_4/Mg/BeF_3	143/2/2/0	60/1/2/1	68/2/1/0	132/2/2/0
RMSD from ideal geometry				
Bond lengths (Å)	0.011	0.013	0.020	0.014
Bond angles (°)	1.37	1.40	1.87	1.42
Ramachandran plot	91.8/7.3/0.9	91.8/7.3/0.9	90.0/8.2/0.9	90.0/8.2/0.9

[a] Values in parentheses are for the last resolution shell. $R_{merge} = (\Sigma h\ \Sigma j|<I(h)>-I(h)j|/\Sigma h\Sigma j<I(h)>)$, where $<I(h)>$ is the mean intensity of symmetry-equivalent reflections. R value $= \Sigma||F_{obs}| - |F_{calc}||/\Sigma|F_{obs}|$, where F_{obs} and F_{calc} are the observed and calculated structure factors, respectively. The distribution of the residues in the most favored / additionally allowed regions of the Ramachandran plot was evaluated by PROCHECK.

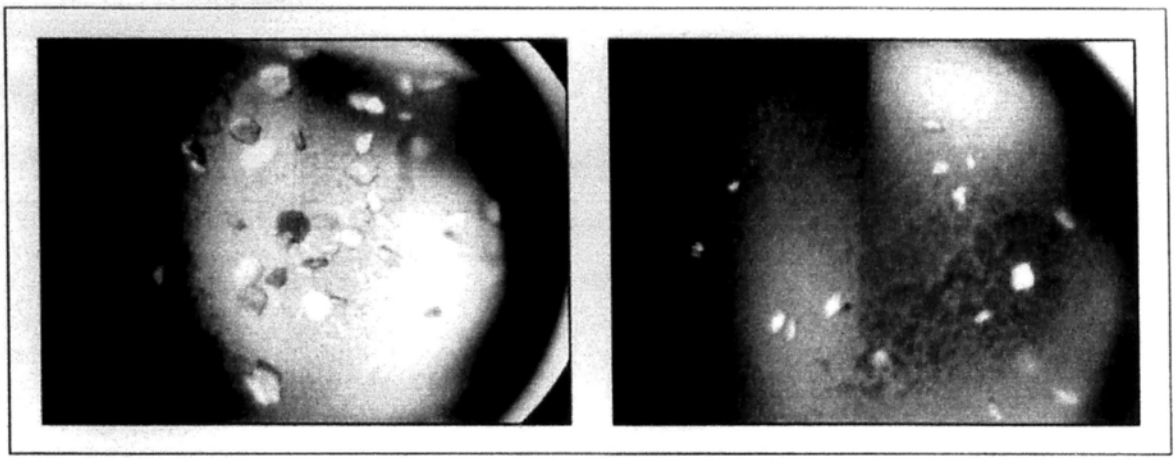

Fig. 2.2. Representative images of beryllofluoride-bound (left) and sulfate-bound (right) CheY1 crystals.

Structural alignment with BeF_3^--EcCheY revealed that the conformation of most of the active site residues and of the hallmark residues for CheY activation, including Thr83 and Tyr106, aligned well when the structures of BeF_3^--CheY1 and BeF_3^--EcCheY were superimposed. This suggests that CheY1 shares a similar activation mechanism (Dyer CM and Dahlquist FW, 2006). On the other hand, a number of structural differences were noted. These differences were clustered at the α2-β3 loop, helix 5 and the C-terminal loop (Fig. 2.3A). The former one corresponded to an insertion of Ala45 in the CheY1 sequence; however, no distortion of the overall protein fold, especially the active site pocket, was observed. Interestingly, helix 5 of CheY1 was five residues shorter and was upshifted by approximately 3.4 Å. The movement of helix 5 may be related to a combination of effects from residues Gly121, which causes an early termination of the helical structure, and Asn123, which is hydrogen bonded to residues in the α1-β2 loop (backbone NH of Asn123 to the backbone carbonyl of Leu23 and Nδ of Asn123 to the backbone carbonyl of Gly24), leaving the C-terminal loop positioned in a rigid

conformation. Gly121 is conserved in most epsilon proteobacteria and in some other proteobacteria (Fig. 1.10). The corresponding Gly126 in the CheY2 structure from *Sinorhizobium meliloti* (PDB-ID: 1P6U) also causes early termination of the helical structure, but the C-terminal loop flips to the other side (Riepl H et al., 2004). Sequence alignment of CheYs showed that the number and types of residues following Gly121 are variable. Residue Asn123 is only conserved in some related bacteria species. We speculate that the helical upshift of CheY1 is a unique feature in *H. pylori* and some closely related species. These structural discrepancies, which could not be predicted from the multiple sequence alignment, in fact provide insights into the molecular interaction with FliM. Analysis of the surface potential of CheY1 and EcCheY clearly demonstrated that although the hydrophobic surface of helix 4 is retained, the electropositive patch contributed by helix 5 for the FliM interaction was much weaker in the CheY1 structure (Fig. 2.4).

A

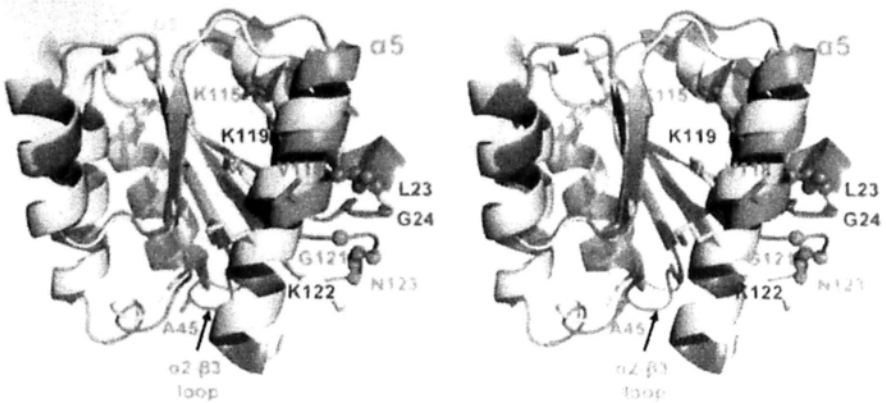
α5
K119
L23
G24
K122
N123
A45
α2 β3
loop

B

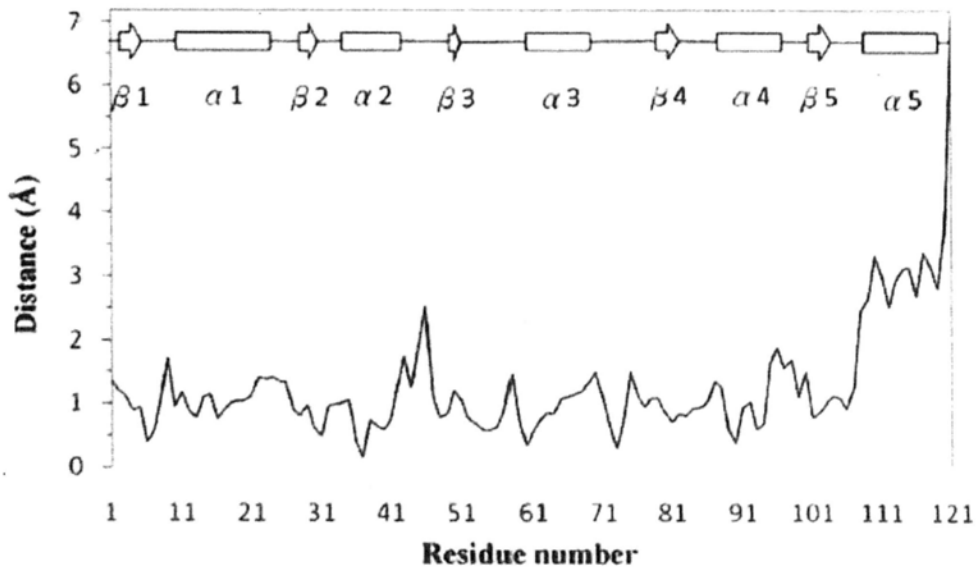
β1 α1 β2 α2 β3 α3 β4 α4 β5 α5
Distance (Å)
0 1 2 3 4 5 6 7
1 11 21 31 41 51 61 71 81 91 101 111 121
Residue number

C

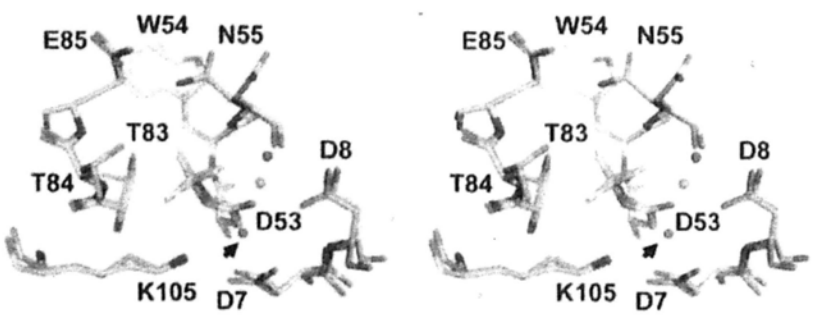
E85
W54
N55
T83
T84
D8
D53
K105
D7

Fig. 2.3. (A) Structural superimposition of BeF_3^--CheY1 (blue) and BeF_3^--EcCheY (white) (PDB-ID: 1FQW) highlights the features of CheY1 α2-β3 loop, α5 and C-terminal loop (orange). Insertion at Ala45 and the major differences in residues involved in $EcFliM_N$ binding (Lys119, Lys122 in EcCheY and Lys115, Val118 in HpCheY1) are shown as stick. Residues contributed to α5 upshift are shown as sphere. Phosphorylation site Asp53 of CheY1 bonded with BeF_3^- is shown as stick. **(B)** Differences in Cα positions between BeF_3^- bound CheY1 and EcCheY. The least square superposition program LSQKAB (CCP4) was used to superimpose CheY1 (residues 1-121) with EcCheY (residues 6 – 125) and to calculate individual Cα distances. Residue 45 of CheY1 was not aligned from the calculation and is not shown on the plot. Residues are numbered according to CheY1 sequence. Secondary structure is shown above the plot. **(C)** Stereo superimposition images of BeF_3^--CheY1 (pink) and EcCheY (yellow) on the basis of structural alignment using Pymol. Residues in the active site pocket are labeled. Metal ions (Mg^{2+} in HpCheY1) and two water molecules (red sphere) (from BeF_3^--CheY1) involved in coordinating the metal ion (pink sphere) are shown. Arrow indicates the water molecule coordinated by Asp7.

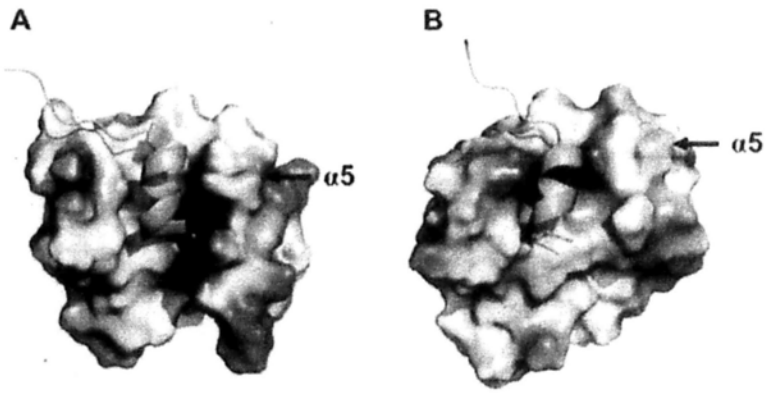

Fig. 2.4. Comparison of FliM binding surface of EcCheY (A) and CheY1 (B). *H. pylori* FliM N-terminal peptide (residues 1-15, orange cartoon) was modeled using EcFliM peptide (green cartoon) as template (Modeller). Molecular surface is drawn as electrostatic potential calculated by APBS at contour level ±3 kT/e. Position of Helix 5 is indicated. Colour code: Blue, electropositive surface; Red, electronegative surface; White, electroneutral surface.

2.3.2.2 Sulfate-bound CheY1

We also attempted to solve the structure of apo-CheY1. To our surprise, a tetrahedral-shaped positive electron density was observed in the active site pocket during model building (Fig. 2.5A). The electron density shown in the active site pocket of the 1.8-Å 'apo-CheY1' structure was interpreted as a sulfate ion because of the addition of 200 mM ammonium sulfate in the crystallization medium. The structure of the CheY1/D53A mutant was also solved to a resolution of 2.2 Å. Interestingly, the sulfate moiety was still found in the active site pocket of CheY1/D53A. The overall structures of sulfate-bound CheY1 and CheY1/D53A were almost identical to the CheY1- BeF_3^- structure, with $RMSD_{C\alpha}$ values of 0.147 Å and 0.199 Å, respectively, suggesting that sulfate-bound CheY1 may represent an activated form. We investigated whether the non-phosphorylatable D53A analog of CheY1 is "activated" by high concentration of ammonium sulfate. We evidenced that sulfate bound CheY1/D53A *in vitro* as tryptophan fluorescence intensity of CheY1/D53A decreased by 30% upon titration with ammonium sulfate. The titration was saturated when the concentration of ammonium sulfate reached around 360 mM, with calculated K_m = 176 ± 21 mM. To further investigate whether sulfate enhanced D53A mutant to interact with $FliM_{NM}$, *in vitro* pull down assay was performed in the presence of 200 mM ammonium sulfate (without KCl). CheY1/D53A showed enhanced binding to $FliM_{NM}$ in the presence of ammonium sulfate (Fig. 2.6), but not in BeF_3^- (Figure 2.1C), agreed with the structural information of SO_4^{2-}-bound CheY1/D53A in an activated configuration. It is noted that the interaction may not be physiological relevance given the high concentration of ammonium sulfate. We attempted to screen for inactive CheY1 in crystallization conditions without ammonium sulfate. However, no crystal was observed.

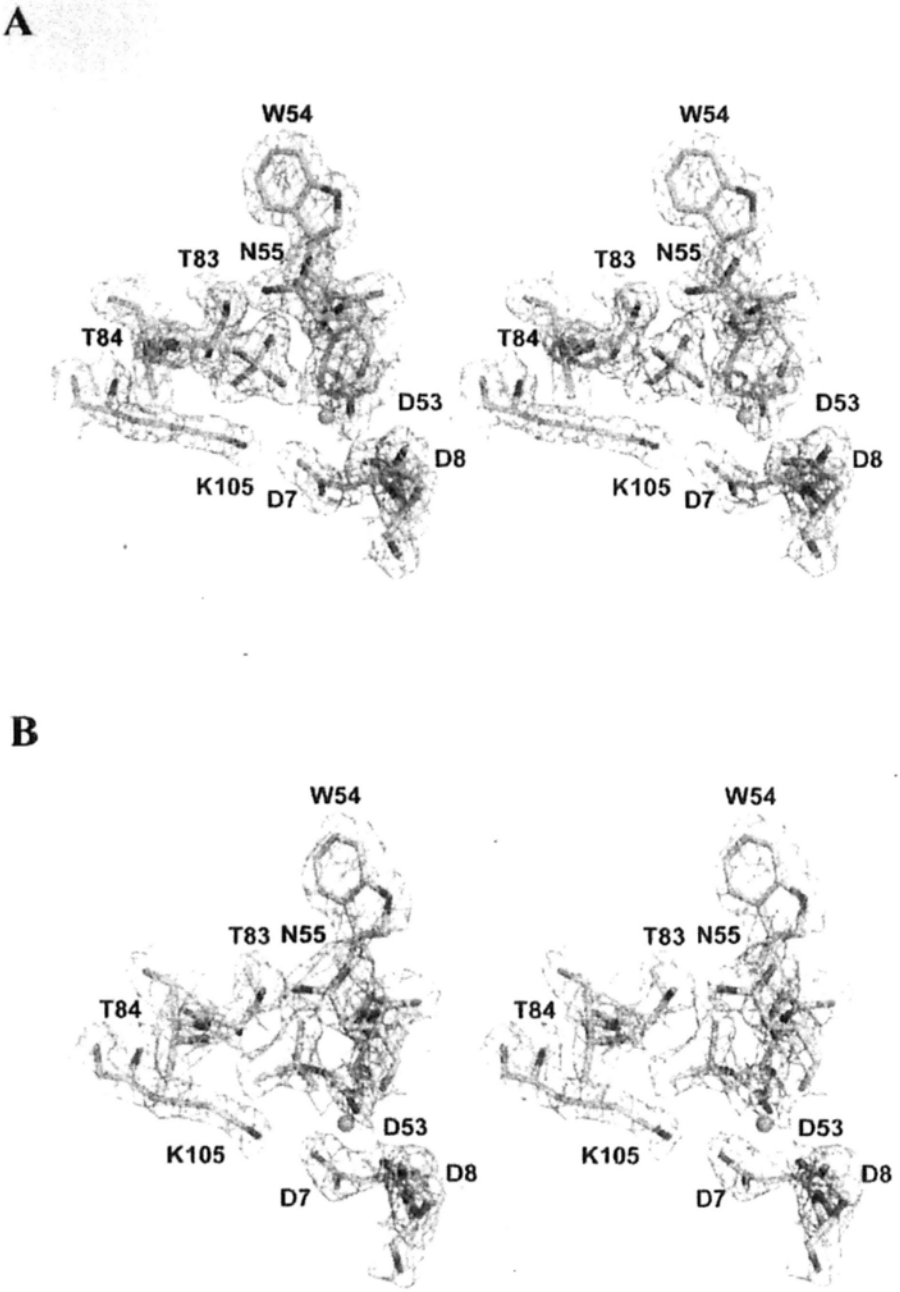

Fig. 2.5. Stereo view of the active site of CheY1. The 2Fo-Fc electron density around SO_4^{2-} **(A)** and BeF_3^- **(B)** moieties contoured at 1.0 σ is represented. Active site residues are labeled and shown as stick. Mg^{2+} is shown as sphere.

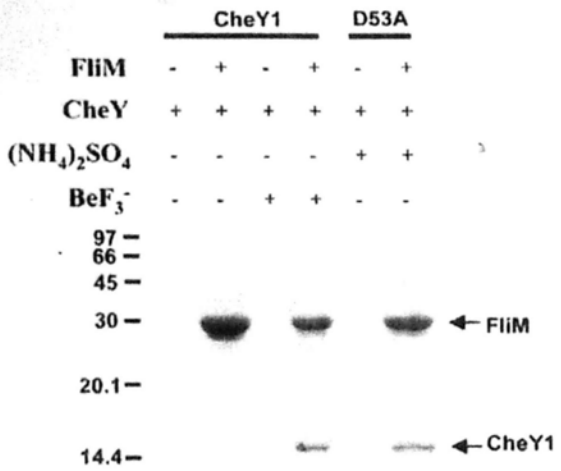

Fig. 2.6. Interaction studies of FliM with CheY1 in the presence of ammonium sulfate. The experiment was conducted as described in 2.2.2.1, except that 200 mM ammonium sulfate was included in the reaction to replace BeF_3.

A sulfate molecule positioned close to the active site pocket has been reported in the crystal structure of apo-EcCheY (PDB-ID: 3CHY), in which the SO_4^{2-} was hydrogen bonded with Lys109 Nε and Asn59 Nδ (in the *E. coli* sequence) (Volz K and P Matsumura, 1991). The position is different in SO_4^{2-}-bound CheY1 which showed that the hydrogen bond networking of SO_4^{2-} with the active site residues in CheY1 was comparable to that found in BeF_3^--CheY1. An 'inward' orientation of the side chain of Asp53, in which the side chain is flipped toward the protein core, was noted in SO_4^{2-}-bound CheY1 (Fig. 2.5). Such rearrangement is very likely induced by the charge-charge repulsion upon sulfate binding. The flipping of Asp53 is stabilized by hydrogen bond formation with its own peptide NH (2.85 Å), peptide NH of Trp54 (3.47 Å), peptide NH of Asp8 (3.41 Å) and Mg^{2+} (2.44 Å).

2.3.3 T84A mutant affect CheY1 phosphorylation

The active site residues of CheY1 aligned well with those in EcCheY, except for the flipping of the Asn55 side chain and the substitution of Thr84 with an alanine in the EcCheY sequence (equivalent to Ala88 in EcCheY). The side chain of the conserved Asn55 in CheY1 was flipped to an alternative conformation and was hydrogen bonded with the carboxylate Oε of Glu85 (2.9 Å). The coupling of Asn55 and Glu85 has been implicated in controlling autodephosphorylation (Thomas SA et al., 2008). Sequence alignment of CheYs showed that Thr84 is conserved within strains of *H. pylori* and in several species of epsilon proteobacteria (Fig. 1.10). Thr84 Oγ in the β4/α4 loop is hydrogen bonded with BeF_3^- (3.50 Å), which may affect the phosphotransfer reaction. The role of Thr84 in CheY1 phosphorylation was investigated by introducing a Thr-to-Ala mutation. Phosphorylation of CheY1 and T84A mutant by acetyl phosphate was measured by equilibrium titration (up to 10 mM). The T84A mutant had an approximately 4–5-fold (0.22 ± 0.055 mM) lower K_m value compared with that of the wild type (1.07 ± 0.31 mM) (Fig. 2.1B). The K_m value of EcCheY is 3.2 ± 0.4 mM (Silversmith RE et al., 1997). The lower *Km* value for CheY1 may be due to the differences in ionic strength in the experiment performed (200 mM buffer salt used in the previous experiment, compared to 50 mM used in our experiment).

2.3.4 CheY1 does not complement *E. coli cheY* mutant but restore swarming of *cheZ* mutant

Although CheY1 and EcCheY share high sequence identity and structural homology, we have noted a major discrepancy at the FliM binding surface. The CheY1

structure differs from the EcCheY structure because of the upshift and shortening of helix 5 (Fig. 2.3A). We hypothesized that this structural difference would lead to a different CheY-FliM interaction in *H. pylori*. We examined the biological function of wild-type and mutant CheY1 in *E. coli* using a swarming assay. Bacterial swarming ability was assessed by transforming pTrc99a vectors encoding CheY1 and CheY1/D53A into wild-type *E. coli* (RP437) and into *cheY*- (RP5232) and *cheZ*- (RP1616) null mutants (Fig. 2.7). A control experiment using the empty pTrc99a vector was also conducted. Our results showed that expression of CheY1 did not restore swarming of the *cheY*-null *E. coli* mutant. On the other hand, CheY1 inhibited swarming of wild-type *E. coli* in an IPTG concentration-dependent manner, suggesting that CheY1 associates with the *E. coli* chemotaxis system. Surprisingly, the expression of the CheY1/D53A mutant, a non-phosphorylatable mutant, inhibited *E. coli* swarming but did not affect cell growth. This result contradicts earlier study that the expression of the wild-type CheY homolog from *A. brasilense* but not the active site mutant inhibited the swarming of *E. coli* (Alexandre G and Zhulin IB, 2003). Our data suggest that CheY1/D53A may interact with the chemotactic system of *E. coli*. Interestingly, CheY1, but not CheY1/D53A, partially restored the swarming ability of the *cheZ*-null mutant (Fig. 2.7A, B).

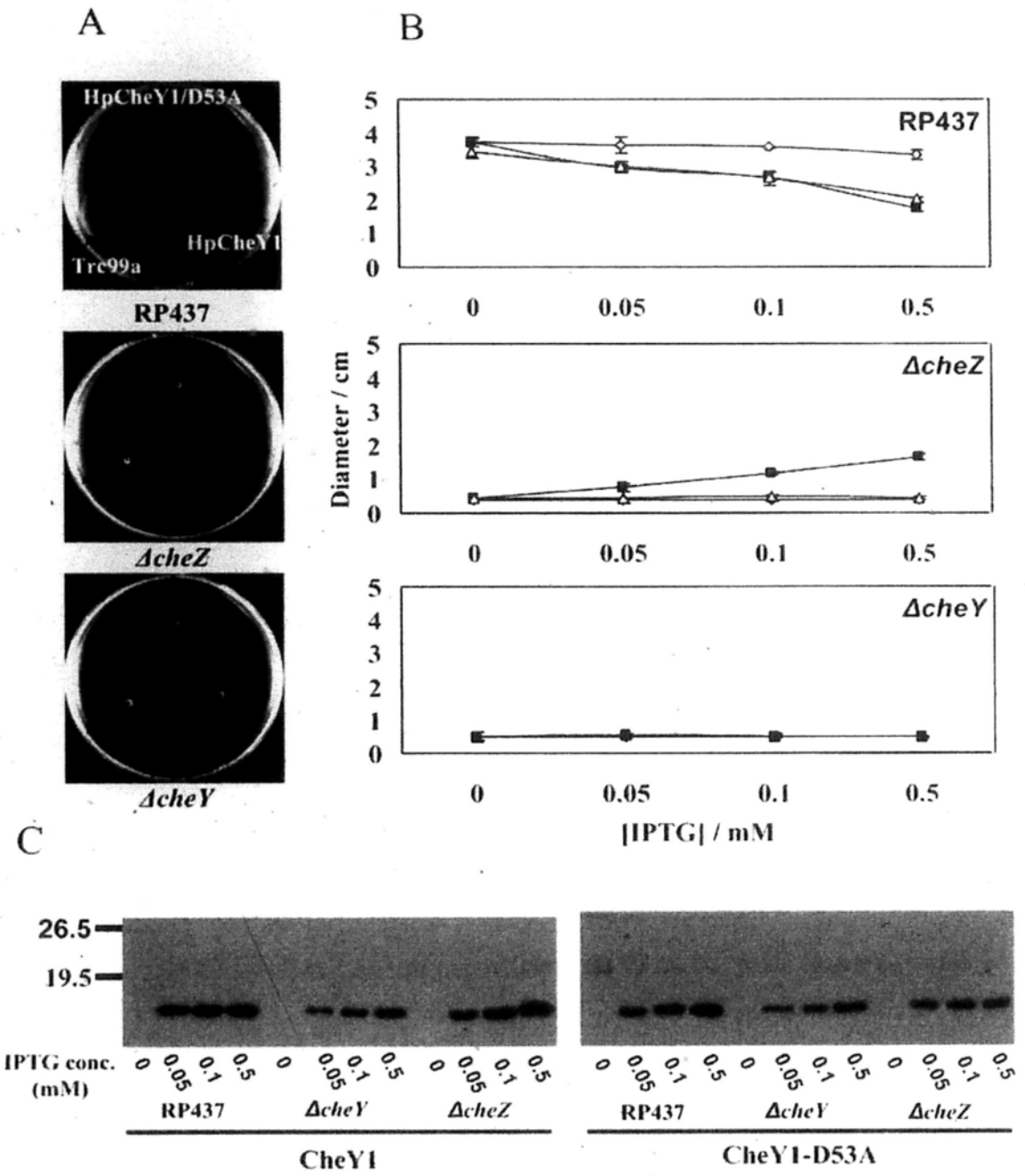

Fig. 2.7. Swarming motility assay of heterologous expression of CheY1 and CheY1-D53A in *E. coli* wild type (RP437), *cheZ* (RP1616) and *cheY* (RP5232) null mutants. Overnight culture of cells carrying plasmids were inoculated onto TB -0.4% semisolid agar plates that were incubated at 30°C for 7 hrs. **(A)** Representative images of the swarming rings produced from the expression of pTrc99a (control), CheY1 or CheY1/D53A in 0.5 mM IPTG are shown. **(B)** Mean diameters of the rings are plotted against IPTG concentrations. The experiment was replicated for 3 times. ◇, pTrc99a; ■,

HpCheY1; Δ, HpCheY1-D53A. **(C)** Protein expression levels of CheYs in *E. coli* wild type and mutant strains were probed by anti-CheY1 antibody.

2.3.5 CheA-P2 preferentially interacts with CheY1

Chemotactic pathway of *H. pylori* is featured with the presence of a CheY-like domain fused to CheA (CheAY2) and three CheV proteins. An *in vitro* experiment showed that CheA displayed a higher preference for CheY1 than CheY2, but had the lowest preference for CheVs (Jiménez-Pearson MA et al., 2005). The P2 domain in CheA consists of a docking site for response regulators and serves to increase the rate of phosphotransfer by concentrating CheY near P1 (Jahreis K et al., 2004). We suspected that the binding affinities of response regulators for CheA-P2 would contribute to the differential rate of phosphotransfer in *H. pylori*. Interaction of CheA-P2 with CheY and CheVs proteins was investigated by a pull-down experiment and by gel filtration analysis. Recombinant CheA-P2-His_8, CheY1, CheY2, CheV1, CheV2 and CheV3 were purified to greater than 95% purity. CheA-P2 was immobilized on Ni-NTA resin, followed by incubation with CheYs or CheVs. As shown in Figure 2.8A, only CheY1 was shown to interact with CheA-P2, suggesting that CheY1 is the sole interacting partner of CheA-P2. The interaction between CheY1 and CheA-P2 was further investigated by gel filtration analysis. CheA-P2 and CheY1 were eluted at 14.57 ml and 16.05 ml, respectively, when run individually. When the two proteins were mixed and then subjected to the gel filtration analysis, the elution profile was shifted to 12.89 ml. Complex formation was further verified by SDS-PAGE analysis (Fig. 2.8B). Our results suggest that CheY1 formed a stable complex with CheA-P2. When the experiment was repeated with CheV3 and CheA-P2, the elution profile of the CheV3/CheA-P2 mixture did not change as compared to the elution profiles of the individual proteins (Fig. 2.9A).

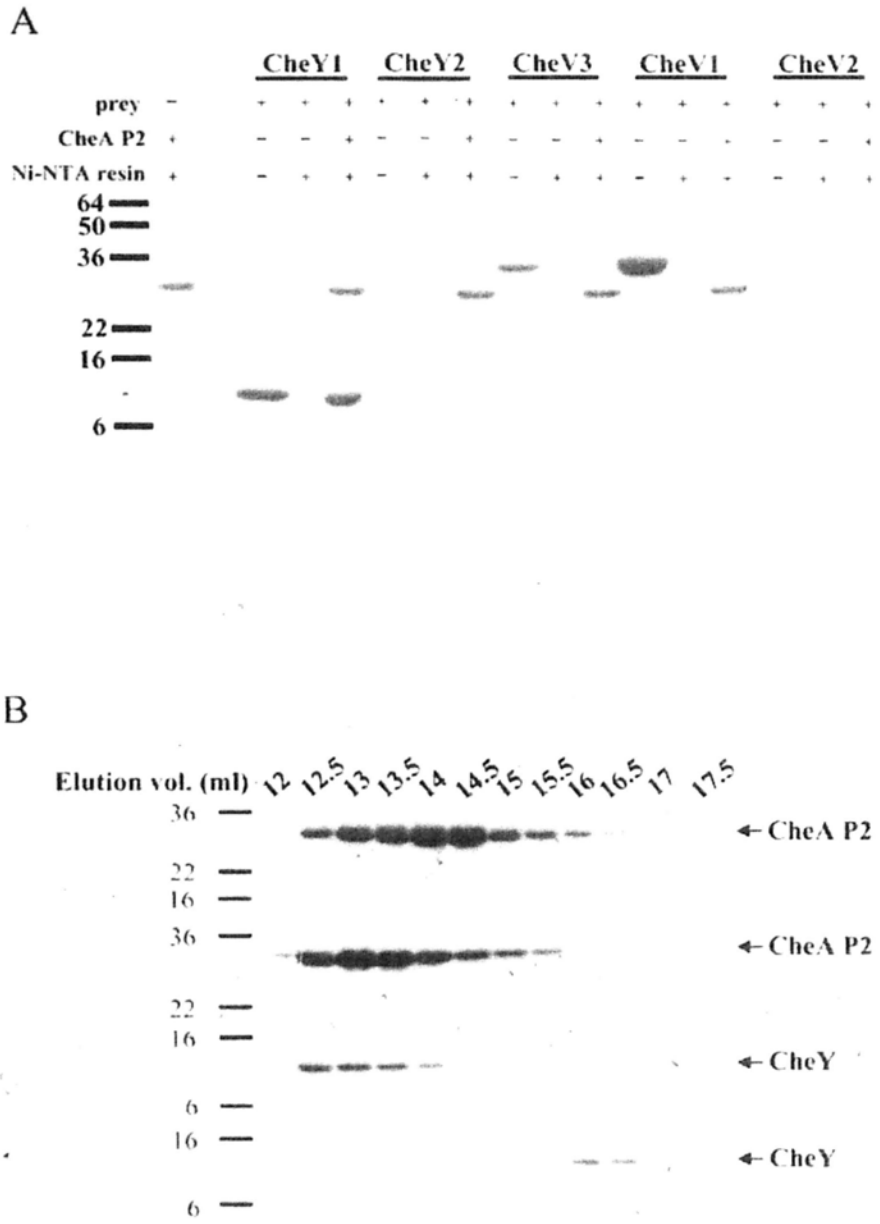

Fig. 2.8. Interaction study of CheA-P2 and CheYs/CheVs. **(A)** Purified CheA-P2 in 0.1 mg/ml was immobilized. Response regulators in 1:1 molar ratio to CheA-P2 were then added and incubated at 4°C for 1 h. After washing, the beads were boiled at 90°C and loaded onto SDS-PAGE. **(B)** Elution profiles of CheY1 (lower panel), P2 (upper panel), CheY1-P2 complex (middle) separated by 10/30 Superdex 200 size exclusion chromatography. The elution volume is indicated above the graph. The elution volume of P2, CheY1 and CheY1-P2 complex are 14.57 ml, 16.05 ml and 12.89 ml respectively.

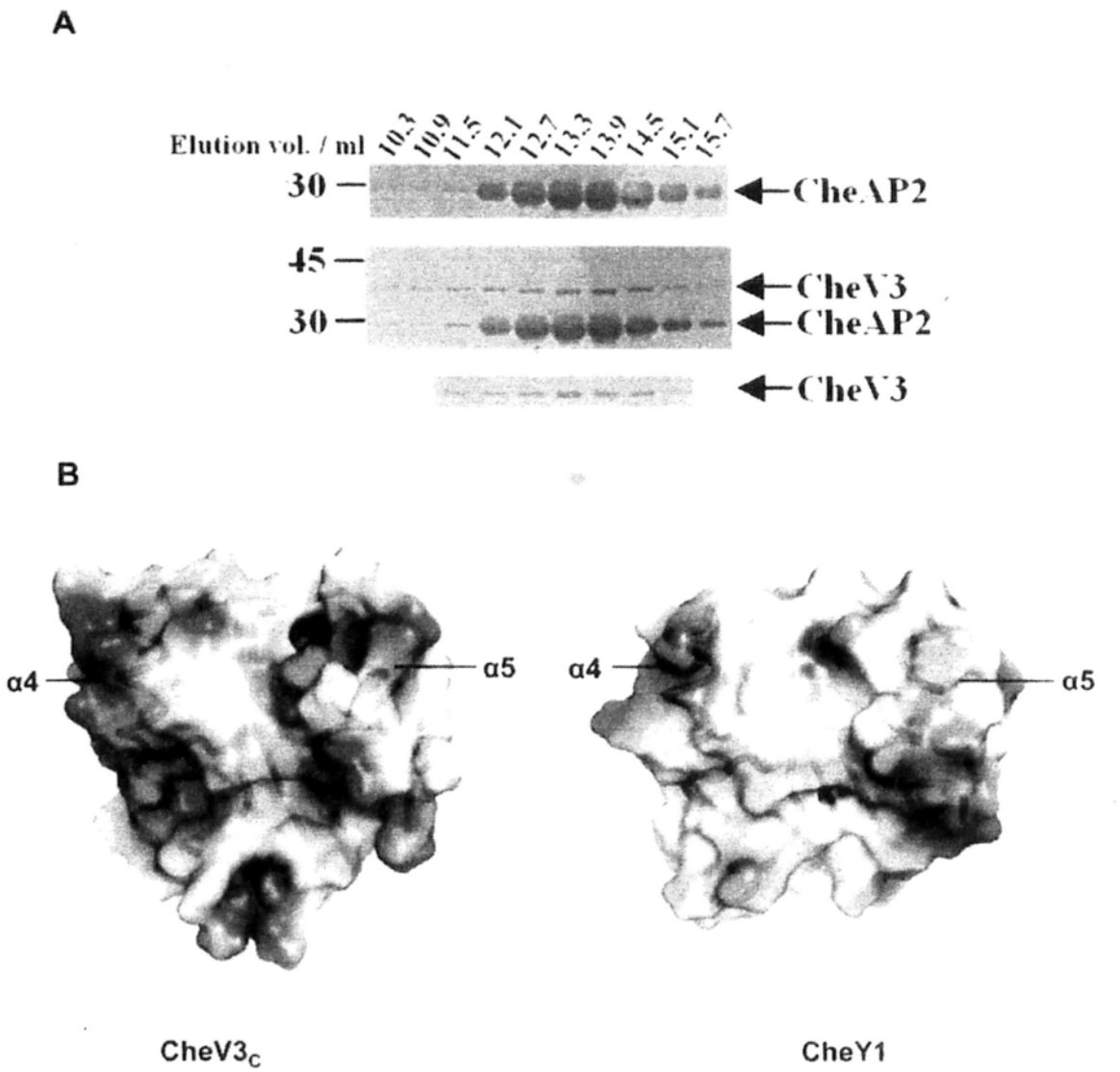

Fig. 2.9. CheV3-CheAP2 interaction. (A) Elution profiles of CheAP2 (upper panel), CheV3 (lower panel), and CheV3-CheAP2 complex (middle) separated by 10/30 Superdex 200 size exclusion chromatography. The elution volume is indicated above the graph. **(B)** Electrostatic surface representation with contour level ± 3 kT/e showing the α4/β5/α5 surface of modeled CheV3 C-terminal domain ($CheV3_C$) and CheY1 (Modeller). Coloring scheme: Blue, electropositive surface; Red, electronegative surface; White, electroneutral surface.

2.4 Discussion

Here the crystal structure of activated CheY1 from *H. pylori* is reported. The activated form of CheY1 by beryllofluoride was verified by fluorescence quenching experiment and pull down assay with $FliM_{NM}$. CheY1 shares high structural homology with EcCheY, but distinctive features were observed at the active site pocket and the motor binding surface. We noted that residue Thr84 is important to CheY1 phosphorylation. Besides, we found that CheY1 cannot complement the biological function of *cheY* mutant but can restore the chemotactic behavior of *cheZ* mutant. CheY1 also preferably interacts with CheA-P2 domain.

The T84A mutant decreased the *Km* value of acetyl phosphate binding by 4 – 5 fold compared with the wild-type, suggesting Thr84 is important to phosphorylation of CheY1 in *H. pylori* and related species. The K_m value is derived from the binding constant and rate constant ($Km=Ks \cdot k_3 / k_2$). A lower K_m value could be due to an increase in the binding affinity between CheY and the phosphodonor (smaller K_s), a faster rate of phosphorylation of bound CheY (larger k_2) or a slower rate of autodephosphorylation (smaller k_3) (Silversmith RE et al., 1997). It has been reported that Ala88 in EcCheY cannot be substituted with amino acid residues with long side chains (Smith JG et al., 2003). Multiple sequence alignment from various response regulators showed that Thr84 is most frequently replaced by small residues, including Ser, Ala and Gly, and more rarely by hydrophobic Val and Ile (Thomas SA et al., 2008). The structure of CheY1/T84A with SO_4^{2-} bound was almost identical to the wild-type ($RMSD_{C\alpha}$ = 0.1 Å), suggesting that the mutation would have no effect on backbone orientation. No significant difference around the active site pocket was observed when comparing the

surface electrostatic potential of wild-type CheY1 and the T84A mutant. A more electronegative surface was observed in the T84A mutant due to the exposed negative charge of Oγ of Thr83 (Fig. 2.10). Future study of the T84V mutant would provide insight into the role of the hydroxyl group in phosphorylation.

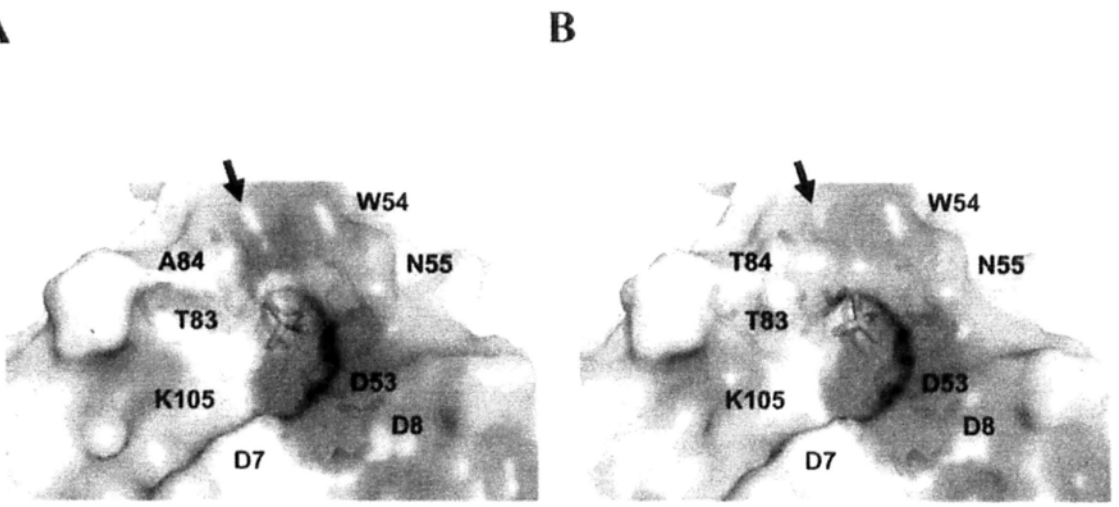

Fig. 2.10. Electrostatic surface representation with contour level ± 5 kT/e showing the active site pocket of SO_4^{2-}-bound CheY1/T84A (A) and SO_4^{2-}-bound CheY1 (B). The position of SO_4^{2-} is shown as stick. Active site residues are labeled. Arrow indicates the difference on the electrostatic surface between the two structures (see text). Electrostatic surface were calculated using software APBS (Baker NA et al., 2001). Ligands were not included in the calculation.

In our study, CheY1, but not CheY1/D53A, restored the swarming ability of the *cheZ*-null mutant. Heterologous expression of CheY homologs from *R. sphaeroides* partially restored *cheZ*-null mutant swarming, suggesting that CheY, with no motor binding affinity, competes with EcCheY for phosphate (Shah DS et al., 2000).It is possible that phosphorylation ability is necessary to bring the run-to-tumble ratio of the

cheZ-null mutant close to that of the wild type. Wild-type CheY1, but not the D53A mutant, was able to receive a phosphate from EcCheA to modulate the concentration of EcCheY-P, therefore controlling the run-to-tumble ratio. Similar effects have also been observed in heterologous gene expression experiments using CheV2 and CheV3 (Pittman MS et al., 2001). CheY1 failed to restore swarming of the *cheY*-null mutant, suggesting that CheY1 does not interact with EcFliM even though CheY1 can be phosphorylated by EcCheA.

Sequence alignment between CheY1 and EcCheY suggested that the hydrophobic residues in α4 and β5 that are involved in $FliM_{NM}$ binding are either identical in the two proteins or are replaced by residues with similar amino acid properties (Fig. 1.10). However, salt bridge formation between the residues in helix 5 and the EcFliM peptide was disrupted (between the Asp12 Oδ of EcFliM-Lys119 and Nζ of EcCheY and between the Asn16 carboxylate of EcFliM-Lys122 and Nζ of EcCheY) (Lee SY et al., 2001). Although Lys119 of EcCheY is conserved in CheY1 (Lys115), the upshift of helix 5 caused displacement of Lys by a distance of approximately 4.4 Å (the distance between the Cα atom of Lys 115 in CheY and that of the equivalent Cα in EcCheY). Additionally, it was noted that the FliM-interacting α4/β5/α5 surface is more hydrophobic in CheY1. Specifically, the corresponding position of Lys122 in EcCheY is occupied by Val118 in CheY1 (Fig. 2.3A). Results of pull down experiment from us and from Lowenthal AC et al., (Lowenthal AC et al., 2009) showed that CheY1-FliM interaction could be detected only if the concentration of KCl in the binding buffer was higher than 250 mM, while EcCheY-EcFliM interaction was detected with no NaCl / KCl added (Wadhams GH and Armitage JP, 2004). We speculated that the CheY1-FliM interaction would involve

more extensive hydrophobic interactions. Sequence alignment of *H. pylori* FliM and EcFliM revealed that the N-terminal fragments responsible for the interactions with CheY differ by four residues (G2A, S4-*del*, A9E and N16E). It is likely that the CheY-FliM interaction in *H. pylori* would be different from that in *E. coli*.

CheY1 but not other response regulators bind to CheA-P2 in pull down experiment. We attempted to identify the surface of CheA-P2 that interacts with CheVs by homology modeling using Modeller (Sali A and Blundell TL, 2003). CheV3 was chosen as the representative of CheV because it shares the highest sequence identity with CheY1. The P2 interaction patch on the α4/β5/α5 surface of CheV3 was found to be more electronegative when compared with those of EcCheY and CheY1 (Fig. 2.9B). The high binding affinity of CheY1 for CheA-P2 observed in the present study is consistent with previous results showing that CheA has a greater phosphotransfer efficiency to CheY1 (Jiménez-Pearson MA et al., 2005). Our data further suggest that the differential phosphotransfer efficiency is regulated by the interaction between the CheY/CheV proteins and the CheA-P2 domain. The P2 domain stands out because of its low sequence conservation among other regions of CheA, and CheA-P2 only shares 15% sequence identity with EcCheA-P2. In fact, the regulation would be complicated in CheV proteins, as the N-terminal CheW-like domain may interact with the P5 regulatory domain of CheA and affect the phosphotransfer activity. How this interaction affects the phosphotransfer reaction remains unclear. Structure determination studies of other CheY-like domains and of their complexes with CheA would help to unravel the complex regulatory mechanisms underlying the chemotactic network in *H. pylori*.

Chapter 3

Structure determination of $FliM_M$ and characterization of FliM-FliG interaction

3.1 Introduction

FliM is a switch protein for rotational switching. Upon CheY-binding at the N-terminus of FliM ($FliM_N$), the activation signal is transmitted to the middle domain ($FliM_M$) on which FliG directly binds. The C-terminal domain of FliM ($FliM_C$) provides the docking site for the assembly of FliN ring. $FliM_C$ is also important for switching as $FliM_C$ and FliN undergo conformational change during the event. Recent study has demonstrated that deletion of FliM showed non-flagellate phenotype. FliM is able to bind CheY-P and a CW-bias mutant has been isolated on residue R54 of FliM (Lowenhal AC et al., 2009). These observations suggested that the function of FliM in *H. pylori* in motor switching is similar to other bacteria. On the other hand, aherence of *H. pylori* to gastric epithelial cells is reduced in fliM mutant suggesting this gene is crucial in gastric infection (Zhang ZW et al., 2002).

To give a further detailed understanding about the structure and function of FliM in *H. pylori*, we have solved the structure of FliM from *H. pylori* and studied its interaction with FliG. Mutagenesis study was also conducted to map the FliM-FliG binding interface. Structural comparison with FliM from *T. maritima* revealed variations on the secondary structure and conformational differences on FliG binding surface.

3.2 Materials and methods

3.2.1 Cloning, expression and purification

FliM (HP1031) middle domain ($FliM_M$, residues 43 – 237) and FliG (HP0352) were cloned into pGEX-6p-1 and pET28m-his_6-sumo1 vectors, respectively. Cloning and mutagenesis ($FliM_{139}YDQ_{141}$/AAA, K136A and K136D in pGEX-6p-1) studies were conducted according to previously described procedures (Section 2.2.1, Table 3.1). Protein expression and purification procedures were performed as described (Section 2.2.1), except that His_6-sumo1 tag of FliG was not removed for pull down experiment. Instead, the protein was eluted with 150 mM Imidazole in Ni-NTA chromatography. Buffer conditions are summarized in Appendix 3.1.

Table 3.1. Primers used for the cloning of FliM and mutants.

Primer Name	Primer Sequence (5' – 3')	Restriction Site
$FliM_M$ – F	catatg**ggatcc**atgaaacgccctaatcgtgtgagtaaggagc	BamHI
$FliM_M$ – R	catatg**gtcgac**tcaaagcatcaaatccctactccccatttt	SalI
FliG – F	gggggg**ggatcc**atggcaaccaagcttacccccc	BamHI
FliG – R	gggggg**gtcgac**ctattcaatgacatcttcctcttcaccg	SalI
$FliM_{K136A}$-F	gattgacagactattaggggtgcggggagcgcgta	
$FliM_{K136A}$-R	tacgcgctccccgcacccctaatagtctgtcaatc	
$FliM_{K136D}$-F	gattgacagactattaggggtgatgggagcgcgtatg	
$FliM_{K136D}$-R	catacgcgctcccatcacccctaatagtctgtcaatc	
$FliM_{YDQ}$-F	ctattagggggtaaggggagcgcggctgctgcaaacagggagtttagcgatattga	
$FliM_{YDQ}$-R	tcaatatcgctaaactccctgtttgcagcagccgcgctcccctaccccctaatag	

3.2.2 Nickel pull down experiment

30 µl nickel-NTA resin was pre-equilibrated with binding buffer 150 mM NaCl, 20 mM Tris pH 7.0, 20 mM imidazole, 2 mM β-mercaptoethanol and subsequently immobilized with His_6-sumo1-FliG by incubation at 4° for 1 hr. $FliM_M$ or $FliM_M$ mutants were added to FliG-bounded beads (molar ratio $FliM_M$: FliG = 2 : 1) and incubated at 4°C for 1 h. After washing with binding buffer for 3 times, the beads were boiled with loading dye at 99°C for 5 min and loaded to SDS-PAGE for analysis.

3.2.3 Size exclusion column chromatography

Purified FliG and $FliM_M$ in a molar of ratio 1 : 1.5 were incubated on ice for 30 mins. FliG-$FliM_M$ complex was analyzed by size exclusion chromatography Superdex 200 column.

3.2.4 Crystallization conditions of $FliM_M$

Crystallization screening was performed as described in section 2.1.7. Diffraction quality crystals of $FliM_M$ were obtained from optimized condition (0.2 M Ammonium sulfate, 0.1M HEPES pH7.5, 25% PEG3350, 20 mM sodium bromide) at 16°C using sitting drop method.

3.2.5 Data collection and processing

A 2.2 Å X-ray data set for $FliM_M$ crystal was collected using in-house X-ray generator. Crystallization buffer with the addition of 20% glycerol was used as cryoprotectant. Data was processed, scaled and reduced as described (Section 2.1.8)

3.2.6 Structure determination and refinement

Initial phase determination was solved by molecular replacement using FliM middle domain from *T. maritima* ($TmFliM_M$) as search model (PDB-ID: 2HP7). Structure refinement was performed as described in Section 2.1.9. Ramachantran plot drawn by PROCHECK showed that 94.3% of all residues fall within favored regions and the remaining 5.7% within additional allowed regions (Appendix 3.2). Orientations of Asn, Gln and His side chain were optimized by MolProbity (Chen VB et al., 2010).

3.3 Results

3.3.1 Description of $FliM_M$ structure

In order to study the structure of FliM, we initially attempted to overexpress full length FliM in *E. coli*. However, over 90% of the recombinant protein was expressed in insoluble fraction (data not shown). We designed truncations of FliM based on sequence alignment and structural information of $TmFliM_M$. Only $FliM_M$ (residues 43 – 237) was stably expressed and purified in considerable yield for crystallization screening. $FliM_{NM}$ (residues 1 – 237) was also successfully purified, however, the N-terminal fragment was not stable and degradation was observed upon storage. Similarly, in $TmFliM_{NM}$, the removal of N-terminal 43 residues is required for crystal growth (Park SY et al., 2006). Hence, the fragment was not considered for crystallization trial.

Rod shaped crystals of $FliM_M$ was obtained under condition 0.2 M ammonium sulfate, 0.1M HEPES pH7.5, 25% PEG3350 with additive 20 mM sodium bromide (Fig. 3.1). A diffraction data with highest resolution 2.2 Å was collected. The crystal belonged to primitive hexagonal space group, with unit-cell parameters a = b = 91.27, c = 57.09 Å. Cell content analysis indicates the presence of 3 molecules per asymmetric unit based on calculated molecular weight 22.3 kDa, corresponding to a Matthews coefficient V_M of 2.05 $Å^3Da^{-1}$ and a solvent content 39.94% (CCP4i). The structure was solved by molecular replacement using $TmFliM_M$ (Park SY et al., 2006) as a search model and was refined to R = 20.28% and R-free = 26.33% (Table 3.2). Refinement statistics were summarized in Table 3.2. The three $FliM_M$ molecules within the asymmetric unit are almost identical to each other ($RMSD_{C\alpha}$ between chains A - B and A - C are 0.274 and 0.244 Å, respectively) (Pymol). Electron density of residues 43 – 47, 135 – 143, 231 –

237 were missing in chain B and chain C. These fragments are possibly flexible. Residues 135 – 143 can only be observed from electron in chain A (Fig. 3.2). The following discussion will be mainly based on structure of chain A that contains most detailed structural information, unless specified (Fig. 3.2C).

Table 3.2. Refinement statistics for the structure of $FliM_M$

Diffraction data statistics	
Spacegroup	P31
Unit cell dimensions (Å)	91.27 91.27 57.09 90.00 90.00 120.00
Resolution range (Å)	35.64 – 2.2 (2.28 – 2.20)
No. of molecules per asymmetric unit	3
Matthews coefficient (VM; $Å^3Da^{-1}$)	2.05
Solvent content (%)	39.94
Number of observations	95893
Number of unique reflections	26487
Average redundancy	3.62 (3.59)
Completeness (%)	98.2 (97.3)
R_{merge}	0.064 (0.296)
Mean I/σI	12.3 (4.0)
Refinement statistics	
Resolution	79.06-2.20
R-value / R_{free} (5% of data)	20.28 / 26.33
Rmsd - bond lengths (Å)	0.022
- bond angles (°)	1.857

Fig. 3.1. Representative image of $FliM_M$ crystals

From structural homology search by DALI, $TmFliM_M$ and CheC from *T. maritima* (PDB-ID: 2f9z, chain A) (TmCheC) show the highest similarity to $FliM_M$ with Z score 26.9 and 19.1, respectively. As previously noted, $FliM_M$ structures shared the same topology with phosphatase CheC with six anti-parallel β-sheets forming the core of the protein (in the arrangement β1-β2'β3'-β3-β2-β1') and six helices wrapping around the β-stranded core. The secondary structure elements of $FliM_M$ are arranged as two αβαββα repeats related by pseudo-two fold symmetry (Park SY et al., 2004, 2006) (Fig 3.2) with α3 – α1' loop connecting these two repeats (Fig. 3.2B).

Comparing the structures of $FliM_M$ and $TmFliM_M$, the α helix and β-sheet are well aligned except β3 is lengthened by 3 residues and α2' is replaced by loop in $FliM_M$ (Fig. 3.3). The secondary structure of the corresponding α2' region in $TmFliM_M$ is a 3_{10} helix (STRIDE, Frishman D & Argos P, 1995). In $TmFliM_M$ structure, 4 residues close to the well conserved GGXG motif, is missing from the electron density ($_{135}$G-P_{138} in $TmFliM_M$) map, these residues can only be reviewed from chain A ($_{135}$G - N_{143} in $FliM_M$) suggesting this region is likely flexible. TmCheC contains two well conserved EXXN motif in α1 and α1' of both active sites participated in the dephosphorylation of CheY (Park SY et al., 2004). Despite $FliM_M$ and CheC share similar fold, this motif is not identified in $FliM_M$ structure. A different set of residues was found to be conserved in α1 of $FliM_M$ but not in α1' (Fig. 3.3).

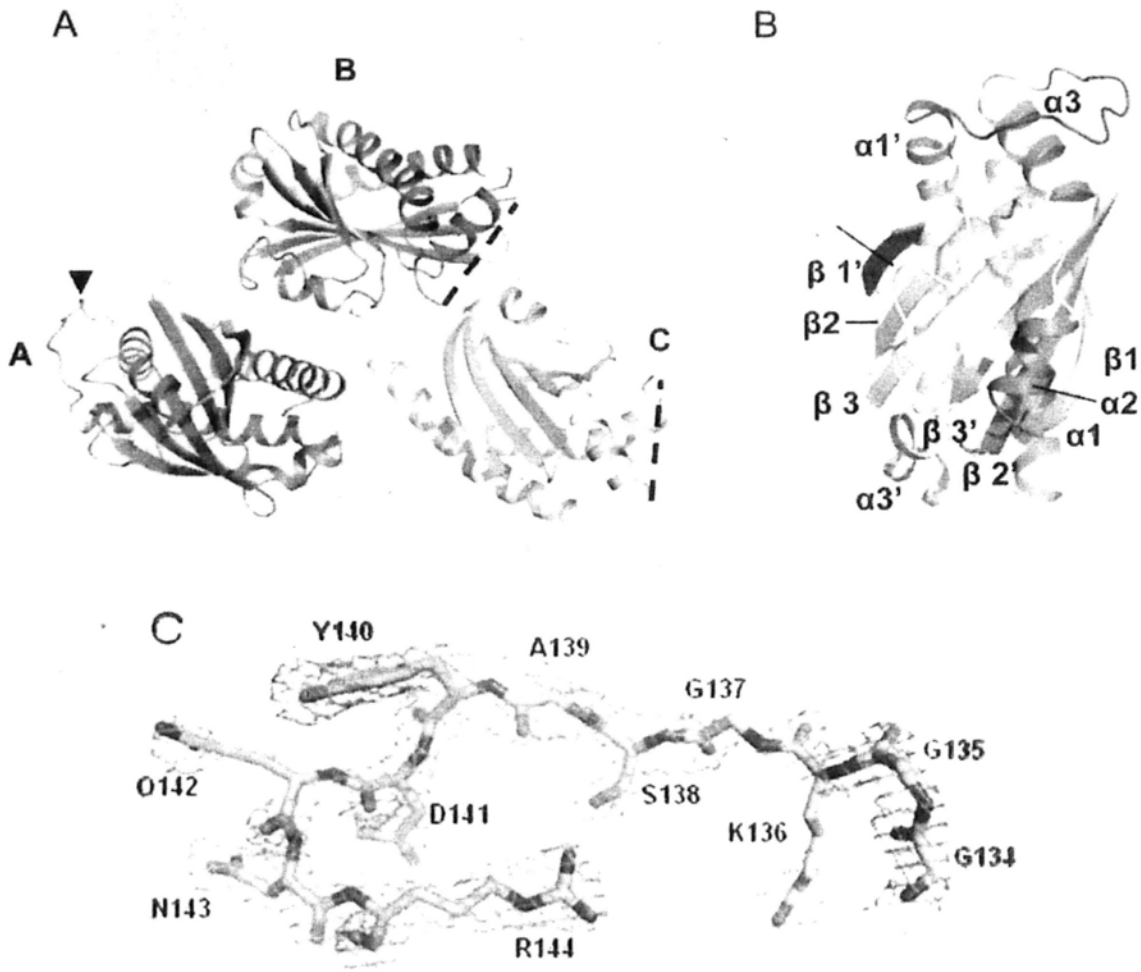

Fig. 3.2. Overall structure of $FliM_M$. (A) Three molecules of $FliM_M$ are found per asymmetric unit, chain A, B and C are shown in discrete colors. Loop region that can only be built on chain A is marked by an arrow and the corresponding missing region is marked as dashed line in chain B and C. **(B)** The secondary structures of $FliM_M$ are organized as αβαββα repeat. Three helices and three beta sheets at the first halve of the structure are colored in green and yellow, while the corresponding structure in second halve are colored in cyan and orange, respectively. The position of α2' (replaced by loop in our structure) is marked. Note that the two repeats are related by two-fold symmetry in the axis perpendicular to the page. α3-α1' loop connecting the two halve is colored in red. **(C)** 2Fo-Fc electron density map of $FliM_M$ structure at contour level 1.0 σ showing α3 – α1' loop (residues G143 – R144) of chain A.

A

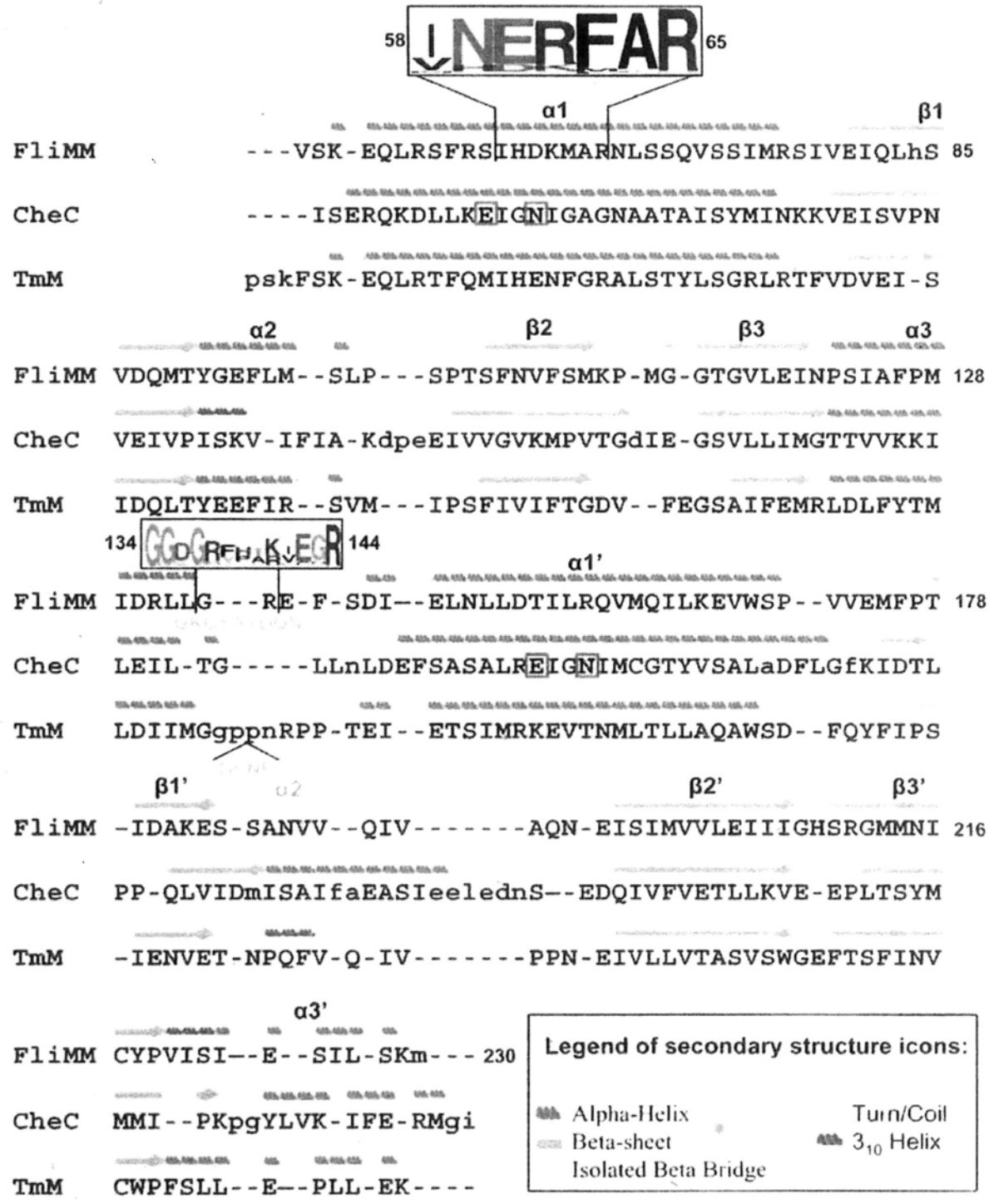
58
65
α1
β1
FliMM ---VSK-EQLRSFRSIHDKMARNLSSQVSSIMRSIVEIQLhS 85
CheC ----ISERQKDLLKEIGNIGAGNAATAISYMINKKVEISVPN
TmM pskFSK-EQLRTFQMIHENFGRALSTYLSGRLRTFVDVEI-S
α2
β2
β3
α3
FliMM VDQMTYGEFLM--SLP---SPTSFNVFSMKP-MG-GTGVLEINPSIAFPM 128
CheC VEIVPISKV-IFIA-KdpeEIVVGVKMPVTGdIE-GSVLLIMGTTVVKKI
TmM IDQLTYEEFIR--SVM---IPSFIVIFTGDV--FEGSAIFEMRLDLFYTM
134
144
α1'
FliMM IDRLLG---RE-F-SDI--ELNLLDTILRQVMQILKEVWSP--VVEMFPT 178
CheC LEIL-TG-----LLnLDEFSASALREIGNIMCGTYVSALaDFLGfKIDTL
TmM LDIIMGgppnRPP-TEI--ETSIMRKEVTNMLTLLAQAWSD--FQYFIPS
β1'
α2
β2'
β3'
FliMM -IDAKES-SANVV--QIV-------AQN-EISIMVVLEIIIGHSRGMMNI 216
CheC PP-QLVIDmISAIfaEASIeelednS--EDQIVFVETLLKVE-EPLTSYM
TmM -IENVET-NPQFV-Q-IV-------PPN-EIVLLVTASVSWGEFTSFINV
α3'
FliMM CYPVISI--E--SIL-SKm--- 230
CheC MMI--PKpgYLVK-IFE-RMgi
TmM CWPFSLL--E--PLL-EK----
Legend of secondary structure icons:
Alpha-Helix
Beta-sheet
Isolated Beta Bridge
Turn/Coil
3 10 Helix

B

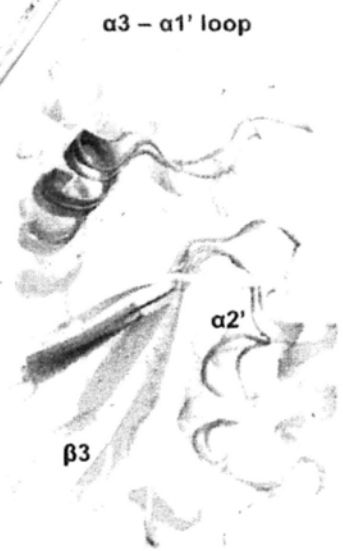

Fig. 3.3. Comparison of the $FliM_M$ with $TmFliM_M$ (TmM) and TmCheC (CheC). (A) Mutiple structural alignment was performed by MatchMaker Tool in Chimera. Secondary structure element was assigned by STRIDE, and the legend of secondary structure icons is shown (box). Inset sequences in logo format showed the conserved residues at α1 (residues 58 – 65) and α3 -α1' loop connecting the two halves of the structure (residues 134 – 144). Differences between $FliM_M$ and $TmFliM_M$ secondary structure are boxed (purple). Residues missing from the chain B, C and $TmFliM_M$ are shown under the sequence and colored green. Conserved EXXN motif in α1 and α1' of CheC is indicated as red box. **(B)** Superposition of $FliM_M$ (green), $TmFliM_M$ (magenta) and TmCheC (white) structures, highlighting the major secondary structural differences at α2' and β3. The alignment is generated by aligning 148 atom pairs (selected by MatchMaker Tool) between TmFliM and $FliM_M$ and 48 atoms between TmCheC and $FliM_M$ with RMSD values 0.998 Å and 1.060 Å, respectively.

Alignment of FliM sequences shows that most conserved residues are clustered around three exposed surface regions. The first patch is localized close to α3-α1' loop and includes residues at C-term of α1, α3 and N-term of α1'. The second patch is at the

side of $FliM_M$, mainly includes residues on the helices and loops around α2 and α2'. The third region is on the opposite side of α2 and α1'. The remaining conserved residues are scattered around the bottom of the domain, including residues on α3', N-term of α1 and β2-β3 loop. Residues around α1' are least conserved (Fig. 3.4). The importance of these regions for the interactions of $FliM_M$ will be discussed.

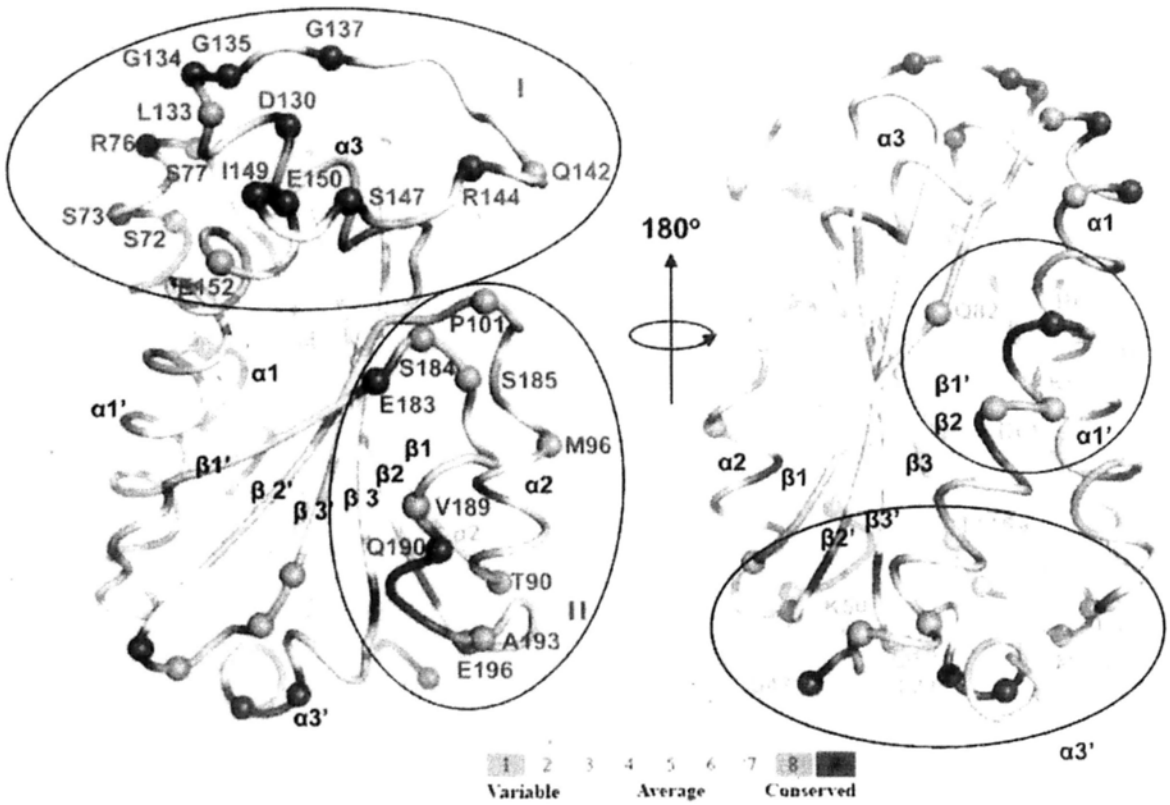

Fig. 3.4. Sequence conservation of $FliM_M$ analyzed by Consurf (http://consurf.tau.ac.il/). The alignment is generated as in Fig. 1.5. Cartoon of $FliM_M$ is colored according to conservation scores following coloring scheme of the software. Residues with conservation scores 8 and 9 on the protein surface are shown as spheres and are labeled according to *H. pylori* sequence. The conserved residues are grouped into 4 regions, each region are differently colored. Positions of α2' is labeled in green.

3.3.2 $FliM_M$-FliG interactions

FliM-FliG interaction identified in *E. coli* and *S. typhimurium* is presumably conserved among all bacterial species. To verify that FliM also binds to FliG in *H. pylori*, purified $FliM_M$ was incubated with untagged FliG in 1.5:1 molar ratio and the complex was separated by size exclusion column chromatography. Figure 3.5 shows that $FliM_M$ was co-eluted with FliG, while excess $FliM_M$ was eluted in later fractions, suggesting that FliG-$FliM_M$ formed a stable complex (Fig. 3.5).

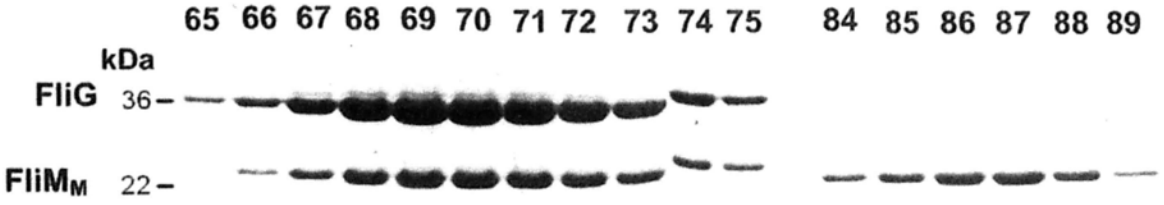

Fig. 3.5. Purification of FliG-$FliM_M$ complex by size exclusion column chromatography. Each elution volume (ml) is indicated above the figure.

3.3.3 $FliM_{M139}YDQ_{141}$/AAA triple mutant impair FliM-FliG interaction

As discussed in Section 1.2.3, regions close to GGXG motif of FliM in *E. coli* and *S. typhimurium* are important for FliG interaction (Park SY et al., 2006). The α3-α1' loop connecting the two symmetry halves of $FliM_M$ is flexible with variable length and different characters of amino acids. To test if these variable residues are involved in FliG interaction, Lys136 within the $_{134}GGXG_{137}$ motif was mutated to Ala and Asp as well as $_{139}YDQ_{141}$ was mutated to $_{139}AAA_{141}$. From the result in Figure 3.7, pull down of $FliM_M$ was significantly reduced in $_{139}YDQ_{141}$/AAA but not K136A and K136D mutants. This suggests that the side chains of $_{139}YDQ_{141}$ likely contributed to FliG interaction.

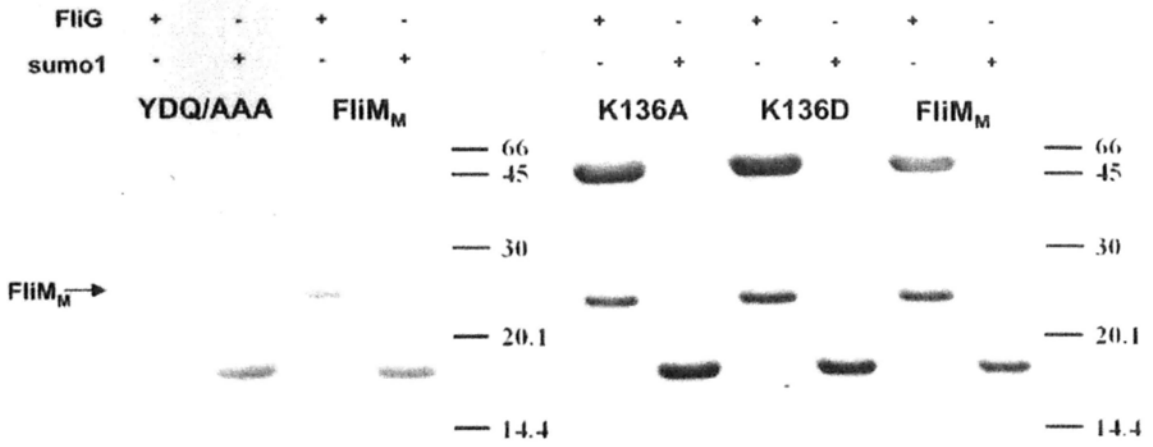

Fig. 3.6. Pull down of $FliM_M$ or $FliM_M$ mutants by His_6-sumo1-FliG. His_6-sumo1-FliG or His_6-sumo1 were immobilized on Ni-NTA beads followed by incubation with purified $FliM_M$ or $FliM_M$ mutants in 2 : 1 molar ratio. Note that the band corresponding to $FliM_M$ (~22 kDa) is significantly diminished for $_{139}YDQ_{141}$/AAA mutant.

3.4 Discussion

FliM-FliG interaction is crucial in rotation and switching of bacterial flagellum. In the present study, the structure and function of FliM in *H. pylori* are investigated. A 2.2 Å crystal structure of $FliM_M$ was determined. $FliM_M$ shares high structural homology to $TmFliM_M$ despite subtle differences in the arrangement of secondary structure are observed. FliM-FliG interaction was further verified by size exclusion column chromatography. By using mutagenesis studies, it was noted that the $_{139}YDQ_{141}$/AAA triple mutant disrupted the $FliM_M$-FliG interactions.

By sequence alignment we identified a highly conserved cluster of surface exposed residues localized around α3 -α1' loop (Region I) (Fig. 3.4). The lack of electron density in this solvent exposed loop in $TmFliM_M$ and $FliM_M$ (chains B and C) implied that the loop likely adopted multiple conformations. Independent studies supported that this exposed surface is close to FliG binding region. Mutants isolated around this region lead to Mot$^-$ (non-motlile) phenotype or suppressed FliG mutations in yeast two hybrid studies (Sockett H et al., 1992; Passmore SE et al., 2008) (Table 3.3 and Fig. 3.7). Among them, L133, G134, G135, S147 are highly conserved; I149 and S184 are conserved but distinct in *H. pylori*; R131, D141, D148 are variable. These residues are located at the periphery of α3. Insertion of Pro to conserved GGXG motif to GPGXG is non-motile (Mathews MA et al., 1998), supporting that FliM-FliG interacting surface is located around α3 to α1'.

Variable residues located around this region may be contributed to the variations in FliM-FliG binding interface among different bacterial species. The residues in the flexible loop are variable in terms of length and character of amino acids. We identified

$_{140}$YDQ$_{142}$/AAA triple mutant impaired FliG-FliM interaction in pull down assay. The mutation unlikely causes change on the backbone of secondary structure (Fig. 3.7). The side chain of these residues may mediate FliG-FliM interactions.

Structural comparison of $FliM_M$ and $TmFliM_M$ shows the different orientations of α3 -α1' loop. Interestingly, the distinct arrangement of three highly conserved residues, D130, R144, E150, leads us to propose that these residues may help to mediate the flexibility of the loop. In $FliM_M$, side chain of R144 is pointing towards α3 by forming salt bridge with D130 and E150. Displacement of α3 -α1' loop is observed in $TmFliM_M$ such that side chain R144 is pointing α1'. We speculate that these residues may help to coordinate the movement of the loop and may be important for FliG binding. Further mutagenesis studies will be performed to investigate the importance of these conserved residues on FliG interaction and their effects on motor switching.

Residue	STY/ECO	suppressor	Mot⁻	Consurf (score)
R131	Asn	√		7
L133	Phe		√	8
G134	Gly		√	9
G135	Gly		√	9
D141	**Val**	**√**		**6**
S147	Thr		√	9
D148	**His**	**√**		**4**
T149	Thr	√		9
S184	Met	√		8

Table 3.3. Surface exposed residues of FliM on Region I important for FliG binding (Sockett H et al., 1992; Passmore SE et al., 2008). Equivalent residues in *E. coli* (ECO) or *S. typhimurium* (STY) are indicated. Mutations that lead to nonmotile (Mot⁻) allele or suppress FliG mutation in yeast two hydrid assay (suppressor) are summarized. Coloring scheme: Highly conserved residues, brown; conserved but unique in *H. pylori* orange, less conserve, shaded yellow. The conservation score is indicated (Consurf).

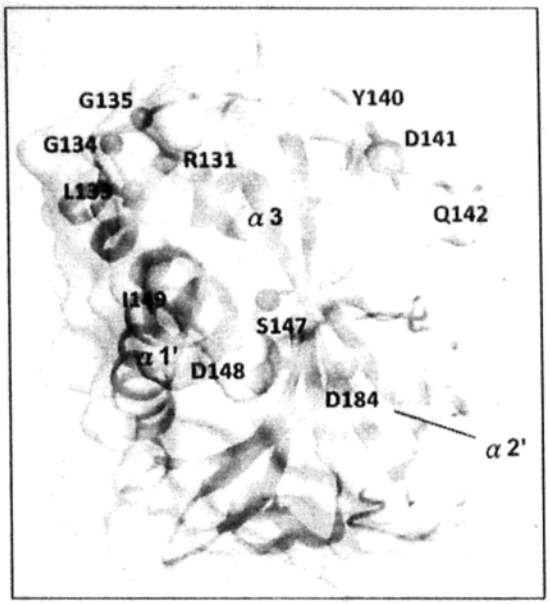

Fig. 3.7. Residues important for FliG interaction are mapped on the structure of $FliM_M$. Residues are colored according to Table 3.2

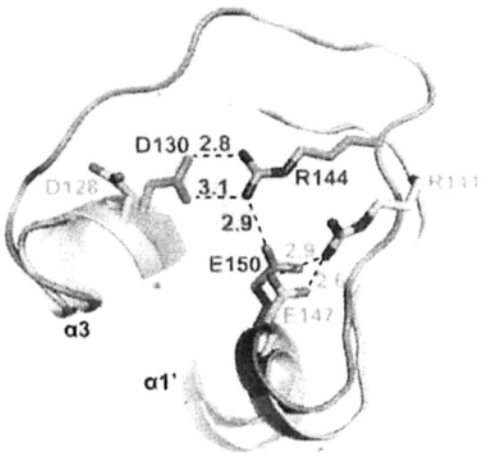

Fig. 3.8. Comparison of $FliM_M$ (green) and $TmFliM_M$ (cyan) reveals different arrangement of D130, R144, E150 (D128, R141, E147 in $TmFliM_M$). Salt bridge formations are indicated as dashed lines with the distance shown in Å.

Another group of conserved cluster of residues gathered around regions II and III. Crosslinking studies suggested that these regions mediate FliM-FliM subunit interaction, including residues S58 and R65 on α1, I78 on α1-β1 loop, M96 on α2, V188 and Q190

on α2'-β2' loop. We noted two differences in this region when comparing the structures of $FliM_M$ with $TmFliM_M$. Firstly, α2' in $TmFliM_M$ is replaced by a loop in $FliM_M$, and is more closely packed against a symmetry molecule in the crystal lattice while the corresponding region is exposed in $FliM_M$ (Fig. 3.9). This suggests that α2' may undergo loop – helix transition during protein-protein interaction. A similar loop-helix difference is observed when comparing α2 from the two chains of CheC in CheC-CheD complex structure (PDB-ID: 2F9Z). Secondly, the electrostatic surface potential on α1 of $FliM_M$ is notably more electropositive than that of $TmFliM_M$ (Fig. 3.10); while the surface potential of α2-α2' of both structures is more or less electronegative. This may create a different binding interface between adjacent FliM molecules in *H. pylori*. A recent study identified a CCW biased mutant R54C of FliM in *H. pylori*. R54 is located at a fairly conserved region in the N-term of α1 connecting CheY binding site. Mutation of this residue may affect the transmission of conformational changes upon CheY binding to $FliM_M$. Or the mutation may affect the interaction between adjacent FliM molecules and therefore the signal transmission within the switch complex (Lowenthal AC et al., 2009). Motor switching is believed to involve the binding of CheY-P to FliM and causes subsequent conformational change of FliM propagated to FliG. CW and CCW bias mutations has been mapped on the structures of FliM and highlighted a distinct pattern (Park SY et al., 2006). Recent studies also suggested that FliM binds to two distinct regions of FliG, however the FliM-FliG binding interface at these two distinct regions has not been well characterized. One of the interface at the middle domain of FliG is dominated with charged residues – EHPQR motif, while the other interface is hydrophobic (Brown PN et al., 2007). It is possible that FliM utilizes an overlap but

distinct surface around α3-α1' loop to interact with two regions of FliG. Further experiments on these binding interfaces will be required to help us to understand the switching mechanism.

In summary, the overall folding of FliM is conserved among thermophilic bacterium *T. maritma* and mesophilic bacterium *H. pylori*. FliM shares the same binding surface for FliG interactions as in other organisms. Variable residues and surface properties on FliM may contribute to binding specificity and affinity with its interacting partners. Further studies will be focused on mapping the role of flexible α3-α1' loop (especially residues D130, R144, and E150) in FliG interaction and motor switching.

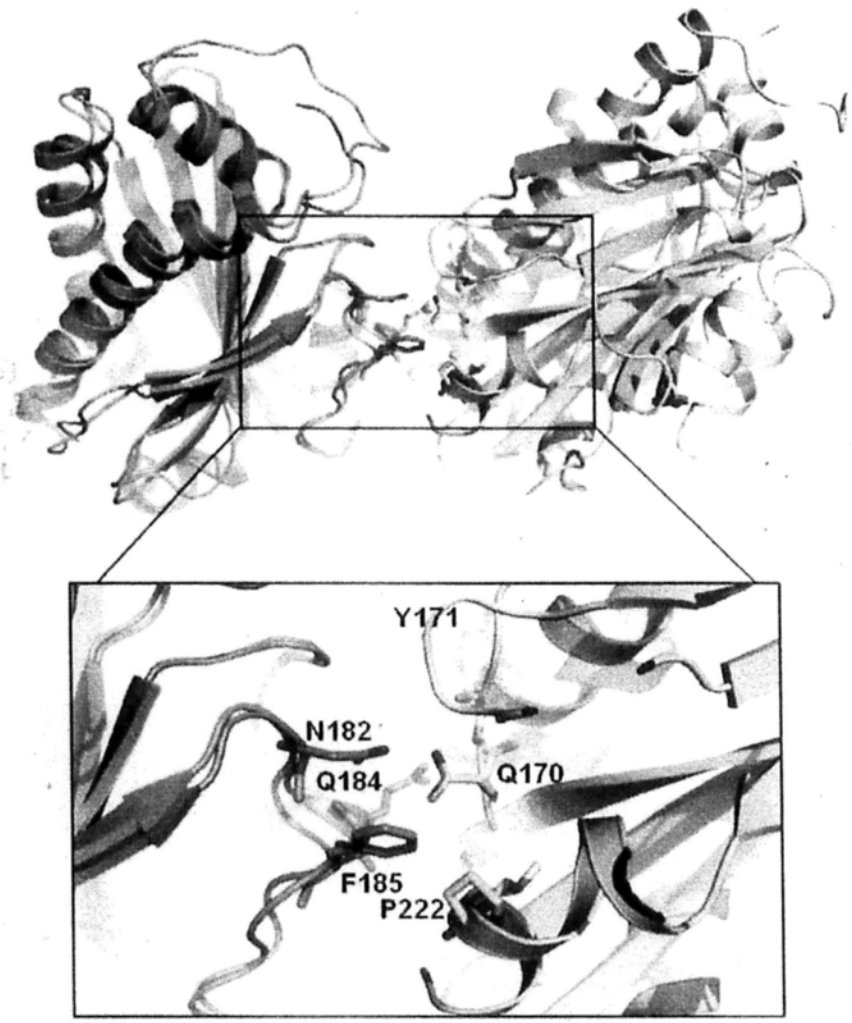

Fig. 3.9. Structural alignment of $TmFliM_M$ (magenta) and $FliM_M$ (orange) comparing the interface between α2' and the symmetry molecules. Symmetry molecules of $TmFliM_M$ and $FliM_M$ are colored in light pink and yellow, respectively. Residues participated in the interaction between $TmFliM_M$ and the symmetry molecule around α2' are shown as sticks and labeled. No interaction between $FliM_M$ and the symmetry molecule is observed in the corresponding region.

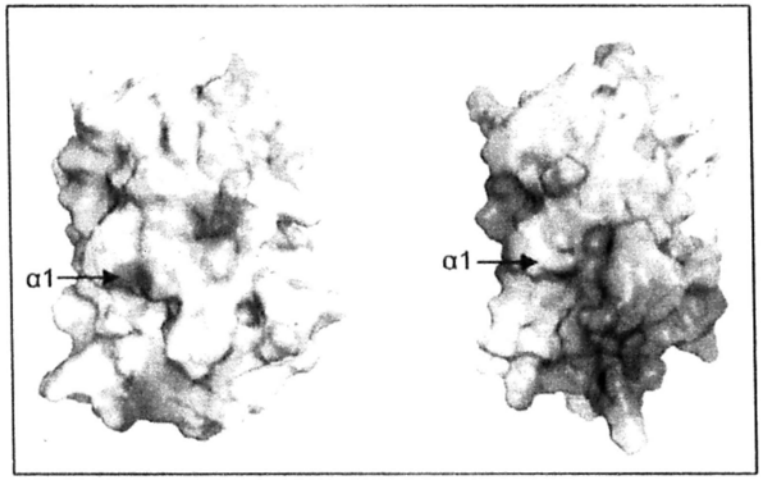

Fig. 3.10. Electrostatic surface of $FliM_M$ (left) and $TmFliM_M$ (right) highlighting the different electrostatic potential of region around α1. Electrostatic surface potential is calculated by APBS, and displayed with contour level ±3 keT.

Chapter 4

Structure of FliG provides insight into the switching mechanism

4.1 Introduction

The rotation of bacterial flagellum is driven by a unique bidirectional motor that allows bacteria to respond to the environmental stimuli. For most bacteria, like *E. coli* and *S. typhimurium,* there are two distinct swimming behaviors. Bacterium runs when the motor turns counterclockwise (CCW), and tumbles when it rotates in clockwise (CW) direction. The core of the rotary device is composed of a transmembrane stator $MotA_4B_2$ complex and a rotor formed by rings of protein oligomers (Kojima S & Blair DF, 2004). Accumulated studies using biochemical, biophysical and genetics approaches have proposed a model for flagellar rotation. Protons flow through $MotA_4B_2$ complex will neutralize a well-conserved aspartic residue on the transmembrane helix of MotB (Kojima S and Blair DF, 2001). This proton flow subsequently induces a conformational change of the cytoplasmic domain of MotA, which exerts torque on the rotor. Switching of rotation between CCW and CW directions is regulated by the binding of the chemotactic response regulator, phosphorylated CheY to FliM and FliN (Welch M et al., 1993). The binding is thought to alter the conformation of the C-terminal domain of FliG which electrostatically

interacts with the cytoplasmic loop of MotA (Zhou J et al., 1998; Brown PN et al., 2002, 2007)

The crystal structure of full length FliG recently resolved in *A. aqeolicus* (AaFliG) reveals that the protein possesses three domains $FliG_N$, $FliG_M$ and $FliG_C$, each of which exhibits specific interaction with other motor proteins (Lee LK et al., 2010). $FliG_N$ is responsible to anchor the whole switch complex to FliF whereas $FliG_M$ carries conserved EHPQR motif for FliM interaction that mediates flagellar assembly and rotational switching. $FliG_C$ is further divided into two sub-domains: an Armadillo repeat motif (ARM_C) and a six-helices of unique fold $FliG_{C\alpha 1\text{-}6}$ at the N- and C-termini, respectively. ARM_C is characterized by a conserved hydrophobic patch that was shown to bind FliM (Brown PN et al., 2007; Grünenfelder B et al., 2003; Passmore SE et al., 2008; Paul K et al., 2011). Three conserved charged residues in helix 5 of $FliG_{C\alpha 1\text{-}6}$ interact complementarily with MotA and participate in the stator-rotor association during torque generation (Zhou J et al., 1998). Connection between the three FliG domains are made by two ~20-residue long helices $Helix_{NM}$ (for $FliG_N$ and $FliG_M$) and $Helix_{MC}$ (for $FliG_N$ and $FliG_M$). Three other loop regions related to switching were identified when compared the AaFliG with $FliG_{MC}$ from *T. maritma* ($TmFliG_{MC}$). They are $Loop_M$-connecting $FliG_M$ to $Helix_{MC}$, $Loop_C$ - connecting $Helix_{MC}$ to $FliG_C$ and carries conserved GlyGly motif, and MFXF motif - connecting ARM_C to $FliG_{C\alpha 1\text{-}6}$ (Fig.

4.4A) (Brown PN et al., 2002; Minamino T et al., 2011). Rotational bias mutations have been mapped onto these linker regions (Irikura VM et al., 1993; Van Way SM et al., 2004), suggesting that the switching mechanism does not localize on one specific region, rather, it may involve a considerable structural movement of FliG molecule. The structure solutions of FliG inevitably set a milestone in understanding the architecture of motor switch complex, however, how FliG assembles into a torque ring and how it undergoes conformational changes during motor switching remains controversial.

Flagellar rotation is a stepping motion and involves 26 steps per revolution in both CW and CCW rotation, despite differences in torque-speed relations (Sowa Y et al., 2005; Nakamura S et al., 2010; Yuan J et al., 2010). It has been proposed that conformational change at FliG C-terminal domain may be responsible to the symmetrical rotation. This was reasoned as $MotA_4B_2$ complex with transmembrane helices would be less mobile for structural changes whereas $FliG_C$ domain is relative isolated in the crystal structure and be susceptible for molecular movement (Nakamura S et al., 2010). In this context, assuming each FliG domain is a rigid body, the conformation of FliG in CW and CCW rotation would then depend on the relative orientation of individual domains connected by the flexible loop. To explain the symmetrical rotation, Lee LK et al., suggested a switching model that coordinated

movement of $Helix_{MC}$ and MFXF motif would lead to reverse arrangement of charges in the C-terminal domain (Lee LK et al., 2010). The involvement of $Helix_{MC}$ in switching event was also highlighted in Minamino T et al.,'s study, as $Helix_{MC}$ was in a distinct orientation in the crystal structure of CW-biased ΔPAA deletion mutant (Minamino T et al., 2011). Still, how individual domain, in particular $FliG_C$, is re-oriented during switching events remains unclear.

Deletion mutants of FliG in *H. pylori* (HpFliG) showed non-flagellate phenotypes (Allan E et al., 2000). In previous chapters, we evidenced HpFliG binds to FliM and FliM binds CheY-P. These studies suggested that both of HpFliG and FliM exhibit similar functional roles as their counterpart in *E. coli* (Lowenthal AC et al., 2009; Lam KH et al., 2010).

In this study, HpFliG – FliF interaction was tested and structures of two HpFliG fragments were examined. Surprisingly, we observed a 180° molecular rotation of $FliG_C$, which help us to explain and delineate the symmetrical torque generation process in both CCW and CW directions. The existence of multiple conformations $FliG_C$ was further evidenced by *in vitro* cysteine cross-linking experiments and the relevance to rotational switching was reviewed by *in vivo* mutagenesis studies.

4.2 Materials and methods

4.2.1 Strains and plasmids

HpFliG, $HpFliG_{MC1}$ (a.a. 86-343), $HpFliG_{MC2}$ (a.a. 116 – 343), $HpFliG_N$ (a.a. 1 – 115), $HpFliG_{NM}$ (181 – 343) and FliF C-terminal domain ($FliF_C$) (HP0351, residues 484 - 567) fragments were amplified from *H. pylori* genomic DNA 26695 (ATCC). HpFliG, $HpFliG_N$, $HpFliG_{NM}$ and $HpFliG_{MC2}$ were cloned into pGEX-6p-1 while $HpFliG_{MC1}$ and $FliF_C$ were cloned into pAC28m (Kholod N & Mustelin T, 2001). FliG from *E. coli* (EcFliG) was amplified from strain RP437 (gift from Parkinson JS) genomic DNA and cloned into pTrc99a vector for complementation. Construction of HpFliG mutants for GST pull down, cysteine cross-linking and EcFliG for *in vivo* assays were performed using QuikChange site-directed mutagenesis kit (Stratagene) according to manufacturer's protocol. All sequences were verified by commercial sequencing service (BGI). For complementation, pTrc99a-EcFliG and its various mutants were individually transformed into *E. coli ΔfliG* strain DFB225 (gifts from Blair D) (Lloyd SA et al., 1996).

4.2.2 Protein expression and purification

HpFliG, truncations and mutants were transformed into *E. coli* strain BL21(DE3) and protein expression was induced when OD_{600} ~0.4 – 0.6 with 0.3 mM IPTG. Cells

were cultured overnight at 20 - 25°C. Proteins were purified by affinity chromatography and gel filtration under standard protocol as described in Section 2.2.1. Procedures for co-purification of HpFliG-$FliM_M$ and $HpFliG_{MC1}$-$FliM_M$ were as described in Section 3.2.3. For co-expression of $HpFliG_N$ and $FliF_C$, plasmids were co-transformed into BL21 (DE3). Cells were growth under 20°C for 16 hrs after 0.3 mM IPTG induction. Co-purification involves two-step affinity column chromatography – Ni-NTA and GST chromatography – and gel filtration. Buffer conditions for the purification process are summarized in Appendix 4.1.

4.2.3 Pull down assay

His-sumo1-FliG – $FliM_M$ interaction assay was described in Section 3.2.2. For GST pull down assay, GST-$HpFliG_{MC2}$ and GST-$HpFliG_{NM}$ 30 µl GST resin (GE Healthcare) was pre-equilibrated with buffer 200 mM NaCl, 20 mM Hepes pH 7.5, 4 mM DTT, 0.2 mM PMSF, 0.2 mM benzamidine. GST-$HpFliG_{MC2}$ and –$HpFliG_{NM}$ were incubated with the resin for 1 hr. $FliM_M$ (in FliG : $FliM_M$ = 1 : 1.5 molar ratio) was incubated with the bounded beads for an additional 1 hr. After washing, the beads were boiled with SDS-containing loading dye and loaded onto SDS-PAGE. Pull down of $FliM_M$ was further confirmed by immunoblotting using polyclonal rabbit-anti-$FliM_M$ antibody (Antibody Production Service, The Chinese University of Hong Kong).

Procedures for nickel pull down HpFliG / mutants by $FliM_{NM}$-His_8 were described in Section 2.2.2.2 with modifications. Binding and washing buffer was 150 mM NaCl, 20 mM Imidazole pH 7.5, 0.15% Tween20. HpFliG / mutants were incubated with immobilized $FliM_{NM}$-His_8 for 1 hr at 4°C for binding.

4.2.4 Crystallization and data collection

Crystals of $FliG_{MC1}$ were obtained under conditions 0.1 M ammonium sulfate, 0.3 M sodium formate, 0.1 M Tris pH 7.8, 1% PGA, 7% PEG8000 at 20°C, using sitting drop method. Hexagonal-shaped crystals grew to full size at about 1 week. The crystals were soaked briefly in crystallization buffer containing 20% glycerol and cooled by plunging into liquid nitrogen. Crystals of $FliG_{MC2}$ were obtained under conditions 0.1 M Hepes pH 7.5, 10% PEG6000, 0.02 M spermidine (4:1) at 16°C using sitting drop method. Crystals were soaked briefly in cryoprotectant with 15% 2-methyl-2,4-pentanediol. Crystals of $FliF_C$-$FliG_N$ were obtained under conditions 1.5 M ammonium sulfate, 0.1 M Tris pH 8.5, 12 % glycerol.

4.2.5 Structure determination and refinement

A 3.3Å $FliF_C$-$FliG_N$, 2.6Å $FliG_{MC1}$ and 2.7 Å $FliG_{MC2}$ X-ray datasets were collected at beamline BL17U Shanghai Synchrotron Radiation Facility (SSRF), China.

The data sets were processed using the HKL2000 and iMosflm package (Otwinowski Z & Minor W, 1997; Leslie AGW, 1992), scaled and reduced with SCALA from the CCP4 suite (Collaborative Computational Project, 1994). Crystals of $FliF_C$-$FliG_N$, $FliG_{MC1}$ and $FliG_{MC2}$ were in the $P3_1$, $P6_5$ and C2 space group, respectively. $FliG_{MC1}$ and $FliG_{MC2}$ were solved by molecular replacement using FliG from *A. aeolicus* (PDB-ID: 3HJL) as a search model. Molecular replacement program Phaser (McCoy AJ et al., 2005), in the CCP4 suite, was used with data in the resolution range 15 – 2.8 Å. Initial model-building was performed by ARP/wARP (Langer G et al., 2008). Rounds of refinements and manual rebuilding were performed using programs REFMAC and COOT (Emsley P et al., 2010). Co-ordinates of $FliG_{MC1}$ and $FliG_{MC2}$ have been deposited in the PDB (PDB-ID: 3PKR, 3PL4). Figures were prepared using PyMol (Delano WL, 2002). Morph structures was calculated using the UCSF Chimera package from the Resource for Biocomputing, Visualization, and Informatics at the University of California, San Francisco (Pettersen EF, 2004). Diffraction and refinement statistics are summarized in Table 4.1.

Table 4.1 X-ray statistics for $HpFliG_{MC1}$, $HpFliG_{MC2}$ (A) and $FliF_C$-$HpFliG_N$ (B). Values in parentheses are for highest-resolution shell.

(A)

	$HpFliG_{MC1}$ (residue 86-343)	$HpFliG_{MC2}$ (residue 116-343)
Data collection		
Space group	$P6_5$	$C2$
Cell dimensions		
a, b, c (Å)	125.5, 125.5, 39.8	85.4, 102.6, 91.6
α, β, γ(°)	90.0, 90.0, 120.0	90.0, 114.7, 90.0
Resolution (Å)	41.07-2.6 (2.74-2.6)[a]	30-2.7 (2.75-2.7)[a]
R_{merge}	0.084 (0.435)	0.090 (0.401)
$I / \sigma I$	10.1 (3.7)	31.5 (4.6)
Completeness (%)	99.8 (100.0)	100 (100)
Redundancy	4.5 (4.5)	7.3 (7.1)
Refinement		
Resolution (Å)	41.07-2.6	30-2.7
No. reflections	10695	18550
R_{work} / R_{free}	23.41/26.79	22.47/28.12
No. atoms		
Protein	1,692	3536
Water	27	32
B-factors		
Protein	58.53	46.74
R.m.s. deviations		
Bond lengths(Å)	0.017	0.017
Bond angles (°)	1.645	1.667
Ramachandran plot	94.5/4.5/1/0	94.3/5.5/0.2

(B)

Diffraction data statistics	
Spacegroup	P31
Unit cell dimensions (Å)	60.10 60.10 85.53 90.00 90.00 120.00
Resolution range (Å)	33.04 – 3.30 (3.48 – 3.30)
No. of molecules per asymmetric unit	1
Matthews coefficient (VM; $Å^3Da^{-1}$)	1.75
Solvent content (%)	29.64
Number of observations	10571
Number of unique reflections	2929
Average redundancy	3.6 (3.7)
Completeness (%)	99.9 (100.0)
R_{merge}	0.109 (0.311)
Mean I/σI	5.7 (2.8)

4.2.6 Swarming assay

E. coli ΔfliG strain DFB225 transformed with pTrc99a-EcFliG or its mutants were grown overnight in LB medium. Cell suspension in 1 μl was spotted onto 0.3% Tryptone Broth (TB) soft agar with 0.05 mM IPTG and ampicilin (100μg/ml). The diameter of the chemotactic ring was measured after incubation at 30°C for 7 h.

4.2.7 Swimming assay

To examine the swimming behavior, overnight culture of the transformed DFB225 was diluted with 1:50 TB medium. Cells were allowed to grow at 30°C for 1.5 h when 0.05 mM IPTG was added for induction. Cells were further grown to exponential phase (OD_{600} = 0.4 – 0.6). Cells were pelleted and washed two times with chemotaxis buffer (10 mM sodium phosphate pH 7.0, 0.05 mM EDTA, 1 mM methioine) and diluted to OD_{600} ~ 0.1. The swimming behavior was examined under phase contrast inverted microscope (Olympus IX71) and 10 s videos with frame rate 15 frames/s and resolution 1360×1024 pixels were recorded. Bacterial swimming behavior was analyzed by software ImagePro Plus. Center-of-area (centroid) of each bacterium for each frame was automatically determined and connected to form a track. X and Y positions of centroid were recorded and smoothing was applied to remove the fluctuating signals due to translational motion of the bacterium or subtle error in recognizing the positions.

Immotile cells or cells with abnormal behavior were manually discarded. The XY positions of the tracks were exported into EXCEL. Tracks were further sorted by mean velocity, and the top and bottom 10% were discarded to eliminate the outliner cells. The tracks were then analyzed by fixed-time diffusion method (Lowenthal AC et al., 2009). Briefly, tracks were truncated into 4 seconds. All (X(t), Y(t)) positions were subtracted by (X(0), Y(0)) such that all tracks appeared to start from the same origin (0, 0). The coordinates was transformed to polar coordinates (r(t), θ(t)) and mean square radius $\langle R^2(t) \rangle$ for each time point was calculated. The diffusion exponent α was determined from the slope by plotting $\log\langle R^2(t) \rangle$ against log(t) according to the equation $\langle R^2(t) \rangle = Dt^{\alpha}$ where D is diffusion constant.

4.2.8 Electron microscopy

Examination of flagellation was performed using cells grown in liquid culture. After washing, cells were fixed with fixative (2.5% glutaraldehye, 2 % paraformaldehyde, 50 mM sodium cacodylate pH 6.5). Fixed cells were attached to the carbon-coated grid (SPI SUPPLIES) by floating the grid on a drop of cell suspension. Attached cells were stained with 1% phosphotungstate. Flagella formation was examined by Tecnai 12 BIOTWIN TEM (FEI/Philips).

4.2.9 Immunoblotting

Cells were grown as described above. Protein expression was checked by immunoblotting using polyclonal anti-FliG antibody (Antibody Production Service, The Chinese University of Hong Kong).

4.2.10 *In vitro* cysteine crosslinking

Purified protein samples were exchanged with buffer (50 mM Hepes pH 8.0, 150 mM NaCl) to remove DTT. To start the crosslinking reaction, FliG single (Q325C) or double mutants (Q325C/R209C, Q325C/R217C, Q325C/S222C, Q325C/E243C) at a protein concentration 0.2 mg/ml was incubated with 0.5 mM Cu^{2+} (phenanthroline) in the same buffer at 4°C for 30 min. To quench the reaction, 10 mM EDTA and 20 mM NEM was added and incubated for 10 min. For control, 10 mM EDTA and 20 mM NEM was added at the start of the reaction without any Cu^{2+} phenanthroline.

For haloalkylation of free cysteine, reactions were set as described above but were stopped by the addition of 10 mM EDTA. Each reaction mixture was further incubated with 500 μM 5'-IAF (Sigma) at pH 7.4 at room temperature for 2 h. Samples were boiled for 5 min and subjected to SDS-PAGE analysis.

4.3 Results

4.3.1 $HpFliG_{MC2}$ but not $HpFliG_{MC1}$ impaired FliG-FliM interaction

We have attempted to purify HpFliG (full length) and to screen for the crystallization conditions. However, no crystal was observed. Elution profile of HpFliG from Superdex 200 showed two close peaks that cannot be separated from each other. The broadened peak may due to self-association or domain movement of HpFliG (data not shown). Thus, the fragment is unlikely suitable for protein crystallization. HpFliG containing C-terminal and middle domain (a.a. 116 – 343) ($HpFliG_{MC2}$) was designed according to $TmFliG_{MC}$ sequence (ClustalW). $HpFliG_{MC2}$ contains the conserved EHPQR motif and hydrophobic patch both of which are critical to FliM binding. We tested $HpFliG_{MC2}$-FliM interaction by pull down assay using His-sumo1 tagged or GST tagged FliG. To our surprise, the amount of $FliM_M$ captured by FliG was significantly reduced in $HpFliG_{MC2}$ compared with wild type (Fig. 4.1A). It may imply that the N-terminal region is important to $FliM_M$ interaction. Another longer fragment composing residues 86 – 343 ($HpFliG_{MC1}$) was designed based on structural prediction by Phyre which indicated a compact N-terminal domain that contains 85 residues terminated by $_{84}GlyGly_{85}$. $HpFliG_{MC1}$ co-eluted with $FliM_M$ through gel filtration column evidenced stable $HpFliG_{MC1}$-$FliM_M$ complex formation (Fig. 4.1B). It leads us to propose a yet unidentified region at residues 86 – 115 may be important to FliM

binding. Accordingly, we mutated charged or bulky residues (Y88, R95, E100, D107) to Ala and test the interaction of mutant proteins with $FliM_{NM}$ (Fig. 4.1C). However, none of the mutant impaired FliG-FliM binding.

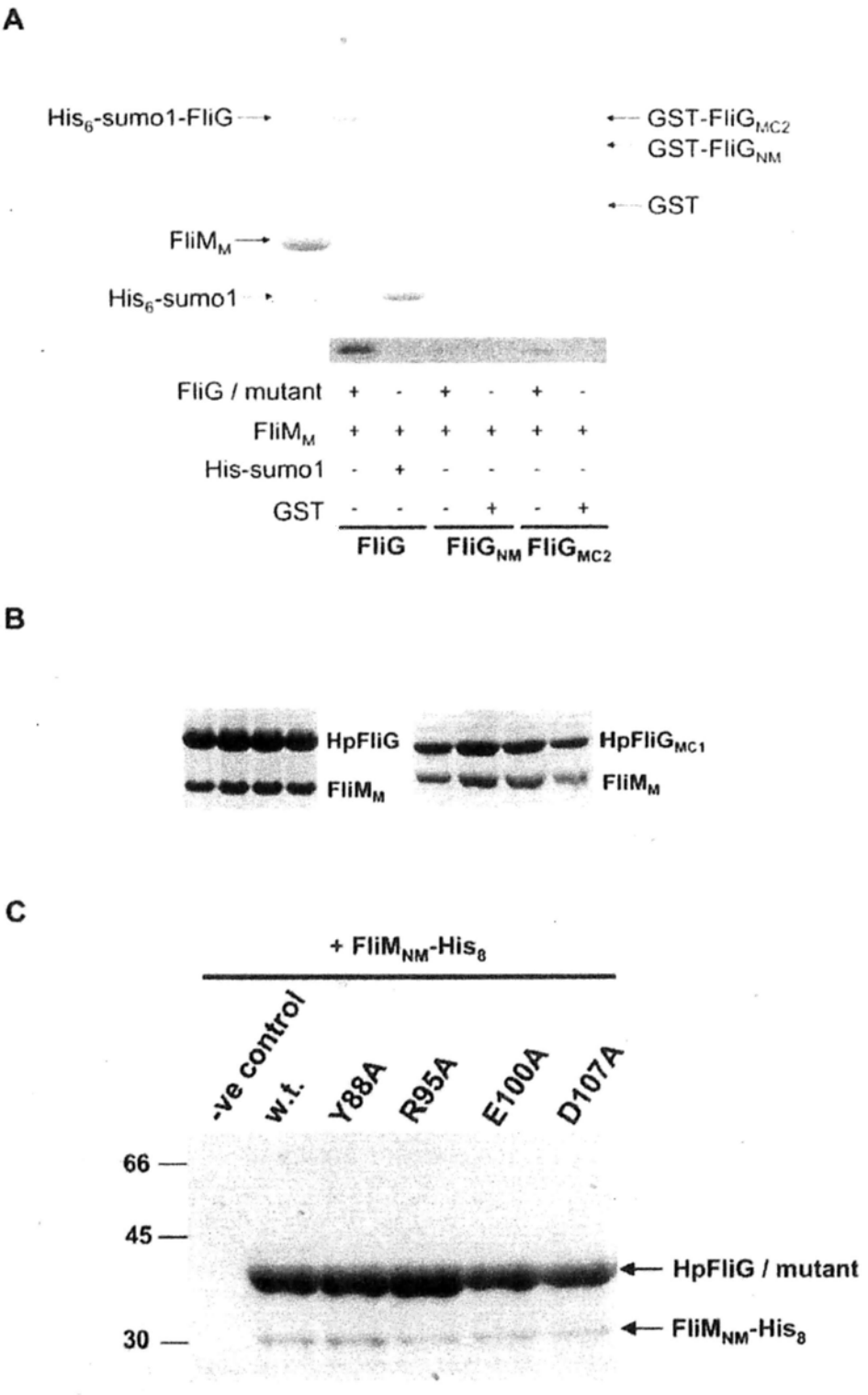

Fig. 4.1. FliG-FliM interaction studies. (A) Interaction between $FliM_M$ and FliG / truncations detected in nickel (His-sumo1-HpFliG) or GST (GST-$HpliG_{MC1}$ and GST-$HpFliG_{NM}$) pull-down assays. Lower strip shows immunoblot probed with anti-$FliM_M$ antibodies. **(B)** Elution profile of FliG-$FliM_M$ (left) and $FliG_{MC1}$-$FliM_M$ (right) complexes from Superdex 200 column analysed by SDS-PAGE. **(C)** Effects of HpFliG mutations on the binding to $FliM_{NM}$. Purified FliG / mutants were incubated with $FliM_{NM}$-His_8 immobilized beads. Empty beads incubated with FliG was used as negative control.

4.3.2 HpFliG N-terminal domain interact with FliF C-terminal domain

To investigate the interaction between HpFliG and FliF, the predicted FliF-FliG binding region composing FliF cytoplasmic domain (residues 484 – 567) ($FliF_C$) and $FliG_N$ (residues 1 – 115) were co-expressed. The complex was stably isolated when passing through Ni-NTA affinity, GST affinity and gel filtration column chromatography, suggesting a stable FliG-FliF interaction (Fig. 4.2).

Attempt was made to obtain $FliF_C$-$HpFliG_N$ crystal for X-ray diffraction. Oval shaped crystals were obtained under condition 1.5 M ammonium sulfate, 0.1 M Tris pH 8.5, 12 % glycerol (Fig. 4.3). The crystals were only diffracted to 3.3 Å resolution. The crystals belonged to the primitive hexagonal space group P3, with unit-cell parameters a = b = 60.10, c= 85.53 Å. Cell content analysis indicated the presence of one molecule per asymmetric unit, corresponding to a Matthews coefficient V_M of 1.75 $Å^3$ Da^{-1} and a

solvent content of 29.64% based on a calculated molecular weight of 25.52 kDa (Table 4.1B). The N-terminal domain of AaFliG was used as a search model in molecular replacement calculations using PHASER (Collaborative Computational Project, 1994). However, no significant solution was obtained. Further experiment will be performed to confirm the presence of $FliF_C$ and $FliG_N$ proteins in the crystals.

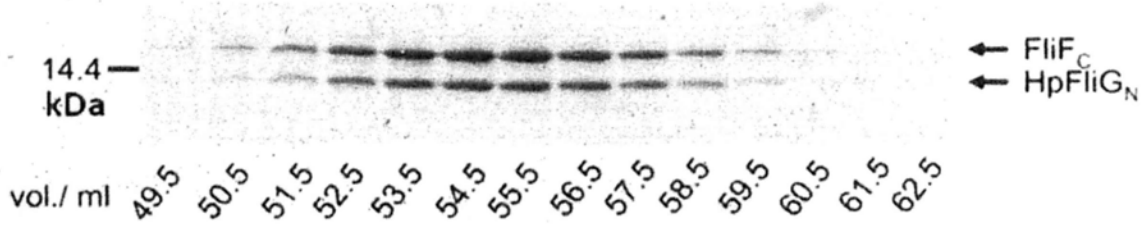

Fig. 4.2. $FliF_C$ – $HpFliG_N$ interaction studies. $FliF_C$ and $HpFliG_N$ were co-expressed in *E. coli* and co-purified by GST- and nickel-affinity chromatography followed by size exclusion chromatography. The elution profile from Superdex 75 is shown and the elution volume is indicated at the bottom.

Fig. 4.3. Representative crystal images of $FliF_C$-$HpFliG_N$, $HpFliG_{MC1}$ and $HpFliG_{MC2}$.

4.3.3 Overall crystal structures of HpFliG$_{MC}$ from *H. pylori*

Hexagonal shaped crystal of HpFliG$_{MC1}$ and trigonal-cylinder-shaped crystal of HpFliG$_{MC2}$ were obtained (Fig. 4.3). The crystal structures of HpFliG$_{MC1}$ and HpFliG$_{MC2}$ were resolved to 2.6 Å and 2.7 Å resolutions, respectively. Phase determination by molecular replacement was achieved only when the middle domain and the two C-terminal sub-domains of AaFliG (PDB-ID: 3HJL) / TmFliG$_{MC}$ (PDB-ID: 1LKV) were separately submitted as search models. These domains and subdomains are connected by flexible loops and displayed distinct spatial arragnement in AaFliG and TmFliG$_{MC}$. From the subsequent structure solutions of HpFliG$_{MC1}$ and HpFliG$_{MC2}$, these domains were found to be oriented differently. This explains why molecular replacement did not give any hit when the whole FliG protein was used as a search model. Both HpFliG$_{MC1}$ and HpFliG$_{MC2}$ consist of structural elements starting from a short Helix$_{NM}$ followed by FliG$_{M}$ (ARM$_{M}$), Helix$_{MC}$, ARM$_{C}$ and FliG$_{C\alpha1\text{-}6}$. Residues 86 – 116 of the N-terminal domain, residues 200 – 202 of Loop$_{C}$ and residues 336 – 343 at the C-terminus of HpFliG$_{MC1}$, and residues 337 – 343 at the C-terminus of HpFliG$_{MC2}$ were disordered and invisible in the electron density map. There is one FliG molecule per asymmetric unit in HpFliG$_{MC1}$, whereas two molecules per asymmetric unit were shown in HpFliG$_{MC2}$. The two molecules HpFliG$_{MC2/A}$ and HpFliG$_{MC2/B}$ are similar, with an RMSD$_{C\alpha}$ of 1.99 Å (Fig. 4.4A). Superimposition of individual ARM$_{M}$, ARM$_{C}$

and $FliG_{Ca1\text{-}6}$ among all solved FliG structures revealed subtle differences (Table 4.2), suggesting that these structural components are highly conserved. Interestingly, when the whole FliG structures were aligned, variations on orientations of $FliG_{Ca1\text{-}6}$ relative to ARM_C, and ARM_C relative to $FliG_M$ are noticeable. Details are discussed below.

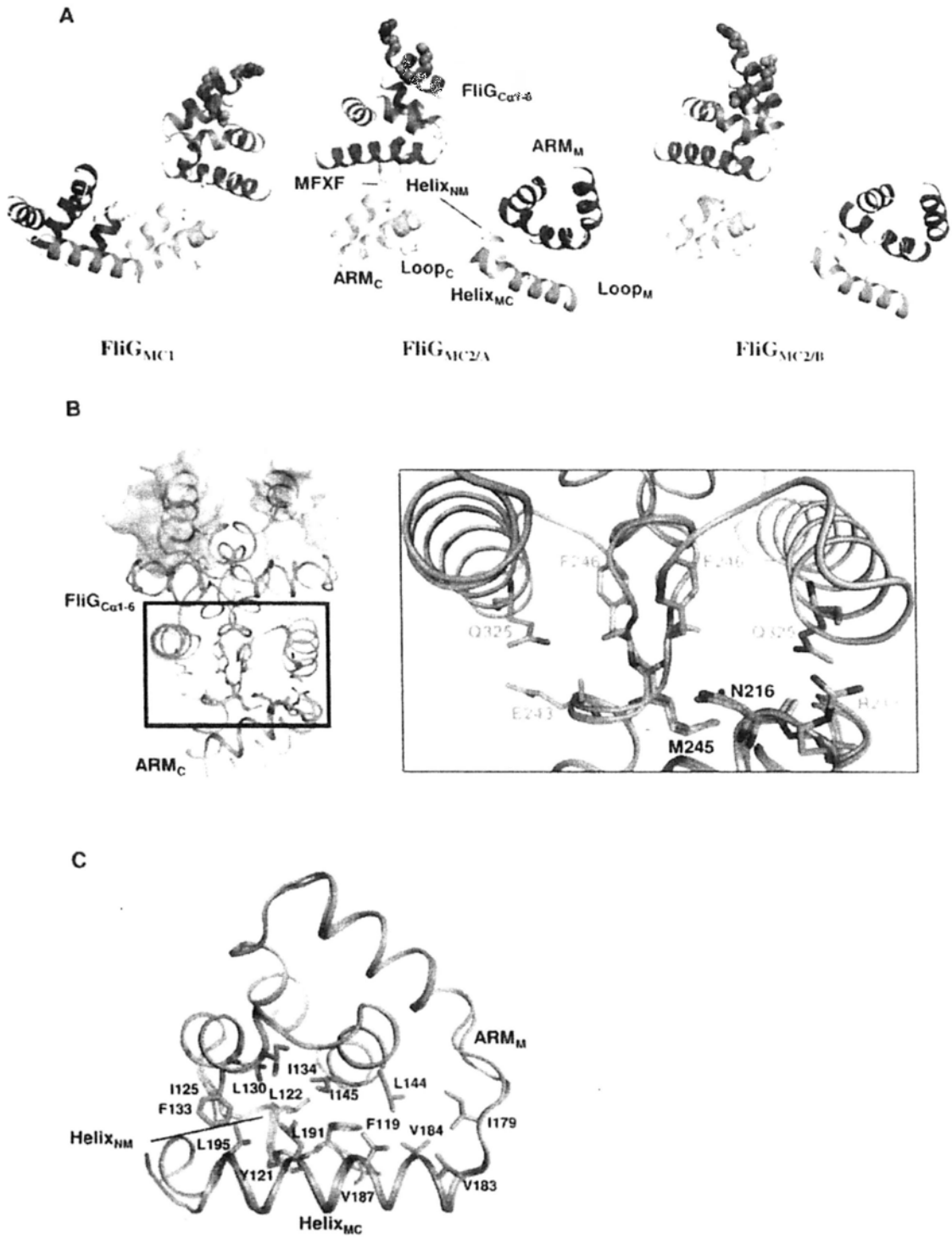

Fig. 4.4. Structures of HpFliG$_{MC1}$ and HpFliG$_{MC2}$. (A) Structures are oriented as ARM$_C$ domains are superimposed. Helices of ARM$_M$, Helix$_{MC}$, ARM$_C$, FliG$_{C\alpha1-6}$ are colored in red, orange, yellow and green, respectively. Loops and truncated helix Helix$_{NM}$ are colored in white. Critical charged residues involved in direct interaction with MotA and conserved di-glycine motif in the Loop$_C$ are highlighted as spheres.

Residues M235 and F246 in the MFXF motif are shown in sticks. **(B)** Structural comparison of $HpFliG_{MC1}$ (green) and $HpFliG_{MC2/A}$ (orange) demonstrating the symmetrical rotation of $FliG_{C\alpha 1\text{-}6}$ via conformational flexibility of $_{245}MF_{246}$. Molecular surface of Helix 5 of $FliG_{C\alpha 1\text{-}6}$ is shown and colored by electrostatic potential, with a contour level ± 5 kT (Baker NA et al., 2001). Interface of ARMc – $FliG_{C\alpha 1\text{-}6}$ are enlarged and residues M245, F246, N216, R217, E243 and Q325 are shown in sticks. Residues of $HpFliG_{MC1}$, $HpFliG_{MC2}$ are labeled in green and orange, respectively; residues aligned in both structures are labeled in black. **(C)** Alignment of the middle domains. Hydrophobic residues at the interface between $Helix_{MC}$, ARM_M and $Helix_{NM}$ are shown in sticks, only residues from $HpFliG_{MC1}$ are represented.

Table 4.2. Superimposition of individual ARM_M (A), ARM_C (B) and $FliG_{C\alpha 1\text{-}6}$ (C) among all solved FliG structures. Alignment was performed in Pymol and the $RMSD_{C\alpha}$ value is reported.

A. ARM_M

	$HpFliG_{MC1}$	$HpFliG_{MC2}$	$TmFliG_{MC}$	$TmFliG_{MC}$ ΔPEV
$HpFliG_{MC2}$	0.249			
$TmFliG_{MC}$	0.789	0.898		
$TmFliG_{MC}$ ΔPEV	0.668	0.675	0.374	
AaFliG	0.660	0.649	0.725	0.556

B. ARM_C

	$HpFliG_{MC1}$	$HpFliG_{MC2}$	$TmFliG_{MC}$	$TmFliG_{MC}$ ΔPEV
$HpFliG_{MC2}$	0.399			
$TmFliG_{MC}$	0.881	0.804		
$TmFliG_{MC}$ ΔPEV	0.745	0.679	0.289	
AaFliG	0.745	0.499	0.592	0.489

C. $FliG_{C\alpha 1\text{-}6}$

	$HpFliG_{MC1}$	$HpFliG_{MC2}$	$TmFliG_{MC}$	$TmFliG_{MC}$ ΔPEV
$HpFliG_{MC2}$	0.273	-		
$TmFliG_{MC}$	0.706	0.629	-	
$TmFliG_{MC}$ ΔPEV	1.123	0.999	0.912	-
AaFliG	0.644	0.614	0.737	0.950

4.3.4 A two-fold rotation of $FliG_{C\alpha1\text{-}6}$ hinged by MFXF motif

Comparison of the whole C-terminal domains revealed significant conformational differences between the two $HpFliM_{MC}$ structures. Remarkably, when ARM_C are aligned, $FliG_{C\alpha1\text{-}6}$ of $HpFliG_{MC1}$ showed a nearly 180° rotation when compared with that of $HpFliG_{MC2}$ (Fig. 4.4B). By analyzing the hinge between ARM_C and $FliG_{C\alpha1\text{-}6}$, M245 on the $_{245}MFXF_{248}$ motif was identified to account for the sub-domain rotation, as the M245 psi angles in the two structures differ by ~180° (Fig. 4.4B). As a consequence, the charge-bearing ridge of $FliG_{C\alpha1\text{-}6}$ coupled with MotA cytoplasmic domain was flipped by a two-fold symmetry about an axis through the Cα-C bond of M245. The two inverse orientated $FliG_{C\alpha1\text{-}6}$ also displayed distinct interacting pattern with ARM_C. In $HpFliG_{MC1}$, hydrogen bonds between side chain amine of Q325 and backbone carbonyl of N216 (3.43 Å) and between side chain of R217 and backbone carbonyl of Q325 (3.21 Å) were found, while in $HpFliG_{MC2}$, side chain amine of Q325 was bonded to backbone carbonyl of E243 (3.31 Å in $HpFliG_{MC2\text{-}A}$, 3.07 Å in $HpFliG_{MC2/B}$). Equivalent residue of Q325 in AaFliG and $TmFliG_{MC}$ is also involved in $FliG_{C\alpha1\text{-}6}$ and ARM_C interaction (Lee LK et al., 2010) (Fig. 4.5A). In addition, residue N216 was found to position the MFXF motif in place and mediate the respective orientation of $FliG_{C\alpha1\text{-}6}$. In $HpFliG_{MC1}$, side chain Oγ of N216 hydrogen bonded to backbone amide of F246 while side chain Nγ of N216 bonded to backbone carbonyl of

M245 in $HpFliG_{MC2}$ (Fig. 4.5B). These interactions may be associated to the relative stability of the structures. Alignment of ARM_C from $TmFliG_{MC}$ and AaFliG also consistently showed that MFXF motif is highly flexible. Among all the solved FliG structures, $FliG_{MC2}$ and $TmFliG_{MC}$ are closely resembled, while AaFliG is distant from $HpFliG_{MC2}$ by ~78° rotation of F246 phi angle. $FliG_{C\alpha1\text{-}6}$ of $HpFliG_{MC1}$ is uniquely arranged on the opposite side (Fig. 4.6A, B). Differences in the phi-psi angles of M245, F246 are summarized in Fig. 4.7.

To explicitly explain the rotational freedom of M245 psi and F246 phi in the MFXF motif, we observed that side chains of M245 and F246 are pocketed into the hydrophobic core of ARM_C and $FliG_{C\alpha1\text{-}6}$, respectively. When compared with residues flanking the motif, relatively less restrained M245 psi and F246 phi would be resulted. It is likely that the restriction on the backbone torsion of these two residues is Ramachandran constraints. When taken into account that rotational bias mutations mapped at or close to MFXF motif (equivalent residues of M245, T247, E249) and on helix 6 of $FliG_{C\alpha1\text{-}6}$ (equivalent residues of Q325) (Brown PN et al., 2007; Irikura VM et al., 1993), this flexible loop region potentiates the CCW/CW switching of the rotor. Mutation of these residues likely alters the orientation of $FliG_{C\alpha1\text{-}6}$.

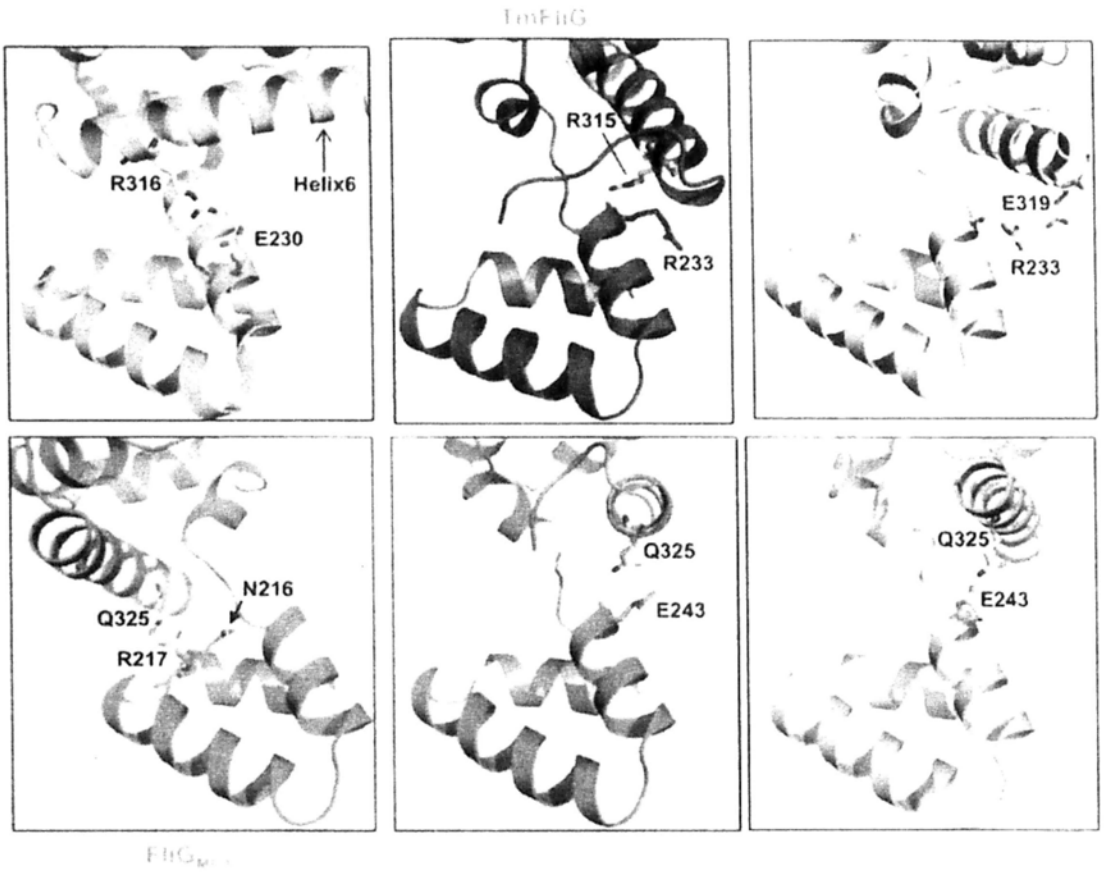

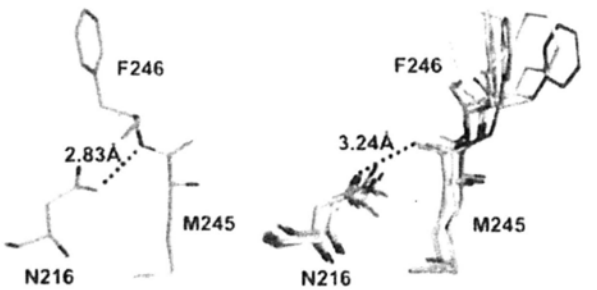

Fig. 4.5. Superimposition of all available FliG structures when ARM_C is aligned. **(A)** Residues involved in the interaction between Helix 6 of $FliG_{C\ 1\text{-}6}$ and ARM_C forming hydrogen bonds / salt bridges within 3.5 Å are shown as sticks. Residue Q325 (equivalent R316 in AaFliG and R315 in TmFliG) is colored in white. **(B)** Distinct hydrogen bond linking side chain of N216 and backbone of $_{245}MF_{246}$ in $HpFliG_{MC1}$ (left) and other FliG structures (right). Distance between side chain of N216 and backbone amide of F246 in $HpFliG_{MC1}$ and backbone carbonyl of M245 in $HpFliG_{MC2}$ is indicated. Sticks are colored as in panel A.

4.3.5 Interdomain flexibility of ARM_C and $FliG_M$

Conformations of the middle domains of the two FliG structures from *H. pylori* are nearly identical ($RMSD_{C\alpha}$= 0.379 Å). $Helix_{MC}$ packed closely to $FliG_M$ by extensive hydrophobic interactions made by residues between $Helix_{NM}$, $Helix_{MC}$ and $FliG_M$. These residues include F119, Y121, L122 on $Helix_{NM}$; V183, V184, V187, L191, L195, L198 on $Helix_{MC}$ and I125, L130, F133, I134, L144, I145, M149, I179 on middle domain (Fig. 4.4C). The conformation closely resemble to that of AaFliG and of $TmFliG_M$ co-crystallized with $FliM_M$, though the helix is slightly farther from $FliG_M$ in HpFliG, possibly due to F119 and Y121 in $Helix_{NM}$ pressed against $Helix_{MC}$ (Lee LK et al., 2010; Paul K et al., 2011). On the contrary, $Helix_{MC}$ dissociates from $FliG_M$ in $TmFliG_{MC}$ and $TmFliG_{MC}\Delta PEV$ (Brown PN et al., 2002; Minamino T et al., 2011) (Fig. 4.6C). As previously noted, $Helix_{MC}$ is amphipathic in nature with hydrophobic residues faced ARM_M and charged residues exposed to the solvent environment (Lee LK et al., 2010). A closely-packed arrangement of $Helix_{MC}$ stabilized by $FliM_M$ was observed in the co-crystallized structure (Paul K et al., 2011). Hence, $Helix_{MC}$-$FliG_M$ interaction is more likely biological relevant among different bacterial species rather than due to crystal contact as suggested by Minamino T et al. (Minaomino T et al., 2011).

Structural alignment of FliG also showed that $Loop_C$ which carries the conserved Gly-Gly motif is highly mobile. In Figure 4.6D, ARM_C of all FliG structures are aligned to compare the arrangement of $Helix_{MC}$. $Loop_C$ of HpFliG are more extended than $TmFliG_{MC}$ and AaFliG. $Helix_{MC}$ of chain A and B of $HpFliG_{MC/2}$ show displacement even in the same asymmetric unit. Three solvent exposed amino acids in $Loop_C$ disordered in $HpFliG_{MC1}$ are disordered. These observations, consistent with previous studies, suggested that $Loop_C$ is flexible (Brown PN et al., 2002; Lee LK et al., 2010; Minamino T. et al., 2011). The flexibility is important to switching since rotational-biasd or infrequent switching mutants have been isolated in $Loop_C$. It has been suggested that $Loop_C$ may be critical to control the relative orientations of $FliG_M$ to $FliG_C$ (Brown PN et al., 2002; Irikura VM et al., 1993; Van Way SM et al., 2004).

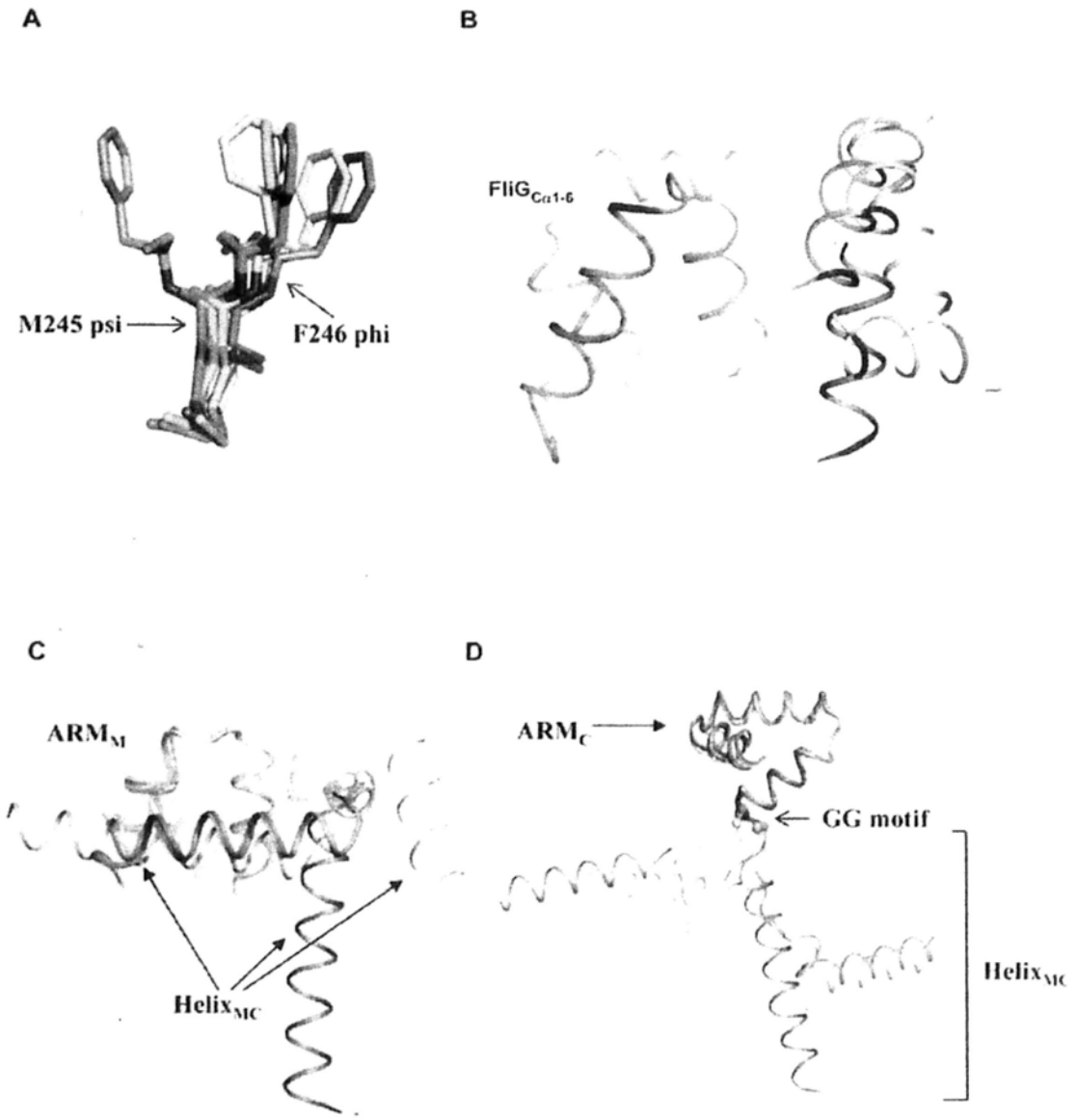

Fig. 4.6. Superimposition of all available FliG structures demonstrating flexibility at MFXF motif, Loop$_C$, and Loop$_M$. (A, B) Alignment through ARM$_C$ showed different backbone orientations of $_{245}$MF$_{246}$ that leads to multiple orientations of the charged ridge as shown in **(B)**. FliG$_{C\alpha 1\text{-}6}$ of HpFliG$_{MC1}$ and Helix 5 of all FliG structures are drawn. Equivalent charged residues that directly involved in interaction with MotA are colored in blue (R293) and red ($_{300}$EE$_{301}$). **(C)** Alignment of middle domain showing multiple arrangement of Helix$_{MC}$. Coloring scheme: HpFliG$_{MC1}$, green; HpFliG$_{MC2/A}$, orange; HpFliG$_{MC2/B}$, yellow; TmFliG$_{MC}$, magenta; TmFliG$_{MC}$ΔPEV, light pink; AaFliG, cyan. **(D)** The flexibility of Loop$_C$. Positions of GG motif (equivalent residues EG motif in AaFliG) are shown as spheres.

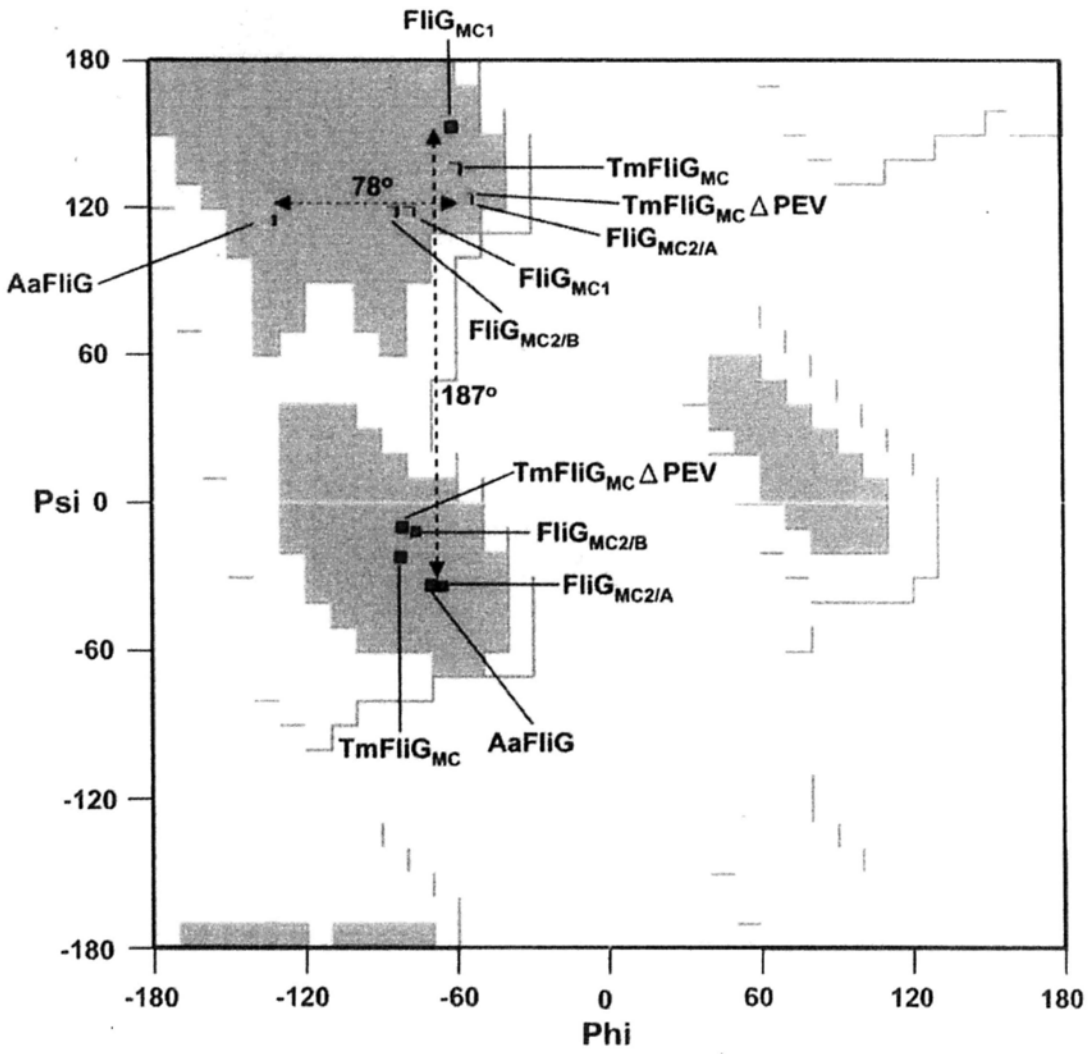

Fig. 4.7. Ramachandran plot showing phi-psi angles of M245 (blue) and F246 (green) from all available FliG structures. Dash line indicates the largest difference of M245 psi and F246 phi. The plot was calculated and modified from Coot (Emsley et al., 2010).

4.3.6 Biological importance of MFXF motif in flagellar motor switching

The 180° rotation of FliG$_{C\alpha 1\text{-}6}$ observed in the HpFliG$_{MC1}$ structure suggested that structural flexibility of MFXF motif is critical for flagellar motor switching. To validate our hypothesis, we mutated conserved residues at or surrounding the MFXF motif in *E. coli* and studied their effects on bacterial swimming. These residues included M245

(equivalent residue M233 in *E.coli*), F246 (F234), N216 (N204) and D250 (N238). The latter two residues hydrogen bonded to the backbone of the MFXF motif (Fig. 4.8A). *E. coli* FliG mutants each contained N204A/D/V/H, N238A, M233P, F234P or M233P/F234P double mutation were constructed using pTrc-EcFliG as a template. The immunoblotting results showed that the expression level of each FliG mutant was comparable to that of the wild type after transformation into DFB225 strain (Fig. 4.8B). From the swarming assay, N204A/D and F234P mutant strains showed significant impairment in soft-agar migration while N204V/H and N238A mutant strains displayed similar swarming activity to that of the wild type. Substitution of M233 with proline abolished bacterial motility as demonstrated from the M233P and M233P/F234P mutant strains (Fig. 4.8C and Table 4.3). The effect of these mutations on flagella formation was also examined by transmission electron microscopy (Fig. 4.8D). M233P and M233P/F234P mutant strains were non-flagellate. From the FliG crystal structures, side chain of M233 is embedded in a hydrophobic patch of ARM_C and may contribute to the structural stability of ARM_C. Mutation of M233 to proline likely induced a dramatic structural change to the MFXF hinge that either lowered the ARM_C stability or distorted the orientation of the C-terminal domain that inhibit its interaction with FliM for the motor switch assembly and the attachment of flagella export apparatus.

To further refine our hypothesis about the association of MFXF motif to switching mechanism, effect of these mutations on rotational switching in *E. coli* was studied by fixed time diffusion analysis. This assay is based on modeling the swimming behavior of bacterium to that of particle diffusion (Lowenthal AC et al., 2009). Basically, the diffusion exponent α measures how close the swimming behavior is to pure diffusion (α = 1). A tumbling bacterium will have an α value close to 1 while a bacterium moves relatively straight will have an α value close to 2. This model has been applied to examine directional changes of *E. coli* (Lowenthal AC et al., 2009). From our results, mutations N204H and N238A had no influence on swimming behavior when compared to the wild type. However, CW bias was found in mutant strains N204V, N204D, N204A and F234P. These results are consistent with the observation from the video tracking of swimming path (Fig. 4.8E). The overall results from fixed time diffusion analysis is also in line with the swarming data, except N204V. This mutant strain exhibited slight tumbling bias in swimming but the effect was not shown from soft agar assay. The soft agar assay may not be sensitive enough to detect the subtle change in rotational bias. A previous study reported that F234A mutation caused severe tumbling bias (Lloyd SA & Blair DF, 1997), this is very similar to the phenotype of F234P mutant. The increase tumbling frequency of N204A/D/V and F234P suggested that these mutations led to various degrees of CW rotational bias of the rotor, while N204H and N238A had no significant effect towards rotational switching.

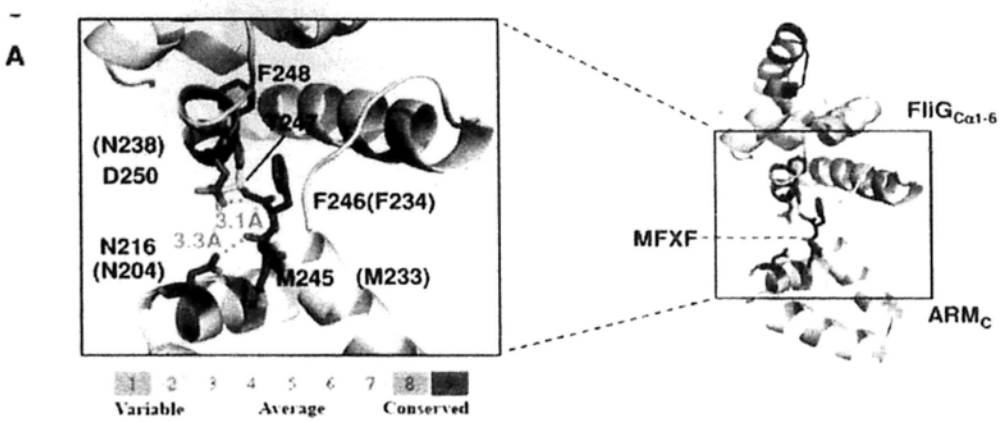
A
F248
(N238)
D250
F246(F234)
3.1A
3.3A
N216
(N204)
M245 (M233)
FliG$_{Cα1-6}$
MFXF
ARM$_C$
1 2 3 4 5 6 7 8
Variable
Average
Conserved

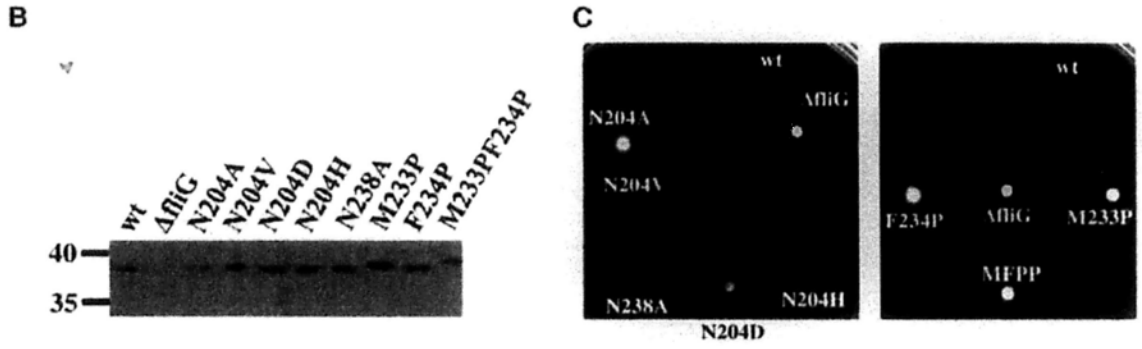
B
wt
ΔfliG
N204A
N204V
N204D
N204H
N238A
M233P
F234P
M233PF234P
40
35
C
wt
ΔfliG
N204A
N204V
N238A
N204H
N204D
wt
F234P
ΔfliG
M233P
MFPP

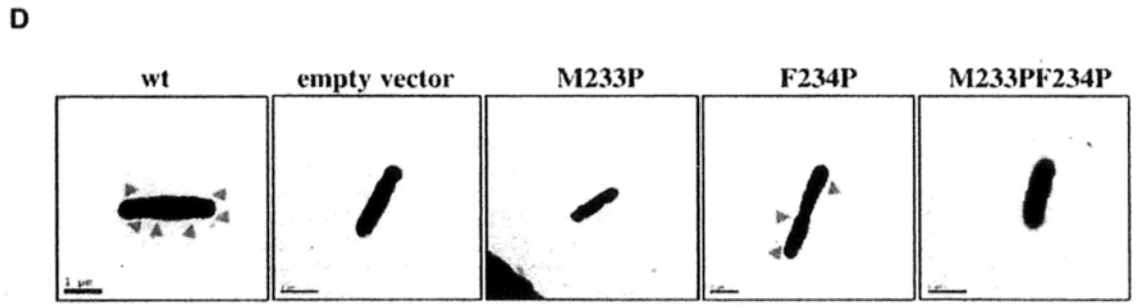
D
wt
empty vector
M233P
F234P
M233PF234P

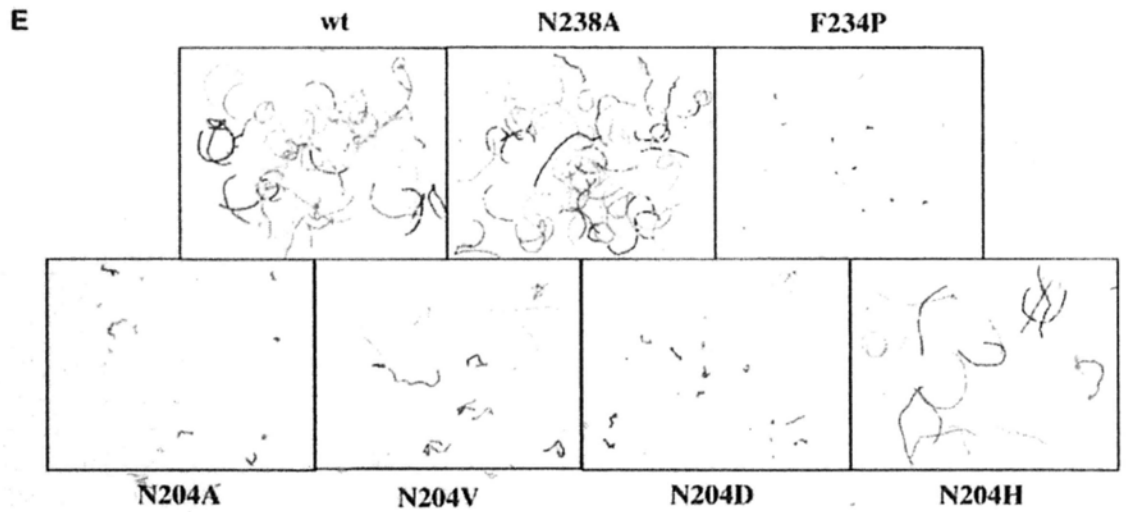
E
wt
N238A
F234P
N204A
N204V
N204D
N204H

Fig. 4.8. Effects of FliG mutations on swimming behavior. (A) Conservation of FliG amino acid sequences. Sequences from 50 microbial species were analyzed by Consurf (http://consurf.tau.ac.il/) (Glaser F et al., 2003). Only $FliG_C$ domain of $HpFliG_{MC2}$ is drawn and regions in proximity to the MFXF motif are highlighted (inbox). Residues related to the stability of MFXF motif are shown as sticks. Hydrogen bond distances between N216 and M245 as well as D250 and T247 are shown. Residues are numbered according to *H. pylori* (equivalent residues in *E. coli* are bracketed) **(B)** Expression of wild type FliG and its various mutants in DFB225. Whole cell lysate were immunoblotted with anti-FliG antibody. **(C)** Soft agar assay. 1 µl overnight culture of cells was spotted on 0.3 % soft agar and incubated at 30°C for 7 hours. **(D)** Electron micrograph of *E. coli* showing flagellar formation in wild type and F234P strains. M233P and M233P/F234P strains were found to be non-flagellate. Flagella are indicated by red arrow. Representative results are shown. **(E)** Swimming tracks of complemented strains used in the calculation of diffusion coefficient. 4 s swimming tracks are plotted with the same scale.

Table 4.3. Effects of FliG mutations on swarming and swimming behavior.

Strain	Diameter / cm	Diffusion coefficient
Wild-type	2.32±0.23 (n=6)	1.7533±0.0182 (n>50)
N204A	0.68±0.06 (n=6)	1.3238±0.0148 (n=23)
N204V	2.43±0.2 (n=6)	1.6897±0.0040 (n=29)
N204D	1.22±0.04 (n=6)	1.5112±0.0125 (n=37)
N204H	2.14±0.13 (n=6)	1.7501±0.0174 (n=35)
N238A	1.95±0.29 (n=6)	1.7709±0.0171 (n=>50)
F234P	0.51±0.09 (n=4)	1.2876±0.0163 (n=33)

4.3.7 Verification of multiple orientations of $FliG_C$ by *in vitro* cysteine cross-linking

Comparison of all solved FliG structures revealed that MFXF linked $FliG_{Cα1-6}$ can be in different orientations relative to ARM_C. Previous section has demonstrated the physiological significance of the flexibility of MFXF motif *in vivo*. We next verified the presence of multiple orientations of $FliG_{Cα1-6}$ in solution by intra-molecular cysteine cross-linking.

From the crystal structures, it was noted that conserved Q325 in $FliG_{Cα1-6}$ is in close proximity to residues in ARM_C – R217 in $FliG_{MC1}$ (4.6 Å) and E243 in $FliG_{MC2}$ (3.59 Å) (Fig. 4.9A). We introduced double cysteine residues in FliG, one at Q325 and the other in one of the helices of ARM_C. A total of four double cysteine mutants Q325C/R209C, Q325C/R217C, Q325C/S222C and Q325C/E243C were created, whereas a single cysteine mutant Q325C was used as a control. We expected that if MFXF motif is intrinsically flexible, $FliG_{Cα1-6}$ will orient differently and intra-molecular disulfide linkage will be observed in these double cysteine mutants. From Figure 4B, all four double mutants showed mobility shift in SDS-PAGE after cross-linking by the addition of catalyst Cu (II) (1,10-phenanthroline)$_3$, suggesting that intra-molecular disulfide linkage were formed. Mutants Q325C/R209C and Q325C/S222C showed prominent downward shift while a smaller quantity of

Q325C/R217C showed band shift (Fig. 4.9B). A complete upward shift of Q325C/E243C upon oxidation was observed. No mobility shift was found in the control mutant Q325C.

Alternative approach was applied to examine the intra-crosslinking product by using fluorescent 5'IAF to probe free cysteine residues (Bass RB et al., 2007). If cysteines are cross-linked, they will be protected from haloalkylation by 5'IAF and this will lead to a reduced fluorescence signal. From Figure 4.9C, all four double mutants showed a reduction in the fluorescence intensity upon 5'IAF haloalkylation. Furthermore, intra-disulfide bond formation of Q325C/R209C and Q325C/E243C double mutants were verified by mass spectrometry (data not shown). When taken together, these data strongly suggested that MFXF motif is intrinsically flexible to allow multiple orientations of $FliG_{C\alpha 1\text{-}6}$ to ARM_C in solution. From the $HpFliG_{MC2}$ structure, Q325 is closed to E243 (Cβ-Cβ distance 6.4 Å) but distant from R217 and S222 (Cβ-Cβ distance >20 Å) (Fig. 4.9A). On the other hand, Q325 and R217 are nearby (Cβ-Cβ distance 6.7 Å) in $HpFliG_{MC1}$. If $FliG_{C\alpha 1\text{-}6}$ is restricted to one orientation, certain double cysteine mutations should not be able to form intra-disulfide cross-linkage.

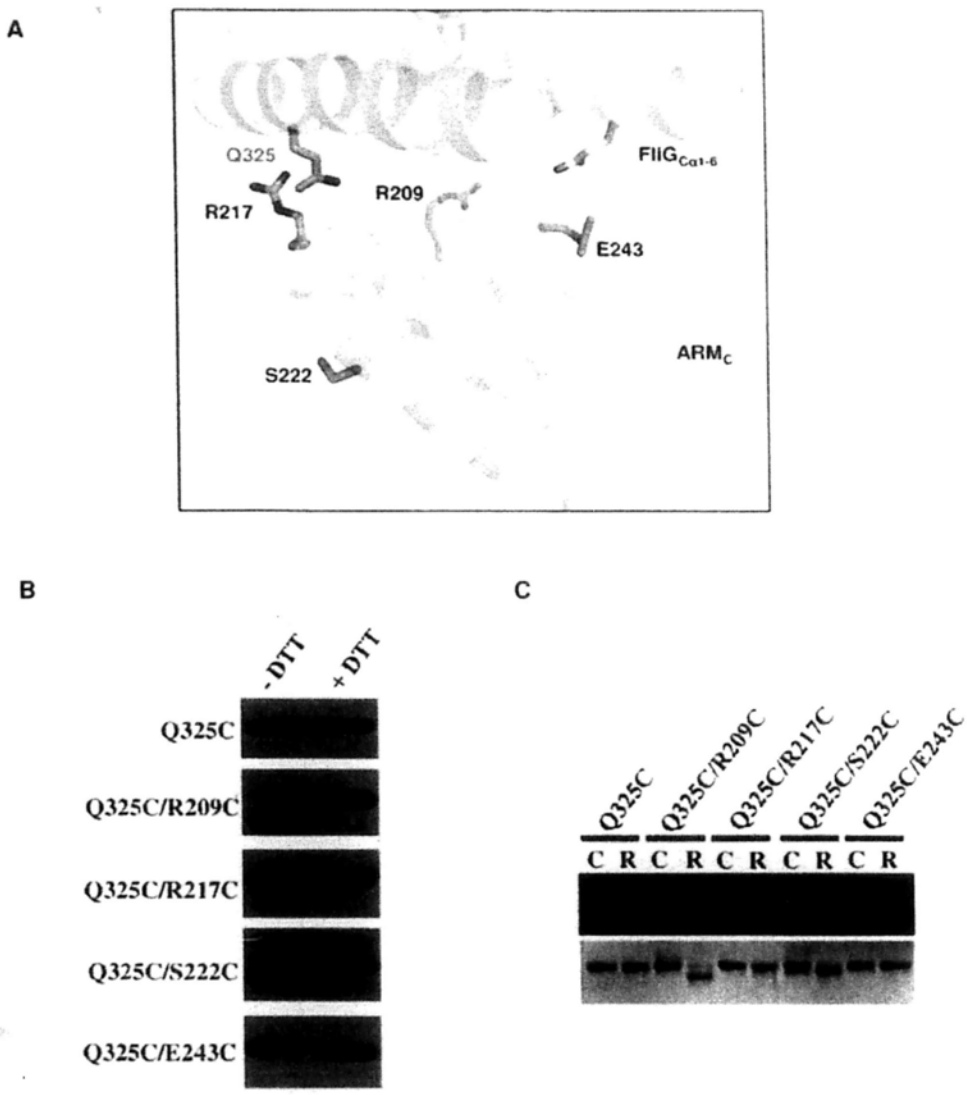

Fig. 4.9. Molecular movement of FliG$_{C\alpha1-6}$ revealed by *in vitro* cysteine cross-linking. (A). Cysteine residues are introduced at the interface between ARM$_C$ and Helix 6 of FliG$_{C\alpha1-6}$ of HpFliG$_{MC1}$ (green) and HpFliG$_{MC2}$ (yellow). ARM$_C$ of the two structures are aligned. Residues mutated to cysteine are shown as stick. Only residues on HpFliG$_{MC1}$ are shown, except Q325 of HpFliG$_{MC2}$ that is also indicated. **(B)** Gel mobility shift assays. After cross-linking, samples were added with loading dye with or without 20 mM DTT and subjected to a 16 × 18 cm 11% SDS-PAGE analysis. (C) Haloalkylation by 5'IAF. Samples with (R) or without (C) Cu (II) (1,10-phenanthroline)$_3$ were loaded onto a 8 × 7.3 cm SDS-PAGE. After electrophoresis, gel was immediately visualized under UV transilluminator (upper panel) followed by staining with Coomassie Blue (lower panel). Experiments were repeated for 4 times and representative images are shown.

4.4 Discussion

In *E. coli*, FliG is the cytoplamic ring protein localized closest to inner membrane (Thomas DR et al., 2006). The interaction studies (FliF-FliG and FliG-FliM) reported here consistently supported that FliG is organized and function in a similar manner as in other organisms. Domain movement of FliG as suggested from the structures and biochemical studies can likely be applied to the border understanding on the general switching mechanism.

Bacterial flagellar motor is a unique bidirectional nano-rotary machine powered by the proton/sodium ion gradient across the cell membrane. For proton driven $MotA_4B_2$ stator, torque generation involves protonation and de-protonation of an aspartic acid residue in MotB and association of MotA with FliG of the motor switch complex (Kojima S & Blair DF, 2001; Zhou J et al., 1998). Accumulating evidences have shown that that the C-terminal domain of FliG bearing conserved charged residues R293, E300 and E301 (in *H. pylori* sequence) is the primary site for electrostatic interaction with the cytoplasmic region of MotA (Zhou J et al., 1998). Switching of rotation between CCW and CW directions is mediated by the coupling of chemotactic signaling pathway with the motor switch complex (Welch M et al., 1993). It is believed that the binding of phosphorylated CheY to FliM/FliN induces conformational changes of FliG and subsequently turns the flagellar rotation from CCW to CW directions

(Brown PN et al., 2002; Sarkar MK et al., 2010). One of the interesting aspects of the flagellar motor is the mechanical movement of FliG associated to rotational switching. In the present study, comparison of the two crystal structures $HpFliG_{MC1}$ and $HpFliG_{MC2}$ reveals a two-fold rotation of $FliG_C$ domain. More specifically, the rotation involves 180° rigid body movement of $FliG_{C\alpha1\text{-}6}$ relative to ARM_C prompted by flipping the M245 psi angle at the MFXF motif. In conjunction with the *in vivo* mutagenesis and swimming assays, the biological importance of the flexibility of MFXF motif and of a conserved residue N216 directly interacting with the motif, in rotational switching is further demonstrated. We also demonstrated the multiple orientations of $FliG_{C\alpha1\text{-}6}$ to ARM_C in solution by showing intra-disulfide linkage between Q325 on $FliG_{C\alpha1\text{-}6}$ and various distant residues on ARM_C, suggesting that the MFXF motif is intrinsically flexible. Our findings in fact are agreed with earlier mutagenesis studies that residues at or near the MFXF motif (N214, M245, F246, T247 and E249) and residue Q325 at the interface between $FliG_{C\alpha1\text{-}6}$ and ARM_C are associated with CW rotation bias (Brown PN et al., 2007; Irikura VM et al., 1993; Lloyd SA & Blair DF, 1997) (Fig. 4.10).

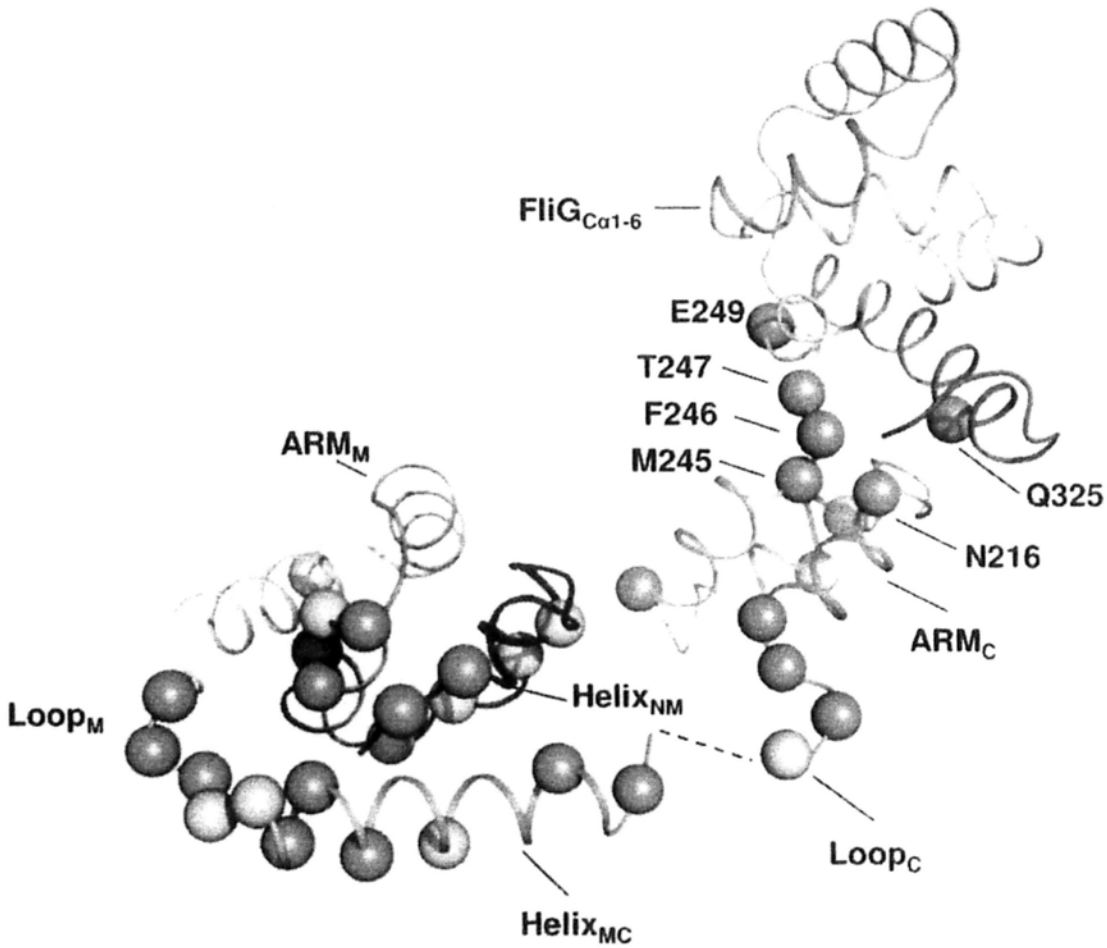

Fig. 4.10. Rotational bias mutations isolated from previous studies are mapped on HpFliG$_{MC1}$. Coloring scheme: CW bias – orange spheres; CCW bias – cyan spheres; both CW and CCW bias: yellow spheres. Residues at FliG$_{C\alpha 1\text{-}6}$-ARM$_C$ interface are labeled.

Structural comparison of FliG molecules highlighted the movement of FliG$_{\alpha C1\text{-}6}$ mediated by the flexibility of MFXF motif. This observation is in concordance with our *in vitro* cross-linking assays, which showed that Q325 at FliG$_{\alpha C1\text{-}6}$ can be cross-linked with multiple distinct sites on ARM$_C$. Rotational movement of FliG$_C$ has been suggested from previous study using *in vivo* double cysteine cross-linking (Lowder BJ

et al., 2005). It was found that oxidation by iodine resulted in cross-linkage between two FliG molecules via $_{309}$KIK$_{311}$ at the loop connecting helices 5-6 of FliG$_{C\alpha 1\text{-}6}$. However, it is not understood how FliG$_C$ moieties are arranged in the motor to yield the results. Taken into account the EM map of CW biased motor from *S. typhimurium* (Thomas D. et al., 2001) and the solved FliG structures (Brown PN et al., 2002; Lee LK et al., 2010; Minamino T et al., 2011), we constructed a model which helped to explain the observation. It is commonly agreed that FliG$_C$ is positioned at the outer globule of the C-ring in the EM map, with the charged ridge of FliG$_{C\alpha 1\text{-}6}$ facing upward toward the membrane and ARM$_C$ at the bottom for FliM interaction, consistent with recently proposed assembly model (Brown PN et al., 2007; Paul K et al., 2011; Lloyd SA et al., 1999). Accordingly, we docked the C-terminal domain of HpFliG$_{MC1}$ to the outer ring of EM map with 34-fold symmetry (either 34 or 26 FliG molecules with local 34 fold symmetry) and a distance of 40 Å between central positions of adjacent FliG$_C$ molecules. In the context that FliG$_{C\alpha 1\text{-}6}$ can undergo molecular rotation, $_{309}$KIK$_{311}$ from adjacent FliG$_C$ molecules will be brought within cross-linking distance if they switch between FliG$_{MC1}$-FliG$_{MC2}$ and FliG$_{MC2}$-AaFliG conformations (Fig. 4.11A). Results from our mutagenesis and swimming assays offer new insights to address the molecular movement of FliG$_C$ in CW and CCW rotational states. The side chain of highly conserved N216 is hydrogen bonded to the backbone amide of F246 in

$HpFliG_{MC1}$ and to the carbonyl of M245 in $HpFliG_{MC2}$/$TmFliG_{MC}$/AaFliG (Fig. 4.5B). We introduced mutations to disrupt these hydrogen bond interactions to evaluate the functional role of these two structural conformations in motor switching. It was expected that mutation N216D would only retain the hydrogen bond to F246 and is favorable to $HpFliG_{MC1}$ while N216H is favorable to the opposite orientation. Intriguingly, the swimming behavior of N216H was comparable to that of the wild type, but N216D mutant clearly showed CW rotational bias. This implies that N216 – F246 hydrogen bonding is critical to the stability of FliG conformation in CCW. Likewise, mutation to hydrophobic Val slightly increased CW bias. Therefore, it is very likely that the $FliG_C$ conformation in $HpFliG_{MC2}$/$TmFliG_{MC}$/AaFliG represents the conformations in CCW state while $HpFliG_{MC1}$ represents the CW conformation. The reason for severe CW bias in N216A is less understood at this stage. In the absence of CheY, flagellum rotates in default CCW rotation. $FliG_C$ may be intrinsically more favorable to $HpFliG_{MC2}$/$TmFliG_{MC}$/AaFliG conformations as the default CCW state. We speculate that any interruption (e.g. N216A) of the default CCW rotations would produce CW bias. This may explain why all mutations at this motif (e.g. M235, F236) and the cleft between $FliG_{C\alpha1\text{-}6}$ and ARM_C (e.g. Q325) were reported to give CW bias (Brown PN et al., 2007; Irikura VM et al., 1993; Lloyd SA & Blair DF, 1997).

The mutagenesis studies were performed in *E. coli* system because of various biochemical and mutagenesis data were available for comparison. The mutation sites chosen were highly conserved among various species and given the structural homology of $FliG_C$ among species from mesophilic and thermophilic bacteria, it is likely that the results in *E. coli* system can be extended to other bacterial systems. However, we do not exclude the possibility of variations on the regulation of switching among bacterial species and ultimately the effect of mutations should be done in *H. pylori*.

Nakamura et al., has recently proposed that the symmetrical torque generation process in both CCW and CW directions may be resulted from 180° rotation of the C-terminal domain of FliG so that the same molecular surface but in opposite orientation is displayed to MotA (Nakamura S et al., 2010). The two FliG crystal structures presented here provide the first ever structural evidence to reveal the two-fold rotation of $FliG_C$ domain and insights into the underlying mechanism. Although the structure of $MotA_4B_2$ remains unresolved, organization of the transmembrane segments based on cysteine cross-linking experiments was modeled (Kim EA et al., 2008). The two MotA subunits which directly involve in forming two proton channels with MotB dimer, are related by two-fold symmetry. The cytoplasmic region between transmembrane helices α2 and α3 bearing oppositely charged residues

for $FliG_C$ interaction likely follows the same arrangement, such that only one of the MotA domains will correctly align with the electrostatic charged residues on $FliG_C$ (Fig. 4.11B). When $FliG_C$ changes from $HpFliG_{MC1}$ to $HpFliG_{MC2}$ conformations, or vice versa, $MotA_4B_2$ would switch to utilize the opposite MotA subunit for FliG interaction to allow symmetrical torque generation in CW/CCW directions (Fig. 4.11B). Given the importance of a rotatable $FliG_{\alpha C1\text{-}6}$ in switching, one may expect that affecting the movement of $FliG_{\alpha C1\text{-}6}$ would lead to rotational bias. Interestingly, recent study has identified c-di-GMP binding protein YcgR that directly binds to $FliG_{C\alpha1\text{-}6}$ and causes CCW rotational bias. The binding of YcgR reduced the $_{309}KIK_{311}$ cross-linked product (Paul K et al., 2010). From our proposed model, interaction of YcgR and $FliG_{C\alpha1\text{-}6}$ possibly hinders the flexibility of C-terminal domain and influences the interconversion between different conformations.

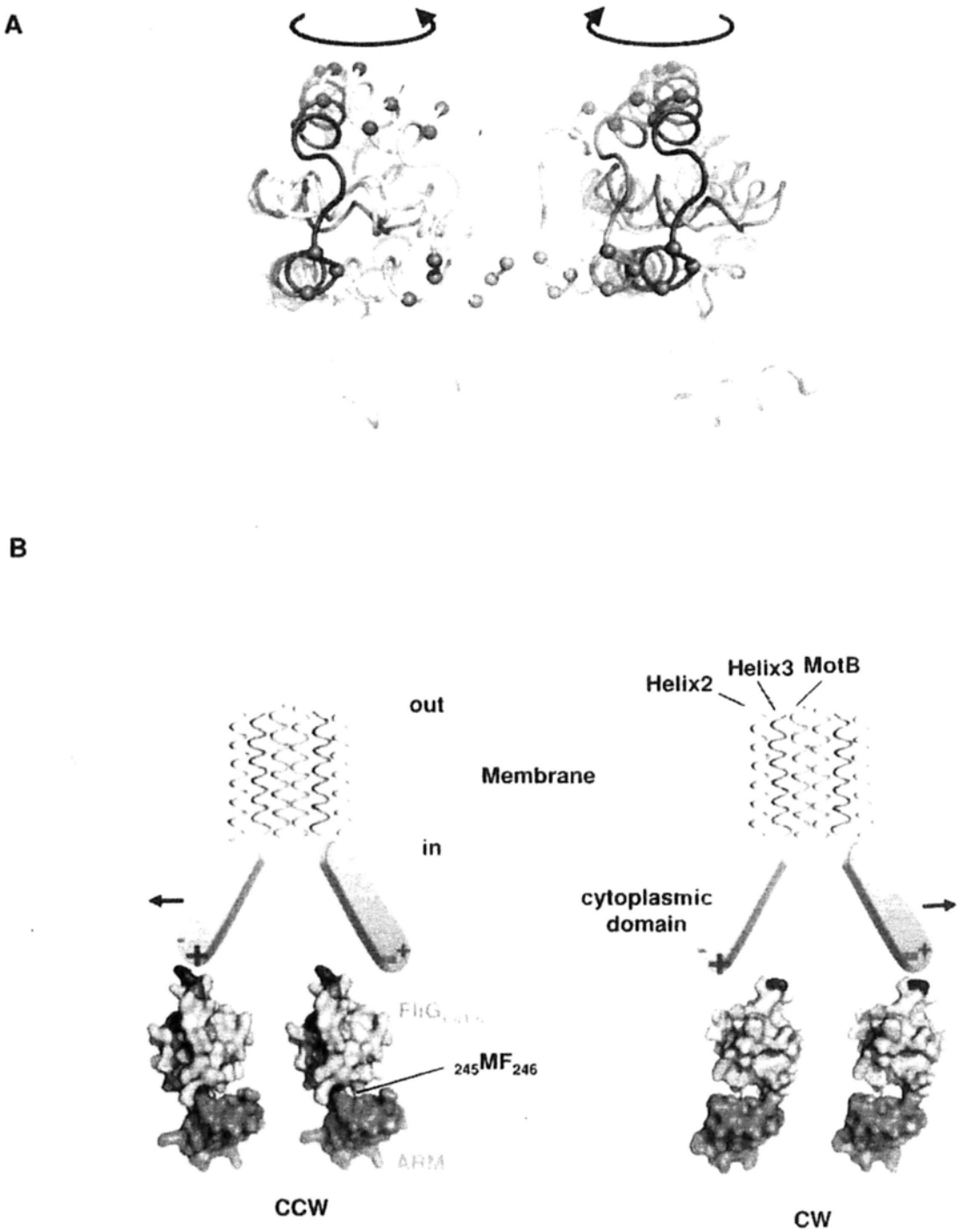

Figure 4.11. Models of rotational movement of $FliG_C$. (A) Two $FliG_C$ domains are docked to the EM map (not shown) as discussed in the text and $HpFliG_{MC2}$ are morphed to the conformations of $HpFliG_{MC1}$ (left) and AaFliG (right). Morphed structures are colored from blue to white ($HpFliG_{MC2}$ to $HpFliG_{MC1}$) and from red to yellow ($HpFliG_{MC2}$ to AaFliG). Conformational flexibility of adjacent $FliG_C$ molecule allows

$_{309}$KIK$_{311}$ (magenta sphere) to be within cross-linking distance. Key charge residues important for interaction with MotA are shown as blue (R293) and red ($_{300}$EE$_{301}$) spheres. Morphing was done using Chimera (Pettersen EF et al., 2004). **(B)** Model of symmetrical torque generation process. Proposed orientation of $FliG_{MC}$ in CCW (left) and CW (right) states. Transmembrane helices of $MotA_4B_2$ complex are adopted and modified from Kim at el. (Kim EA et al., 2008). Only Helices 2 (cyan) and 3 (magenta) close to the transmembrane helix of MotB (yellow) are drawn. The cytoplasmic domains connecting helices 2 and 3 that contain conserved charged residues for $FliG_C$ interaction are shaded in blue. The positive and negative charges are labeled as (+) and (-), respectively. Molecular surface of $FliG_{C\alpha 1\text{-}6}$ (cyan) and ARM_C (orange) are presented. Critical charges for MotA interaction are colored in blue (R293) and red ($_{300}$EE$_{301}$).

It is believed that torque generation occurs when MotA presses against an angled surface of $FliG_C$. Alignment of multiple FliG structures suggested that $FliG_{\alpha C1\text{-}6}$ can be arranged both tangentially or radially to the periphery of outer C ring by rotating F246 phi angle (Fig. 4.12A). Both arrangements are possible since the domain is not restricted by other switch proteins. Patterns of synergism observed from FliG and MotA double mutants indicates that charged residues (K276, R293, E300, K309 in *H. pylori*; K264, R281, D288, R297 in *E. coli*) that interact with a conserved Glu (Glu97 in *H. pylori*; Glu98 in *E. coli*) on MotA are distantly positioned on $FliG_C$ (Zhou J et al., 1998). Domain flexibility of $FliG_C$ may allow different surfaces along the charge-bearing ridge to be displayed to MotA during rotation (Fig. 4.12C).

Flagellar motor switching is highly cooperative. Recent studies support conformational spread model in explaining the switching event. Cooperative switching response is achieved by stochastic coupling and conformational spread of neighboring subunit sharing a particular state (Duke TA et al., 2001; Bai F et al., 2010). Considering $FliG_C$ packed in a local 34-fold symmetry in the outer C-ring, the arrangement of $FliG_{\alpha C1\text{-}6}$ likely influences adjacent FliG molecules. Adjacent $FliG_{\alpha C1\text{-}6}$ share similar conformation would be more favorable to avoid steric clash (Fig. 4.12A). We speculate that the conformational dynamics of FliG would be important to the highly cooperative response of the switch. Further study will be needed to address how the intra- and inter-molecular movement of FliG links to the switching response.

Rotational bias mutations have been identified at $FliG_M$-$Helix_{MC}$ interface, $Loop_C$ as well as two distinct FliM-FliG interfaces near the EHPQR motif and the conserved hydrophobic patch of FliG (Brown PN et al., 2007; Paul K et al., 2011; Irikura VM et al., 1993; Van Way SM et al., 2004). It has been proposed that motor switching involves CheY-mediated conformational change of FliM that alters the relative movement of $FliG_C$ to $FliG_M$ connected by $Helix_{MC}$ and $Loop_C$ (Brown PN et al., 2007; Paul K et al., 2011). While how the relative domain movement is related to rotational bias remains unclear, it is possible that the movement induced by FliM is transmitted through ARM_C to disturb the $FliG_{\alpha C1\text{-}6}$ – ARM_C interface (e.g. Q325 – ARM_C interaction) and increases the probability of $FliG_{\alpha C1\text{-}6}$ in CW orientation.

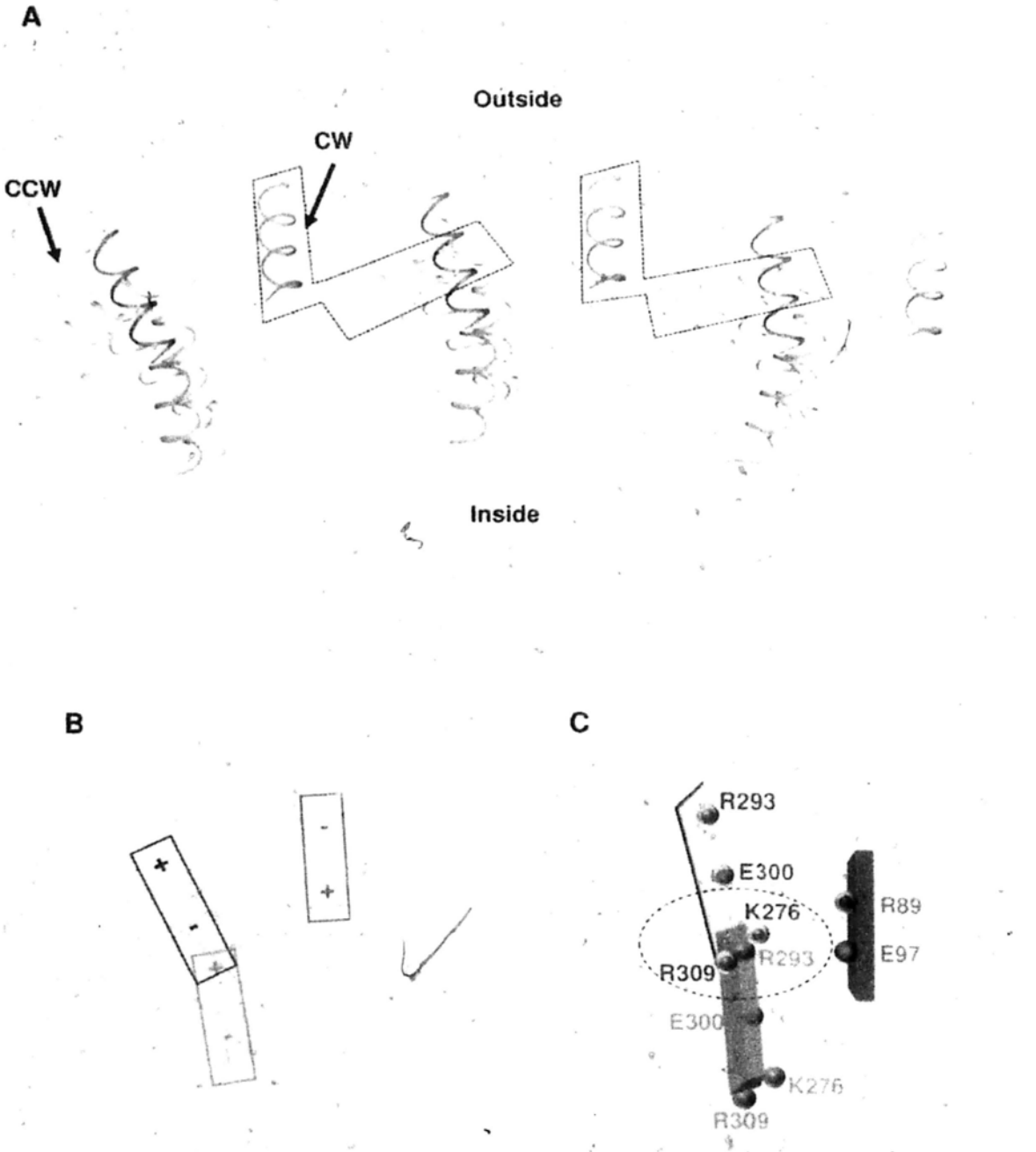

Fig. 4.12. Docking of all the $FliG_C$ structures on the torque ring highlights the possible spatial arrangement of charged ridge. (A) $FliG_C$ are aligned through ARM_C which is constrained by FliM interaction. Only helix 5 of $FliG_{C\alpha 1\text{-}6}$ is drawn Top view (from membrane to cytosol) shows the charged ridge of three consecutive $FliG_C$ (outlined in grey). The structures are colored according to Fig. 4.6. The arrangement of charges that are primary importance to MotA interactions are outlined in panel **(B)**. Conformations of adjacent molecules that cannot coexist are highlighted by dashed line.

(C) Schematic diagram showing the hypothesized FliG-MotA interface. Relative positions of $HpFliG_{MC2/A}$ (orange) and $TmFliG_{MC}$ (purple) are shown. Charged residues that interact with conserved Glu on MotA (E97 in *H. pylori*) (Zhou J et al., 1998; Lloyd SA et al., 1999) are drawn as sphere and labeled. Note that R293 and R309/K276 are positioned at the two ends of the charged ridge. Domain movement of $FliG_C$ would bring these residues close to the proposed position of MotA (Circled).

Lee LK et al., recently proposed a model of switching mechanism deduced from structural differences between AaFliG and $TmFliG_{MC}$, including the "open" and "closed" interaction of $Helix_{MC}$-$FliG_M$ interaction and a conformational changes of $FliG_{C\alpha 1\text{-}6}$ by rotation of M245 psi by ~26° and F246 phi by ~78° (Lee LK et al., 2010). Since most CW bias mutants isolated were at the $Helix_{MC}$-$FliG_M$ interface, they proposed that $TmFliG_{MC}$ represented CW conformation and AaFliG represented the opposite. Switching was explained by assuming co-operative conformational changes of $Helix_{MC}$ and MFXF motif that leads to reversal of charge ridge. Considering all available FliG structures, we do not observe any simple correlation between $Helix_{MC}$ and MFXF motif. Instead, $FliG_{MC1}$ and $FliG_{MC2}$ are identical in middle domain but they differ in $Helices_{C1\text{-}6}$ by 180° rotation, suggesting that there may not be any direct mechanical relationship between the two structural elements. Our model takes into account our mutagenesis assays at the sites at and near MFXF motif, thus it is more valid to demonstrate the conformation changes of $FliG_C$ during switching.

A long-lasting question is how individual switch component assembles into a motor switch complex. Analysis of the crystal packing of $HpFliG_{MC1}$ and $HpFliG_{MC2}$ showed interaction between ARM_M and ARM_C of adjacent symmetry molecules. Such ARM_M-ARM_C arrangement aligned well with available FliG structures in their respective crystal packing (Brown PN et al., 2002; Lee LK et al., 2010; Minamino T et al., 2011), despite these structures are crystallized in different crystallographic symmetry (Fig. 4.13A, B). Interestingly, symmetry molecules in $HpFliG_{MC1}$ crystal are packed in a linear array with intermolecular distance of 4 nm that is close to the intermolecular spacing of 3.9 nm in the outer C ring of the EM model (Thomas DR et al., 2006; Young HS et al., 2003) (Fig. 4.13C). However, recent *in vivo* study in *E. coli* did not support this model as no direct $FliG_M$-$FliG_C$ binding was observed (Paul K et al., 2011). Further investigation on the biological relevance of ARM_M-ARM_C interaction *in vivo*, if any, is required.

Dynamic of flagellar motor implies that the turnover of specific components (e.g. FliM and FliN) and structural flexibility of multi-domains containing components are needed (Delalez NJ et al., 2010; Fukuoka H et al., 2010). This makes this biological rotary device more fascinating, but also more challenging to be understood. In summary, the structural and molecular genetics analysis presented here not only reveal the high conservation of individual structural domain of FliG, but also illustrate the relationship

between multiple states of $FliG_C$ and CW/CCW rotations. The mechanistic details of the intrinsic flexibility of $FliG_C$ would provide a fundamental basis to unravel the switching mechanism of flagellar motor.

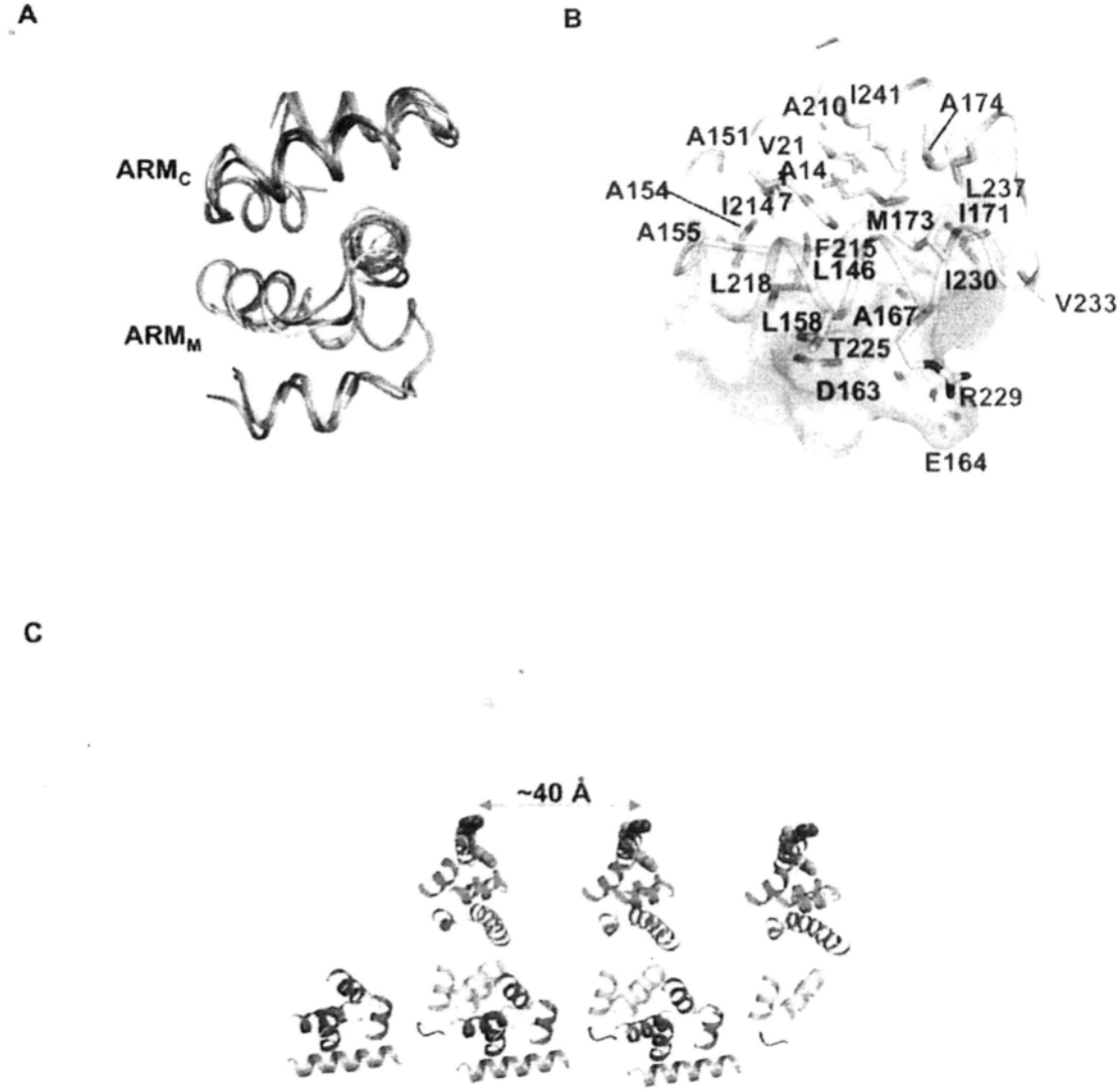

Fig. 4.13. ARM_M-ARM_C interactions. (A) Structural alignment of ARM_M-ARM_C from $HpFliG_{MC1}$ (green), AaFliG (cyan) and $TmFliG_{MC}$ (magenta) ($HpFliG_{MC1}$ – $TmFliG_{MC}$ RMSD = 0.96 Å, $HpFliG_{MC1}$ – AaFliG RMSD = 0.86 Å) (Pymol). **(B)** Binding interface between ARM_M and ARM_C. The molecular surface of ARM_M is shown and colored by electrostatic potential, with a contour level ± 5 kT (APBS)

(Baker NA et al., 2001). Residues of ARM_M (deepteal, labeled in blue) and ARM_C (yellow, label in brown) on the interface are presented as sticks. **(C)** $FliG_{MC}$ molecules are arranged as linear array from the crystal lattice of $HpFliG_{MC1}$. Secondary structures are colored according to Figure 4.4A. Conserved charged residues on Helix 5 of $FliG_{C\alpha 1\text{-}6}$ are shown as sphere. Note that the central position of adjacent molecule is separated by ~40 Å.

Chapter 5

Structural and functional characterization of FliY from *Helicobacter pylori*

5.1 Introduction

An uncharacterized switch protein FliY was identified from the genomic sequence of *H. pylori*. Amino acid sequence analysis of FliY indicates its N-terminal domain ($FliY_N$) belongs to CYX phosphatase family with EXXXN motif conserved among ε-proteobacteria; whereas its C-terminus contains a FliN-like domain ($FliY_C$) (Section 1.6.1) (Bischoff & Ordal, 1992). Deletion of FliY in *H. pylori* is partially non-flagellate while an additional disruption of FliN is completely non-flagellate, suggesting that FliY is a switch protein and it shares a functionally reductant role in flagellation with FliN (Lowenthal AC et al., 2009).

However, how FliY interacts with other switch proteins remains unclear. Furthermore, the biological function of its individual N- and C- terminal domain in motility has not been demonstrated. This section aims to unravel the roles of FliY in motility and its organization in the switch protein complex. The interaction of FliY and $FliY_C$ with FiN was investigated by co-expression and co-purification strategy. Purified complexes were subjected to crystallization trial. Further, the binding of FliY/FliN complex to FliH was studied by pull down experiment. The *In vivo* function of $FliY_C$ was examined by complementation of *ΔfliY* mutant the motility phenotype was characterized by swarming assay and electron microcopy. Further, the putative phosphatase activity of $FliY_N$ towards CheY was studied by Enzchek Phosphate Kit assay.

5.2 Materials and methods

5.2.1 Cloning, expression and purification of FliY and FliN proteins

FliY (HP1031), $FliY_N$ (residues 1 – 195), $FliY_C$ (residues 198 – 287) were cloned into pGEX-6p-1 vector while FliN (HP0584) was cloned into pAC28m vector according to standard protocol as described in Section 2.2.1. pGEX-6p-1-FliY or –$FliY_C$ was co-transformed with pAC28m-FliN in *E. coli* strain BL21 and were co-expressed by induction with 0.3 mM IPTG under growth conditions at 16°C for overnight. The same growth condition was applied for the expression of $FliY_N$. $FliY_N$ was purified according to protocol for the purification of GST-tagged proteins (Section 2.2.1). For co-purification of FliY/FliN, clear cell lysate was first purified by Ni-NTA resin with buffer containing 20 mM imidazole. After washing, proteins were eluted with 200 mM imidazole and immediately incubated with GST resin with the addition of 4 mM DTT and 0.5 mM EDTA. The GST tag was cleaved and the eluted protein was further subjected to size exclusion chromatography. For purification of proteins in GST pull down experiment, proteins were eluted with buffer containing 20 mM reduced glutathioine. Buffer conditions are summarized in Appendix 5.1. Purified FliH was provided by a colleague in Dr. Au's lab (Lam WW et al., 2010).

5.2.2 GST pull down assay

GST-FliY/His-FliN, GST-$FliY_C$ / His-FliN were co-expressed and GST, GST-$FliY_N$ were individually expressed in *E. coli* strain BL21 and purified by affinity chromatography followed by gel filtration. 1 ml 0.54 μM GST, GST-FliY/FliN, GST-$FliY_C$ /FliN or GST-$FliY_N$ was incubated with 30 μl GST resin pre-equilibrated with

buffer 150 mM NaCl, 10 mM Hepes pH 7.3, 4 mM DTT, 0.15% Tween20 for 1 hr at 25°C. After washing, FliH (FliH : bait = 1.5 : 1 molar ratio) was incubated with the immobilized beads for 1 h at 25°C with gentle shaking. The beads were washed with the 1 ml buffer for 3 times and subjected to boiling and SDS-PAGE analysis.

5.2.3 *H. pylori* growth conditions

H. pylori G27 strains was cultured on Columbia blood agar with 5% defibrinated horse blood and *H. pylori*-selective antibiotics (including trimethoprim, amphotericin, vancomycin, cycloheximide, cefsulodin, polymyxin, β-cyclodexrin) at 37°C under conditions of 7 to 10% O_2, 10% CO_2 and 80 to 83% (Ottemann KM and Lowenthal AC, 2002). 5 μg/ml chloramphenicol was included for selection of *H. pylori* with transformed plasmid. For long term storage, a thick 3-day growth lawn of cells from blood agar plate was scraped into brucella broth (BB) with 10% heat inactivated fetal bovine serum (FBS), 1% (wt/vol) β-cyclodextrin, 25 glycerol and 60% brain heart infusion broth.

5.2.4 Cloning and transformation of *fliY* and *fliY$_C$* into *H. pylori*

For complementation studies, his$_6$-*fliY* and *fliY$_C$* his$_6$ were amplified from genomic DNA of *H. pylori* G27 strain. The genomic DNA was extracted from *H. pylori* according to DNeasy Blood and Tissue Kit (Qiagen). Amplified genes were cloned into IPTG-inducible pILL2157 vector (kindly provided by de Reuse H) (Boneca IG et al., 2008) (Appendix 1). Primers for cloning are summarized in Table 5.1.

Table 5.1. Primers used for cloning of FliY and FliN.

Primer Name	Primer Sequence (5' – 3')	Restriction Site
FliY – F	cgggatccatgcaagattttattaagatttttattcaagag	BamHI
FliY – R	catatggtcgacttaatgtttcaattgttctaagcgttct	SalI
$FliY_N$– R	catatggtcgacttaagacgcatcatgggttttaacctcttcagc	SalI
$FliY_C$ – F	catatgggatccatgaacatagaaatccgcaatatcagcatgctttaga	BamHI
FliN – F	gggggggatccatgtcagaaacagaagctaataagttaaaagtagccg	BamHI
FliN – R	gggggggtcgactcatgaatttttagcgagataatatacaatggcg	SalI
FliYG27-F	gggggcatatgcatcaccatcaccatcaccaagattttattaagatttttattcaagaggttgtt	NdeI
FliYG27-R	gggggggatccttaatgtttcaattgttctaagcgttctttttttagtg	BamHI
$FliY_C$G27-F	gggggcatatgaacatagaaatccgcaatatcagcatgc	NdeI
$FliY_C$G27-R	gggggggatccttagtgatggtgatggtgatgatgtttcaattgttctaagcgttctttttttagtg	BamHI
pILL-R	cagggcggggcgtaattttt	

The plasmids were introduced into *H. pylori ΔfliY* strain by natural transformation (kindly provided by Prof. Ottemann KM, Lowenthal AC et al., 2009). Plasmids (~20 μg) were methylated by the addition of *H. pylori* G27 cell-free extract in order to bypass *H. pylori* restriction barrier. For transformation, *H. pylori* was struck onto blood agar plate and was allowed to grow for one day. The cells were collected and restruck as a small patch and were further grown for 6 h. Plasmids (~20 μg) were stirred with the cells and the plate was incubated for overnight. The cells were re-collected and were struck onto blood agar plate with chloramphenicol. After incubation for 3 days, eight isolated colonies were selected and re-streaked on selective plate twice. To check for positive transformants, plasmid DNA of the selected cells was extracted by minipreparation kit (Qiagen) and PCR was performed with primers flanking 5' of target gene and 3' of vector specific sequence (Table 5.1).

5.2.5 Immunoblot detection of FliY

Wild type, *ΔfliY* mutant or complemented mutants were grown for 1 day with BB broth supplemented with 10% FBS. The absorbance of the culture was measured by OD_{600}. Same amount of cells were pelleted and resuspended with phosphate buffered

saline (in volume $OD_{600} \div 6 \times 1$ml). Total cellular proteins were prepared by boiling with loading dye. Protein expression level of complemented mutants was probed by 1:5000 anti-$FliY_N$ (provided by collaborative work with Prof. Lau KF, CUHK) or anti-His_6 antibody (GE Healthcare).

5.2.6 Characterization of flagella formation by electronmicroscopy

Wild type *H. pylori* strain G27, *ΔfliY* mutants and the complemented mutants were grown on blood agar plates for one day. Formvar carbon-coated grid was floated on a thin patch of cells on blood agar plate for seconds. The cells were immediately fixed by floating the grid on a drop of 1% glutaraldehyde for 1 min followed by negative staining with 1% phosphotungstate for 1 min. Excess staining was removed with Whatman paper. Cells were imaged using a JEOL 1230 electron microscope (Facilities provided by the University of California, Santa Cruz).

5.2.7 Characterization of swarming activity by soft agar assay

Wild type, *ΔfliY* mutant and complemented strains were cultured on blood agar plate for 2 days. Strains were inoculated into soft agar plate (brucella broth with 5% FBS, 0.4% agar, chloramphenicol and IPTG if required) using a pipette tip. The swarming halo was examined after 5 – 7 days incubation.

5.2.8 Phosphate release assay

Dephosphorylation of CheY-P was monitored by Enzchek Phospate Kit (Invitrogen) as described (Lertsethtakarn P and Ottemann KM 2010). Basically, the rate of phosphate release was continuously monitored by measuring OD_{360} in a reaction

mixture containing the kit reagent 1 mM MESG (2-amino-6-meracapto-7-methyl-purine riboside) and 0.5 U PNP (purine nucleoside phosphorylase). To start the reaction, 5 μM CheY and 2.5 mM monophosphoimidazole (concentration that allowed saturating autophosphorylation activity of CheY) was mixed into a 450μl reaction mixture containing buffer (100 mM HEPES pH 7.0, 20 mM $MgCl_2$) and the kit reagent (Lertsethtakarn P and Ottemann KM, 2010). The reaction was allowed to proceed for 10 min. To monitor the putative phosphatase activity of FliY, the reaction was performed as above in the presence of 2.4 μM FliY/FliN complex or 10 μM $FliY_N$. The amount of phosphate released was determined using extinction coefficient at 360 nm of 0.0091 $\mu M^{-1}cm^{-1}$ at pH 7.0 (Silversmith RE et al., 2001). The release rate was calculated from the slope of plotted phosphate release as a function of time.

5.3 Results

5.3.1 FliY-FliN interaction study

The FliN-like domain in $FliY_C$ shares a high sequence homology with FliN from *T. maritima*. Previous study of FliN showed that it dimerized in solution (Brown PN et al., 2005) and two FliN dimers interacted to form tetrameric ring-like structure. This information leads us to speculate that FliY, which contains FliN-like domain, is incorporated into the switch complex by binding to FliN to form heterodimer. To test our hypothesis, we overexpressed individual GST-tagged FliY or 6×His-thioredoxin-tagged FliN (in pET32h vector) in *E. coli* and to purified the proteins by affinity and size exclusion chromatography. Most proteins were eluted in void volume from gel filtration column, suggesting that both proteins form high molecular weight aggregate. Purification of FliN but not FliY was improved by including 5 mM CHAPS in the gel filtration buffer (FliN monomer was observed), however the protein was unstable and prone to degradation. Alternatively, we tried to purify FliY/FliN complex by co-pellet purification that involved mixing the *E. coli* cells separately expressing FliY and FliN. Interestingly, FliY and FliN formed soluble complex and co-eluted from gel filtration column (data not shown).

To further verify FliY-FliN interaction, co-expression/co-purification strategy was employed. Compatible vectors, pGEX-FliY and pAC28m-FliN were co-transformed in *E. coli* and the recombinant proteins were co-purified by GST and Ni-NTA affinity column chromatography followed by gel filtration. This purification strategy would allow the isolation of protein complexes with high purity since excess FliY or FliN were removed by two-step affinity column chromatography each targeting different tagged proteins

(Lam WW et al., 2010). Figure 5.1 shows that FliY and FliN were coeluted in ~1:1 ratio from Superdex S200 with over 90% purity, suggesting FliY and FliN formed a stable complex (Fig. 5.1A). To further identify the domain involves in their interacton, GST-tagged $FliY_C$ was co-expressed with FliN. $FliY_C$ was co-eluted with FliN from gel filtration column, indicating that the C-terminal domain of FliY stably complexes with FliN (Fig. 5.1B). The purified FliY/FliN, $FliY_N$ and $FliY_C$/FliN proteins were subjected to crystallization screening using commercially available screening conditions, including Index I & II, Crystal Screen I & II and Wizard Screen I & II, however no crystal was obtained.

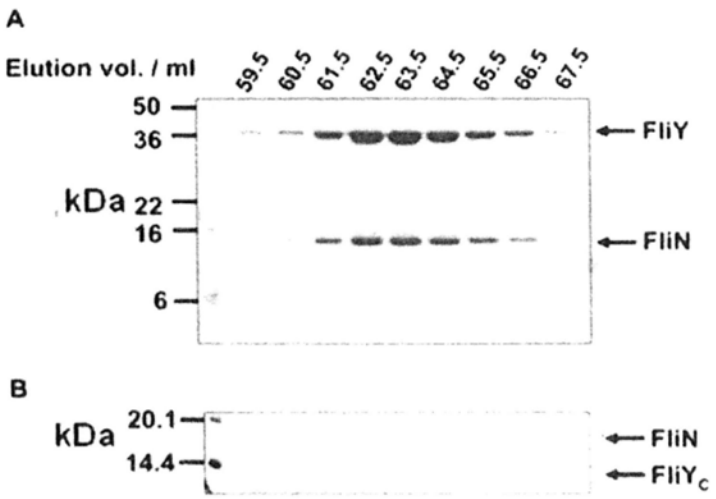

Fig. 5.1. Elution profile of FliY/FliN (A) and $FliY_C$/FliN (B) complexes from Superdex S200 analyzed by SDS-PAGE. Elution volume for the purification of FliY/FliN complex is indicated above the gel photo.

5.3.2 FliY/FliN complex interacts with FliH

FliN contains a conserved hydrophobic patch that is crucial for the localization of export regulatory protein FliH near the flagellar export gate. These conserved residues can be identified on both $FliY_C$ and FliN, hence it is likely that complex could bind to

FliH. FliY/FliN-FliH interaction was studied by pull down assay. Purified FliH was mixed with immobilized GST-FliY/FliN, GST-$FliY_C$/FliN or GST-$FliY_N$ resin. Figure 5.2 shows that both GST-FliY/FliN and GST-$FliY_C$/FliN but not GST-$FliY_N$ captured FliH, suggesting that FliH binds to FliY/FliN complex and $FliY_N$ is not required for the interaction.

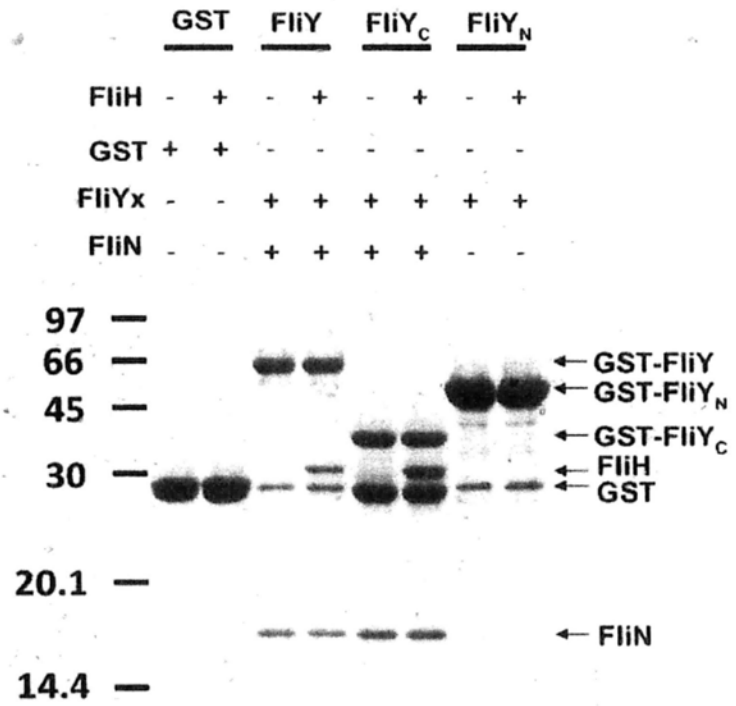

Fig. 5.2. FliY/FliN – FliH pull down experiment. Using glutathione sepharose, GST-FliY or N- and C-terminal truncated fragments were partially purified and some protein impurities (mainly GST) are observed from the lanes.

5.3.3 Motility assays of *fliY*- and *fliY$_C$*- complemented mutant

Previous study suggested that *ΔfliY H. pylori* mutant was immotile and partially flagellated. To further verify the effect was due to the loss of fliY gene, we performed a complementation study by overexpression of FliY in the *ΔfliY* null mutant (Lowenthal

AC et al., 2009). His_6-fliY was cloned into pILL2157 IPTG-inducible *E. coli – H. pylori* shuttle vector. The vector contains promoter *pUreI* and two LacI-binding sites that allows expression modulated by IPTG concentration (Boneca IG et al., 2008). Methylation of plasmid by *H. pylori* cell-free extract was performed. The method was shown to enhance the successful rate of transformation by overcoming the restriction barrier in *H. pylori* (Donahue JP et al., 2000). Methylated plasmid was transformed into *H. pylori* by natural transformation. Successful transformants were selected by chloramphenicol and checked by PCR. Expression of FliY was detected by mouse anti-$FliY_N$ antibody under various IPTG concentrations. Figure 5.3A showed that FliY was overexpressed (>10 fold expression compared with wild-type) even without IPTG and the expression level independent to IPTG concentration. Probably, expression by plasmid pILL2157 is leaky, as previously reported (Boneca IG et al., 2008).

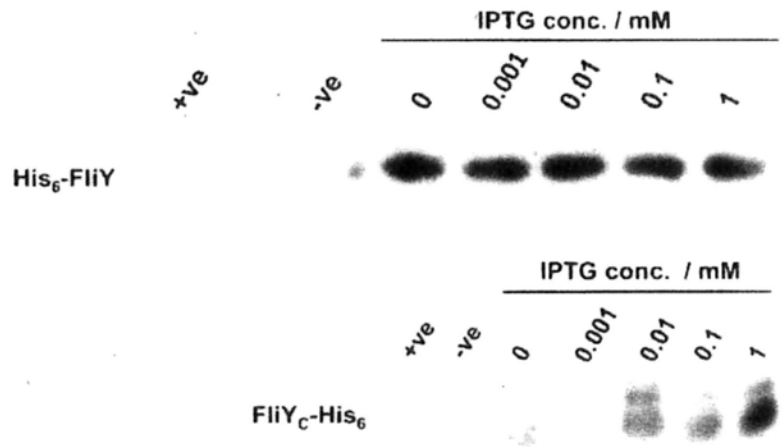

Fig. 5.3. Expression of His_6-FliY and $FliY_C$-His_6 from complemented mutants. Equal amount of cells (measured by OD_{600}) were lysed and loaded on each lane. Immunoblot of His_6-FliY and $FliY_C$-His_6 were probed with anti-$FliY_N$ and anti-His antibodies respectively. For His_6-FliY: +ve control: wild type *H. pylori* G27; -ve control: *ΔfliY* strain. For $FliY_C$-His_6: +ve control: His_6-FliN; -ve control: *H. pylori* lysate.

To determine if the expression of fliY gene restores flagellation of complemented mutant, the cells were visualized by electron microscopy. Both wild type and complemented strain, but not *ΔfliY* strain, were flagellated and the flagella showed to have the featured terminal bulb structure, suggesting FliY is involved in flagellar formation (Fig. 5.4A). To further test the biological function of FliY, soft agar assay was performed. The swarming ring of complemented mutant was comparable to that of wild type but no swarming was observed in the deletion mutant (Fig. 5.4B). Swimming behavior was also observed under phase-contrast microscopy, agreed with that the complemented mutant is motile.

The two distinct domains in FliY likely carry unique function in motility of *H. pylori*. To investigate the biological importance of FliY domains, His-tagged $fliY_N$ and $fliY_C$ were cloned into pILL2157 and transformed into *ΔfliY* strain. Only pILL2157-$fliY_C$-His_6 was successfully transformed. The transformation was confirmed by PCR and the overexpression of $FliY_C$ was verified by anti-His antibody (Fig. 5.3B). The expression level of $FliY_C$ seems to be IPTG-dependent.

The motility phenotype of the $fliY_C$ complemented mutant was investigated. Electron microscopy of the strain showed flagellation with the terminal bulb structure (Fig. 5.4). The bacteria was motile in solution as observed by phase contrast microscopy (data not shown). However, the swarming diameter of $fliY_C$-complemented strain (mean diameter = 13.7 mm) was significantly reduced compared with wild type (mean diameter = 19.9 mm), suggesting that $FliY_N$ is required for full motility function.

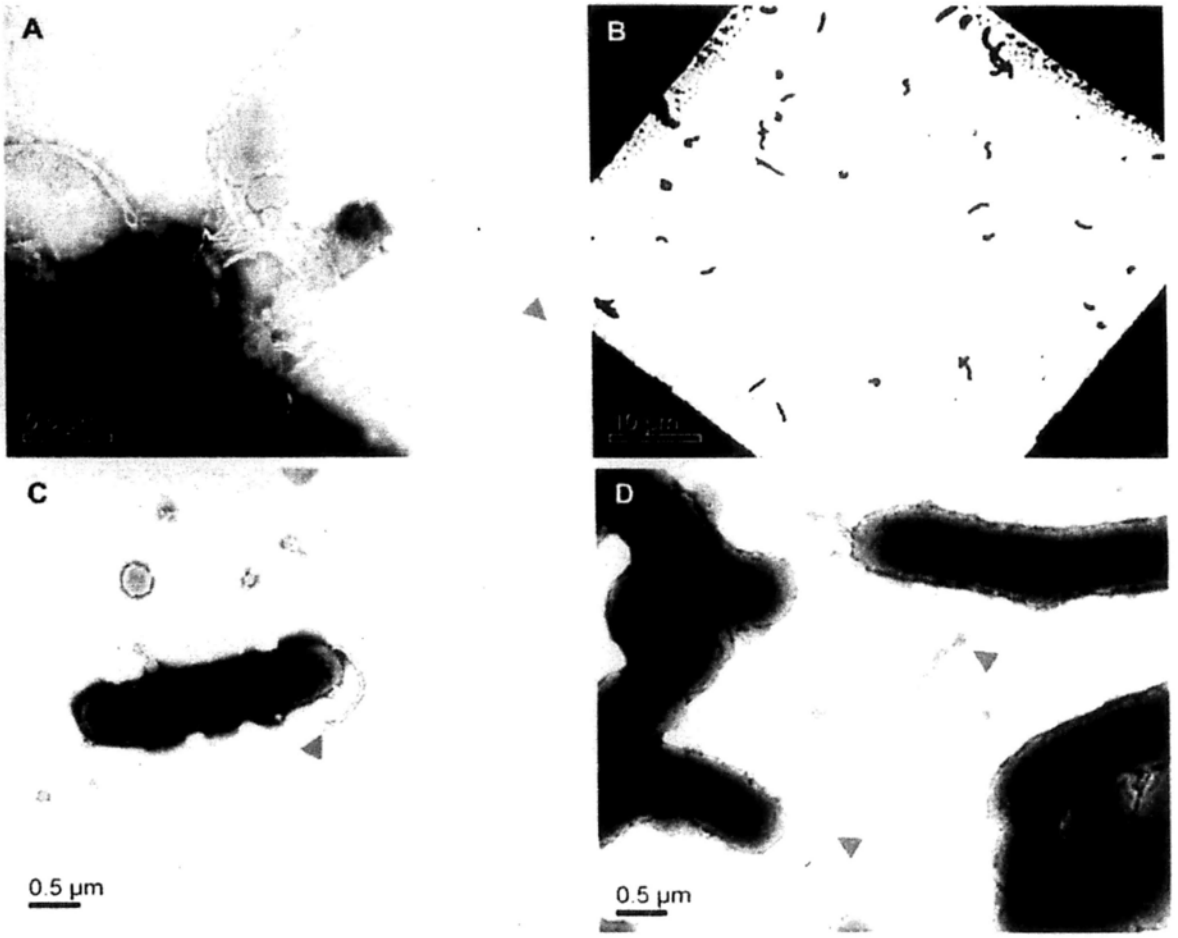

Fig. 5.4. Flagellation of *H. pylori* complemented mutants. Arrows mark the terminal bulb structure of the flagellum. **(A)** Wild type G27; **(B)** *ΔfliY* mutant; **(C)** his6-fliY complemented mutant; **(D)** fliY-his_6 complemented mutant. Scale bar is shown in microns.

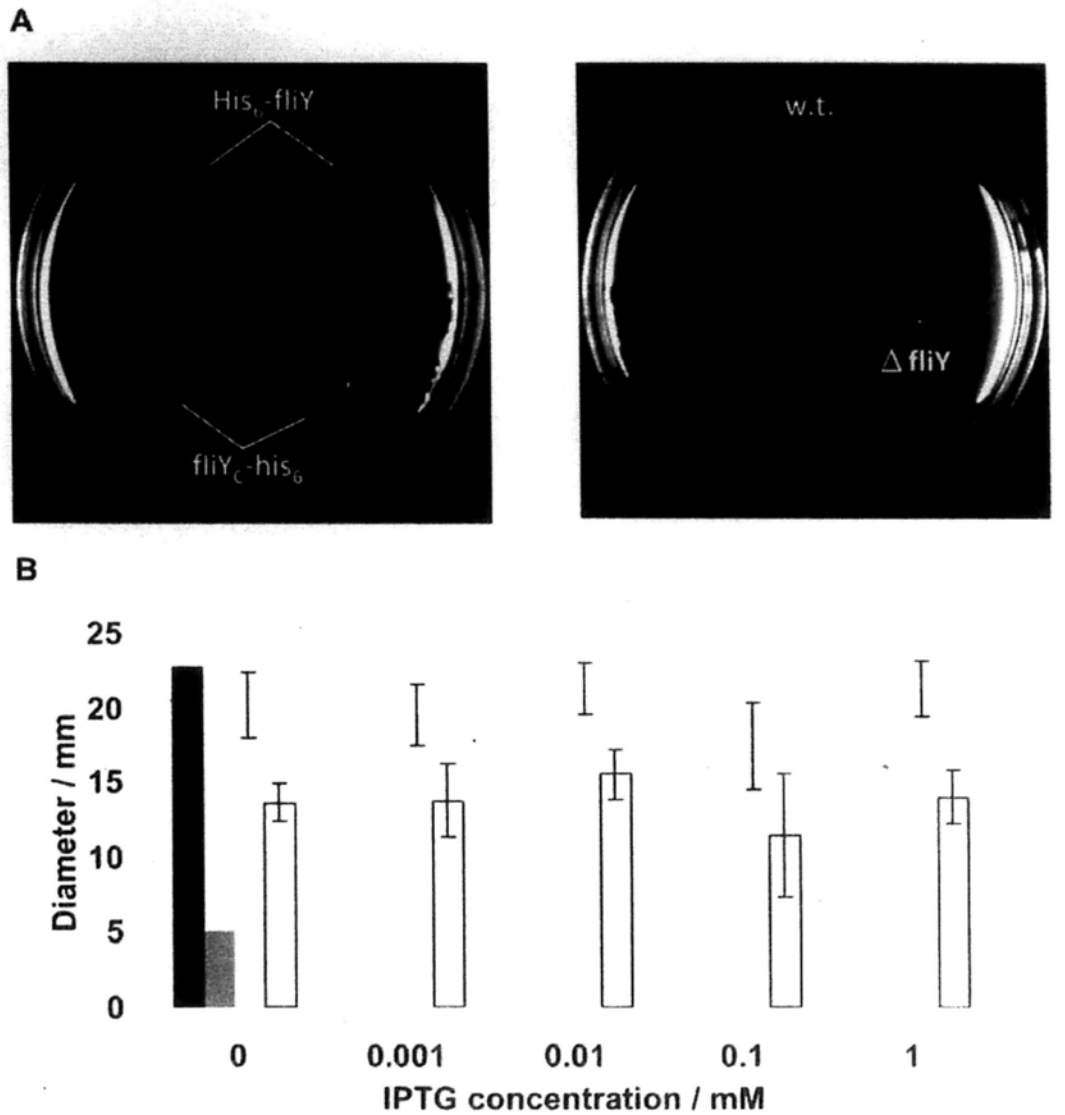

Fig. 5.5. Swarming phenotype of fliY complemented mutants. (A) Representative images of the swarming rings observed in pILL2157-his$_6$-FliY and -fliY$_C$-his$_6$ complemented strains. **(B)** Swarming diameter of the complemented mutant induced with various IPTG concentration. Wild type G27 strain, black; *ΔfliY* srain, dark grey; his$_6$-fliY complemented mutant, light grey; fliY$_C$-his$_6$ complemented mutant, white. For complemented mutants, the mean value from four independent experiments and the error bar shows the standard deviation are shown. For wild type and *ΔfliY* strain, the diameter is an average value of duplicate experiment.

5.3.4 Neither $FliY_N$ nor FliY/FliN enhance the dephosphorylation of CheY-P

A conserved EXXXN motif identified in $FliY_N$ (Section 1.6.1) indicating that FliY may carry phosphatase activity. The putative dephosphorylation activity of $FliY_N$ was investigated by EnzChek Phosphate Assay Kit as previously employed to study the phosphatase activity of *H. pylori* CheZ (Lertsethtakarn P and Ottemann KM, 2010). In this assay, CheY is autophosphorylated by phosphodonor monophosphoimidazole (MPI), and the steady state phosphate release by autodephosphorylation of CheY is measured. If $FliY_N$ carries phosphatase activity, it is expected that phosphate release rate would be enhanced as demonstrated by CheZ (HP0170). Preliminary experiment measured the phosphate release rate of CheY was 0.0506 μMs^{-1}, CheY with 10 μM $FliY_N$ was 0.0483 μMs^{-1} and CheY with 5.4 μM FliY/FliN complex was 0.0451 μMs^{-1}. The data suggested that there is no increase in the phosphate release rate in the presence of $FliY_N$ domain (Fig. 5.6).

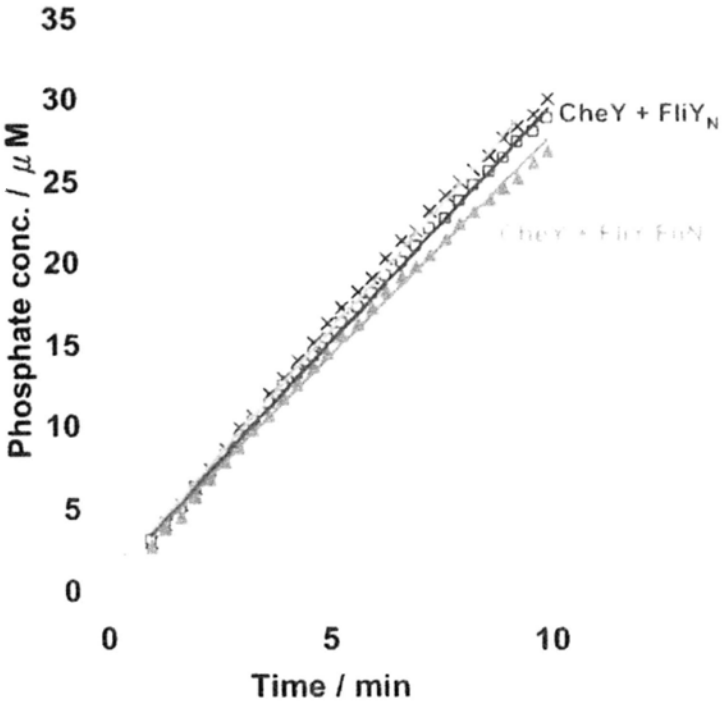

Fig. 5.6. Phosphate release by autodephosphorylation of CheY and dephosphorylation in the presence of FliY$_N$ and FliY/FliN. Amount of phosphate released using monophosphoimidzole as phosphodonor is shown. Line is marked as in the diagram.

5.4 Discussion

Recent study on the deletion mutants of *H. pylori* supported that FliY is a member of switch proteins (Lowenthal AC et al., 2009). The presence of both FliY and FliN as switch proteins is unique among ε-proteobacteria, that their co-existence may be associated to the adaptation of the motility system among these bacteria. This study aims to further our understanding about the structure-function relationship of FliY as a switch protein and to examine the biological function of its individual domains. We demonstrated that FliY complemented the flagellar formation and restored swarming of *ΔfliY* mutant, once again supporting that the motility defect observed in *ΔfliY* mutant was due to the absence of FliY. Further, we showed that FliY stably bound to switch protein FliN, thus providing molecular insight to the incorporation of FliY into the switch complex.

Both our *in vivo* and *in vitro* studies agree that $FliY_C$ but not $FliY_N$ contributes to the flagellation in *H. pylori*. $FliY_C$ complemented *ΔfliY* mutant showed normal flagella and motility. Interactions studies showed that $FliY_C$/FliN complex but not $FliY_N$ is needed to bind FliH. Sequence analysis of $FliY_C$ and FliN showed that both proteins contain the residues necessary for protein export and motility. It is intriguing why *H. pylori* have two FliN domain containing proteins. Deletion of either FliY or FliN caused immotile and partial flagellation, while both proteins resulted in non-flagellate phenotypes, implying that FliY and FliN are functionally redundant. Lowenthal AC et al., proposed that these two proteins may carry equivalent roles in flagellation and the phenotype for the single knockout mutant might simply because of an inadequate FliN domains to create normal flagella. Their idea is in coherence to the experimental findings

from *E. coli*, that the expression level of FliN was reduced led to impaired flagella function (Tang H et al., 1995). In *E. coli*, FliN forms a tetrameric ring-like structure by two homodimers. It was assumed that FliY assembles into tetramer in a similar manner as in FliN. Based on our interactions studies, we proposed an alternative model of FliY/FliN complex organization (Fig. 5.7). FliY forms a stable complex with FliN in 1:1 molar ratio. Thus it is more likely that FliY and FliN interact with each other to form tetramer composed of either two hetero-dimers of two homo-dimers (Fig. 5.7B). We observed that both FliY and FliN are prone to soluble aggregation when individually expressed, while soluble FliY/FliN complexes can be isolated by co-pellet purification. It appears that their cognate interacting partner is required to maintain their proper folding. From the structure of *T. maritima* FliN, FliN domain is dominated by solvent exposed hydrophobic residues, but they are buried and stabilized by the formation of dimeric structure (Fig. 5.7A) (Brown PN et al., 2005). FliY or FliN may not be able to dimerize individually results in the exposure of hydrophobic residues that non-specifically bind with other proteins and form soluble aggregate. The addition of CHAPS helps to stabilize FliN probably by binding to the exposed hydrophobic surface. Our results more likely support FliN tetramer involves the formation of FliY/FliN heterodimer. Nevertheless, to elucidate the organization of FliY/FliN complex, further experiments are needed to map the binding interface between the proteins.

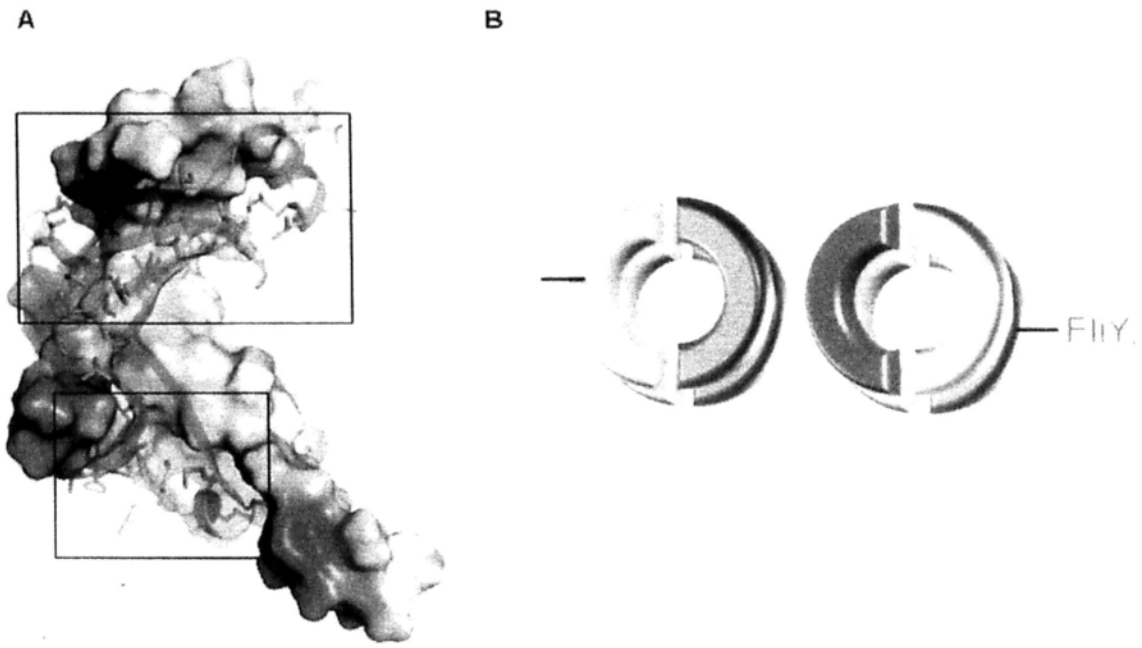

Fig. 5.7. Possible organizations of $FliY_C$/FliN complex. (A) *T. maritma* FliN (PDB-ID: 1YAB) forms homodimer mediated by extensive hydrophobic interactions. Chain A and chain B of the structure are represented as molecular surface and cartoon (green) respectively. The hydrophobic residues at the interface of the dimer are shown as stick (PISA). Clusters of hydrophobic residues involved in the dimer formation are boxed. Electrostatic surface is calculated by APBS tools and represented in contour level ±5 keT. **(B)** Two possible organizations of $FliY_C$/FliN complex.

Deletion of $FliY_N$ impaired motility of *H. pylori* in soft agar assay. However, the role of $FliY_N$ is still ambiguous since a reduced swarming ring would be due to impaired chemotactic behavior (CW or CCW bias), reduced growth rate or defect in flagellar formation (Berg HC & Turner L, 1979). Although EM of complemented mutant showed normal flagellar structure, but our current results are not statistically significant enough to rule out the involvement of $FliY_N$ in flagellar formation. Our *in vitro* phosphate release

assay did not detect the phosphatase activity of FliY and no FliY-CheY-P interaction was observed from pull down experiment (data not shown). Still, due to the presence of conserved phosphatase motif, it is possible that FliY carry phosphatase activity *in vivo* but cannot be measured under our experimental conditions. It could be that the absence of CheY-binding domain in *H. pylori* FliY precludes the binding of CheY-P to FliY. However, when FliY is assembled into switch protein complex, cheY-P may be brought close to the phosphatase active site of FliY by FliM-N-terminal domain, which also interacts with FliN (Sarkar MK et al., 2010). Further experiments are needed to verify the possible phosphatase activity of FliY towards CheY-P in complex with FliM N-terminal peptide.

In summary, our study consistently showed that FliY is a switch protein. $FliY_C$ is important to flagellation, possibly through complex formation with FliN to bind FliH. We also demonstrated that $FliY_N$ is necessary to full motility function, although the specific role of $FliY_N$ remains to be elucidated.

Chapter 6

General discussion

Bacterial motility is controlled by a nano-rotary motor composed of proton pump stator and rotor. Various models for the organization of the switch complex have been constructed, based on 3D electron microscopy of isolated rotor and various structural, biochemical and mutagenesis studies in enteric bacteria *E. coli* and *S. typhimurium* (Lee LK et al., 2010; Minamino T et al., 2011; Paul K et al., 2011). The diverse organization and function of switch complex among bacteria has not been reviewed until recent advances in genomic sequencing and cryo-electron tomography (Pallen MJ et al., 2005; Chen S et al., 2011).

The target organism of present study is *Helicobacter pylori*. Motility is crucial to the colonization and persistence of *H. pylori* in human stomach (Eaton KA et al., 1992, 1996). A specific niche of this bacterium, includes a chemotaxis system that helps the pathogen to move away from acidic gastric lumen to epithelial cells as well as to come across the viscous mucin layer (Celli JP et al., 2009). Deletion of chemotaxis or flagellar structural genes impaired the infection of *H. pylori* (Ottemann KM et al., 2002; Terry K et al., 2005). These proteins may be novel drug targets for the eradication of *H. pylori* (Duckworth MJ et al., 2010).

The major aim of this study is to characterize the structure and function of regulatory and switch proteins from *H. pylori*. Genomic sequence analysis of *H. pylori* revealed the presence of additional CheY-like chemotaxis proteins and a putative switch protein FliY when compared with well-studied model organism *E. coli*. The additional

switch and chemotaxis proteins lead us to speculate that the architecture of switch protein complex and the regulatory mechanism of motor switching are distinct in *H. pylori*.

Prior to this study, Lowenthal AC et al., showed that the deletion of all four switch proteins in *H. pylori* is partially or completely non-flagellate while deletion of CheY showed rotational biased phenotype. Besides, FliM-CheY1 interaction has been demonstrated. However, the interactions among the switch proteins as well as their molecular structures, that are important to understand the architecture of the switch complex, have not been elucidated.

In this study, we reported the crystal structures of activated CheY1, $FliM_M$ and $FliG_{MC}$ from *H. pylori* and identified the crystallization condition for $FliF_C$-$FliG_N$ complex. CheY1-FliM, FliM-FliG, FliF-FliG, FliY-FliN interactions were verified (summarized in Fig. 6.1). These interactions are consistent with those observed from *E. coli* and *S. typhimurium* (Toker AS & Macnab RM 1997; González-Pedrajo B et al., 2006), except FliY-FliN association which is unique to *H. pylori*. The high structural homology of CheY1, $FliM_M$ and $FliG_{MC}$ may be organized in a similar manner as in *E. coli* and *S. typhimurium*. FliG is in close proximity to the membrane with its C-terminal domain positioned at periphery. The charge ridge is facing to the membrane and the conserved EHPQR motif and hydrophobic patch pointing towards FliM. A triple mutant $_{140}$YDQ/AAA$_{142}$ located on the GGXG-bearing flexible loop impaired the binding to FliG imply that this surface is close to FliG-FliM interface. Activated CheY1 bind to $FliM_{N\alpha}$ peptide and may dock to FliN domains as in *E. coli*. Based on the results from our interaction studies, we propose that $FliY_C$/FliN complex form a heterodimer. The

structure of the complex is modeled according to FliN from *T. maritima*. The ring-like structure probably located at the bottom of the switch complex. One interesting question is how $FliY_N$ is arranged in the complex. The overall protein folding of $FliY_N$ predicted by Phyre is similar to $FliM_M$, consistent with the notion that $FliY_N$ belongs to CYX family (Park SY et al., 2006; Kirby JR et al., 2001; Lowenthal AC et al., 2009). Alternative positions of $FliY_N$ are proposed in Figure 6.2 with minimal steric hindrance on the binding surface of $FliY_C$/FliN to other proteins (e.g. FliH) (Fig. 6.2).

A most recent study compared the flagellar motors from 11 bacteria by cryo-electron tomography and revealed unique structural features of the switch protein complex among ε-proteobacteria (*Campylobacter jejuni* and *Helicobacter hepaticus*), including a larger C-ring diameter (49 nm compared with 40 nm in *S. typhimurium*) and a stronger densities between MS- and C-ring (Fig. 6.2). The increase in the diameter of C-ring may suggest a different stoichiometric relationship between the switch proteins. Taken together a 49 nm diameter of C-ring and a constant intersubunit spacing of 3.9 nm observed from outer C-ring with variable symmetries (Young HS et al., 2003), the outer C-ring of ε-proteobacteria may contain ~39 subunit, compared with calculated ~ 32 subunit in *E. coli*. One the hand, no extra density can be assigned to additional FliY. One possibility is that the loop region connecting $FliY_N$ and $FliY_C$ is flexible and $FliY_N$ is dynamically oriented in multiple positions that cannot be visualized from the map of electron-tomography.

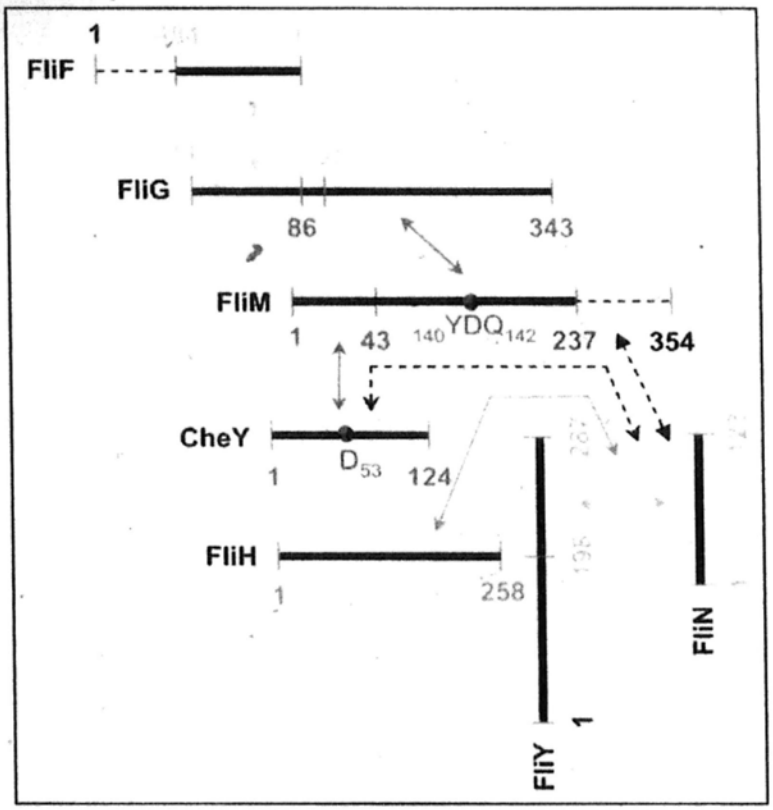

Fig. 6.1. A summary of the interactions of switch proteins from *H. pylori*. Arrow indicates protein-protein interaction. The minimal domain for respective stable interactions are of the same color as the arrow. The lines are not drawn to scale. Dashed lines represent regions that are not covered in this study. Dashed arrows indicate protein-protein interaction identified in *E. coli* but not yet confirmed in *H. pylori*. Mutant identified that impaired the interaction are highlighted as red spheres.

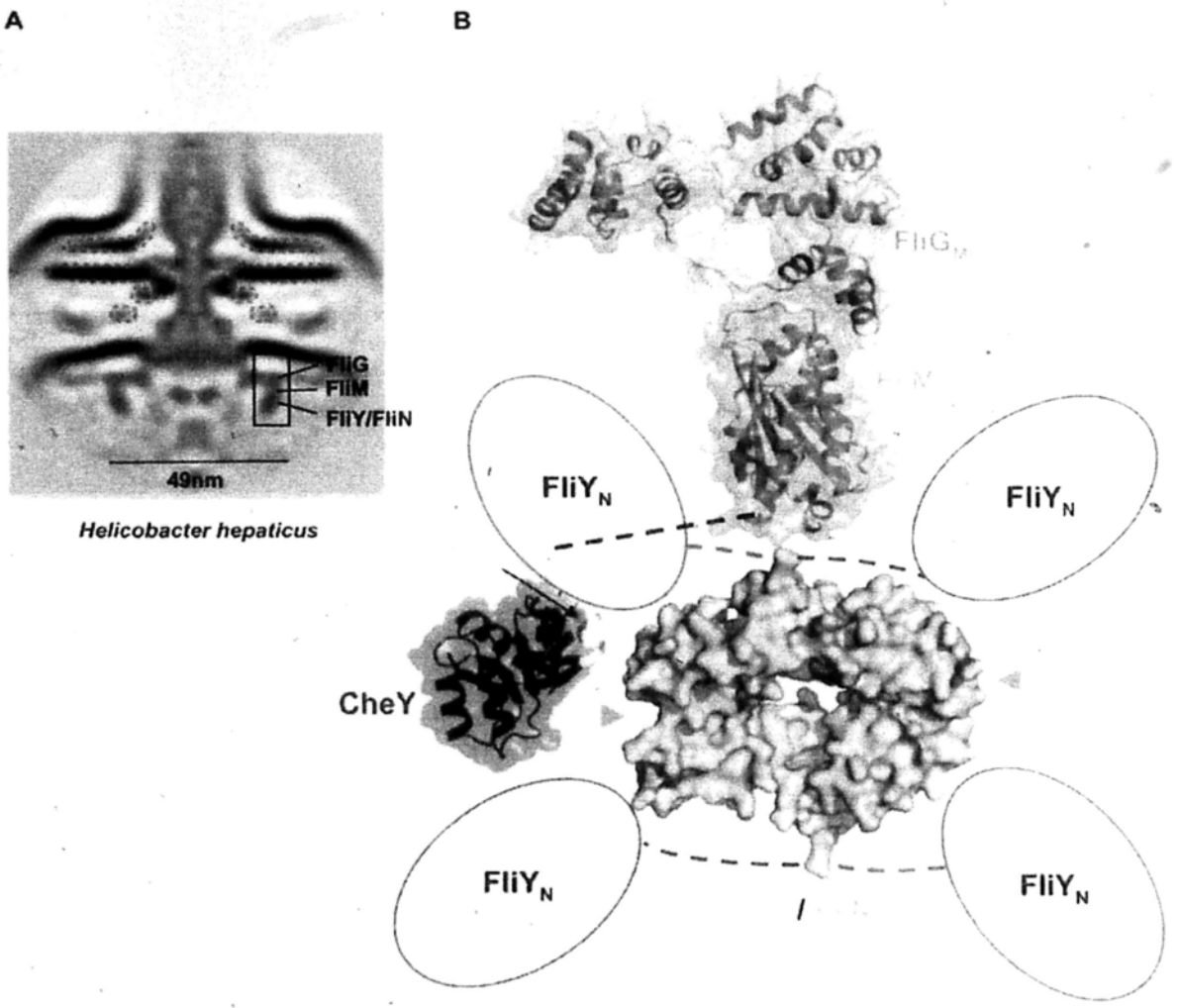

Fig. 6.2. Architecture of *H. pylori* SPC proposed by this study. (A) Electron cryotomograph of motor from *Helicobacter hepaticus*, a closely related species of *H. pylori* (adapted from Chen S. et al., 2011). The density of C-ring is colored red. The relative positions of FliG, FliM and FliY/FliN complex are indicated. **(B)** Model for the organization of SPC. Structures of $HpFliG_{MC2}$, $FliM_M$, CheY and the modeled structures of $FliY_C$/FliN tetramer are represented. $FliY_C$/FliN and $FliM_{N\alpha}$ are modeled using *T. maritma* FliN and *E. coli* $FliM_{N\alpha}$ as template, respectively (Phyre). Blue arrow indicates the surface hydrophobic patch on $FliY_C$/FliN for docking FliH. Purple and red circle indicates two possible arrangements of $FliY_N$ that would minimally affect the binding of $FliY_C$/FliN to other switch proteins. Dashed line indicates the loop connecting distinct domain.

A long-lasting biological question concerning the function of the motor is how bi-directional rotation is achieved. All the switch proteins undergo conformational change upon CheY-P binds to FliM and led to CW-biased rotation (Sarkar MK et al., 2010; Lee LK et al., 2010; Minamino T et al., 2011). However, the dynamic motion of switch proteins during motor switching is poorly understood, due to the limitations of experimental techniques to measure these relative movements in the assembled macromolecular complex. Nevertheless, by comparing multiple structures of FliG and FliM, we unravel the relative sub-domain movement of $FliG_C$ and the displacement of $FliM_M$ surface loop. Remarkably, a 180^o rotation of charge ridge that is critical to FliG-MotA interaction is reported and helps to explain the symmetrical stepping motion in both CCW and CW rotation (Nakamura S et al., 2010). How CheY-FliM interaction mediate the conformational change of FliG remains controversial, it is possible that the flexible loop of $FliM_M$ close to FliG-FliM interface is important for regulating this process.

In summary, our pilot study on the structure and function of switch proteins from *H. pylori* helps to explore the molecular architecture of switch protein complex from *H. pylori*. Multiple structural comparisons of the switch proteins uncover their dynamic properties that contribute to the understanding of the mechanistic details of motor switching.

References

Alexandre G & Zhulin IB (2003) Different evolutionary constraints on chemotaxis proteins CheW and CheY revealed by heterologous expression studies and protein sequence analysis. *J Bacteriol* 185(2):544-552.

Allan E, Dorrell N, Foynes S, Anyim M, & Wren BW (2000) Mutational analysis of genes encoding the early flagellar components of Helicobacter pylori: evidence for transcriptional regulation of flagellin A biosynthesis. *J Bacteriol* 182(18):5274-5277.

Alm RA, *et al.* (1999) Genomic-sequence comparison of two unrelated isolates of the human gastric pathogen Helicobacter pylori. *Nature* 397(6715):176-180.

Armitage JP & Schmitt R (1997) Bacterial chemotaxis: Rhodobacter sphaeroides and Sinorhizobium meliloti--variations on a theme? *Microbiology* 143 (Pt 12):3671-3682.

Ashkenazy H, Erez E, Martz E, Pupko T, & Ben-Tal N (2010) ConSurf 2010: calculating evolutionary conservation in sequence and structure of proteins and nucleic acids. *Nucleic Acids Res* 38(Web Server issue):W529-533.

Bai F, *et al.* (2010) Conformational spread as a mechanism for cooperativity in the bacterial flagellar switch. *Science* 327(5966):685-689.

Baker NA, Sept D, Joseph S, Holst MJ, & McCammon JA (2001) Electrostatics of nanosystems: application to microtubules and the ribosome. *Proc Natl Acad Sci U S A* 98(18):10037-10041.

Baltrus DA, *et al.* (2009) The complete genome sequence of Helicobacter pylori strain G27. *J Bacteriol* 191(1):447-448.

Bardy SL, Ng SY, & Jarrell KF (2003) Prokaryotic motility structures. *Microbiology* 149(Pt 2):295-304.

Bass RB, Butler SL, Chervitz SA, Gloor SL, & Falke JJ (2007) Use of site-directed cysteine and disulfide chemistry to probe protein structure and dynamics: applications to soluble and transmembrane receptors of bacterial chemotaxis. *Methods Enzymol* 423:25-51.

Basso D, Plebani M, & Kusters JG (2010) Pathogenesis of Helicobacter pylori infection. *Helicobacter* 15 Suppl 1:14-20.

Berg HC (2008) Bacterial flagellar motor. *Curr Biol* 18(16):R689-691.

Berg HC & Brown DA (1972) Chemotaxis in Escherichia coli analysed by three-dimensional tracking. *Nature* 239(5374):500-504.

Berg HC & Turner L (1979) Movement of microorganisms in viscous environments. *Nature* 278(5702):349-351.

Berry RM & Armitage JP (1999) The bacterial flagella motor. *Adv Microb Physiol* 41:291-337.

Bischoff DS & Ordal GW (1992) Identification and characterization of FliY, a novel component of the Bacillus subtilis flagellar switch complex. *Mol Microbiol* 6(18):2715-2723.

Blair KM, Turner L, Winkelman JT, Berg HC, & Kearns DB (2008) A molecular clutch disables flagella in the Bacillus subtilis biofilm. *Science* 320(5883):1636-1638.

Boneca IG, *et al.* (2008) Development of inducible systems to engineer conditional mutants of essential genes of Helicobacter pylori. *Appl Environ Microbiol* 74(7):2095-2102.

Briegel A, *et al.* (2009) Universal architecture of bacterial chemoreceptor arrays. *Proc Natl Acad Sci U S A* 106(40):17181-17186.

Brown LM, *et al.* (2002) Helicobacter pylori infection in rural China: demographic, lifestyle and environmental factors. *Int J Epidemiol* 31(3):638-645.

Brown PN, Hill CP, & Blair DF (2002) Crystal structure of the middle and C-terminal domains of the flagellar rotor protein FliG. *EMBO J* 21(13):3225-3234.

Brown PN, Mathews MA, Joss LA, Hill CP, & Blair DF (2005) Crystal structure of the flagellar rotor protein FliN from Thermotoga maritima. *J Bacteriol* 187(8):2890-2902.

Brown PN, Terrazas M, Paul K, & Blair DF (2007) Mutational analysis of the flagellar protein FliG: sites of interaction with FliM and implications for organization of the switch complex. *J Bacteriol* 189(2):305-312.

Celli JP, *et al.* (2009) Helicobacter pylori moves through mucus by reducing mucin viscoelasticity. *Proc Natl Acad Sci U S A* 106(34):14321-14326.

Cerda O, Rivas A, & Toledo H (2003) Helicobacter pylori strain ATCC700392 encodes a methyl-accepting chemotaxis receptor protein (MCP) for arginine and sodium bicarbonate. *FEMS Microbiol Lett* 224(2):175-181.

Chen S, *et al.* (2011) Structural diversity of bacterial flagellar motors. *EMBO J.* 30(14):2972-2981.

Chen VB, *et al.* (2010) MolProbity: all-atom structure validation for macromolecular crystallography. *Acta Crystallogr D Biol Crystallogr* 66(Pt 1):12-21.

Cho HS, *et al.* (2000) NMR structure of activated CheY. *J Mol Biol* 297(3):543-551.

Choong IC, *et al.* (2002) Identification of potent and selective small-molecule inhibitors of caspase-3 through the use of extended tethering and structure-based drug design. *J Med Chem* 45(23):5005-5022.

Cohen-Ben-Lulu GN, *et al.* (2008) The bacterial flagellar switch complex is getting more complex. *EMBO J* 27(7):1134-1144.

Collaborative Computational Project Nm (1994) The CCP4 suite: programs for protein crystallography. *Acta Crystallogr D Biol Crystallogr* 50(Pt 5):760-763.

Correa P & Houghton J (2007) Carcinogenesis of Helicobacter pylori. *Gastroenterology* 133(2):659-672.

Croxen MA, Sisson G, Melano R, & Hoffman PS (2006) The Helicobacter pylori chemotaxis receptor TlpB (HP0103) is required for pH taxis and for colonization of the gastric mucosa. *J Bacteriol* 188(7):2656-2665.

Delalez NJ, *et al.* (2010) Signal-dependent turnover of the bacterial flagellar switch protein FliM. *Proc Natl Acad Sci U S A* 107(25):11347-11351.

DeRosier DJ (1998) The turn of the screw: the bacterial flagellar motor. *Cell* 93(1):17-20.

Di Tommaso P, *et al.* (2011) T-Coffee: a web server for the multiple sequence alignment of protein and RNA sequences using structural information and homology extension. *Nucleic Acids Res* 39 Suppl 2:W13-17.

Donahue JP, Israel DA, Peek RM, Blaser MJ, & Miller GG (2000) Overcoming the restriction barrier to plasmid transformation of Helicobacter pylori. *Mol Microbiol* 37(5):1066-1074.

Duckworth MJ, Okoli AS, & Mendz GL (2009) Novel Helicobacter pylori therapeutic targets: the unusual suspects. *Expert Rev Anti Infect Ther* 7(7):835-867.

Dyer CM & Dahlquist FW (2006) Switched or not?: the structure of unphosphorylated CheY bound to the N terminus of FliM. *J Bacteriol* 188(21):7354-7363.

Dyer CM, *et al.* (2004) Structure of the constitutively active double mutant CheYD13K Y106W alone and in complex with a FliM peptide. *J Mol Biol* 342(4):1325-1335.

Dyer CM, Vartanian AS, Zhou H, & Dahlquist FW (2009) A molecular mechanism of bacterial flagellar motor switching. *J Mol Biol* 388(1):71-84.

Eaton KA, Morgan DR, & Krakowka S (1992) Motility as a factor in the colonisation of gnotobiotic piglets by Helicobacter pylori. *J Med Microbiol* 37(2):123-127.

Eaton KA, Suerbaum S, Josenhans C, & Krakowka S (1996) Colonization of gnotobiotic piglets by Helicobacter pylori deficient in two flagellin genes. *Infect Immun* 64(7):2445-2448.

Eisenbach M (1996) Control of bacterial chemotaxis. *Mol Microbiol* 20(5):903-910.

Emsley P & Cowtan K (2004) Coot: model-building tools for molecular graphics. *Acta Crystallogr D Biol Crystallogr* 60(Pt 12 Pt 1):2126-2132.

Emsley P, Lohkamp B, Scott WG, & Cowtan K (2010) Features and development of Coot. *Acta Crystallogr D Biol Crystallogr* 66(Pt 4):486-501.

Erhardt M, Namba K, & Hughes KT (2010) Bacterial nanomachines: the flagellum and type III

injectisome. *Cold Spring Harb Perspect Biol* 2(11):a000299.

Foynes S, *et al.* (2000) Helicobacter pylori possesses two CheY response regulators and a histidine kinase sensor, CheA, which are essential for chemotaxis and colonization of the gastric mucosa. *Infect Immun* 68(4):2016-2023.

Frishman D & Argos P (1995) Knowledge-based protein secondary structure assignment. *Proteins* 23(4):566-579.

Fukuoka H, Inoue Y, Terasawa S, Takahashi H, & Ishijima A (2010) Exchange of rotor components in functioning bacterial flagellar motor. *Biochem Biophys Res Commun* 394(1):130-135.

Geis G, Suerbaum S, Forsthoff B, Leying H, & Opferkuch W (1993) Ultrastructure and biochemical studies of the flagellar sheath of Helicobacter pylori. *J Med Microbiol* 38(5):371-377.

Glaser F, *et al.* (2003) ConSurf: identification of functional regions in proteins by surface-mapping of phylogenetic information. *Bioinformatics* 19(1):163-164.

González-Pedrajo B, Minamino T, Kihara M, & Namba K (2006) Interactions between C ring proteins and export apparatus components: a possible mechanism for facilitating type III protein export. *Mol Microbiol* 60(4):984-998.

Graham DY & Rimbara E (2011) Understanding and appreciating sequential therapy for Helicobacter pylori eradication. *J Clin Gastroenterol* 45(4):309-313.

Grünenfelder B, Gehrig S, & Jenal U (2003) Role of the cytoplasmic C terminus of the FliF motor protein in flagellar assembly and rotation. *J Bacteriol* 185(5):1624-1633.

Hamblin PA, Maguire BA, Grishanin RN, & Armitage JP (1997) Evidence for two chemosensory pathways in Rhodobacter sphaeroides. *Mol Microbiol* 26(5):1083-1096.

Hilser VJ (2010) Biochemistry. An ensemble view of allostery. *Science* 327(5966):653-654.

Holm L, Kääriäinen S, Rosenström P, & Schenkel A (2008) Searching protein structure databases with DaliLite v.3. *Bioinformatics* 24(23):2780-2781.

Irikura VM, Kihara M, Yamaguchi S, Sockett H, & Macnab RM (1993) Salmonella typhimurium fliG and fliN mutations causing defects in assembly, rotation, and switching of the flagellar motor. *J Bacteriol* 175(3):802-810.

Jahreis K, Morrison TB, Garzón A, & Parkinson JS (2004) Chemotactic signaling by an Escherichia coli CheA mutant that lacks the binding domain for phosphoacceptor partners. *J Bacteriol* 186(9):2664-2672.

Jiménez-Pearson MA, Delany I, Scarlato V, & Beier D (2005) Phosphate flow in the chemotactic response system of Helicobacter pylori. *Microbiology* 151(Pt 10):3299-3311.

Jones CJ, Macnab RM, Okino H, & Aizawa S (1990) Stoichiometric analysis of the flagellar hook-(basal-body) complex of Salmonella typhimurium. *J Mol Biol* 212(2):377-387.

Josenhans C & Suerbaum S (2002) The role of motility as a virulence factor in bacteria. *Int J Med Microbiol* 291(8):605-614.

Kavermann H, *et al.* (2003) Identification and characterization of Helicobacter pylori genes essential for gastric colonization. *J Exp Med* 197(7):813-822.

Kersulyte D, *et al.* (2010) Helicobacter pylori from Peruvian amerindians: traces of human migrations in strains from remote Amazon, and genome sequence of an Amerind strain. *PLoS One* 5(11):e15076.

Kholod N & Mustelin T (2001) Novel vectors for co-expression of two proteins in E. coli. *Biotechniques* 31(2):322-323, 326-328.

Kim EA, Price-Carter M, Carlquist WC, & Blair DF (2008) Membrane segment organization in the stator complex of the flagellar motor: implications for proton flow and proton-induced conformational change. *Biochemistry* 47(43):11332-11339.

Kirby JR, *et al.* (2001) CheC is related to the family of flagellar switch proteins and acts independently from CheD to control chemotaxis in Bacillus subtilis. *Mol Microbiol* 42(3):573-585.

Ko M & Park C (2000) Two novel flagellar components and H-NS are involved in the motor function of Escherichia coli. *J Mol Biol* 303(3):371-382.

Kojima S & Blair DF (2001) Conformational change in the stator of the bacterial flagellar motor. *Biochemistry* 40(43):13041-13050.

Kojima S & Blair DF (2004) Solubilization and purification of the MotA/MotB complex of Escherichia coli. *Biochemistry* 43(1):26-34.

Lam KH, Ling TK, & Au SW (2010) Crystal structure of activated CheY1 from Helicobacter pylori. *J Bacteriol* 192(9):2324-2334.

Lam WW, *et al.* (2010) Molecular interaction of flagellar export chaperone FliS and cochaperone HP1076 in Helicobacter pylori. *FASEB J* 24(10):4020-4032.

Langer G, Cohen SX, Lamzin VS, & Perrakis A (2008) Automated macromolecular model building for X-ray crystallography using ARP/wARP version 7. *Nat Protoc* 3(7):1171-1179.

Laskowski RA, MacArthur MW, & Thornton JM (1998) Validation of protein models derived from experiment. *Curr Opin Struct Biol* 8(5):631-639.

Lee LK, Ginsburg MA, Crovace C, Donohoe M, & Stock D (2010) Structure of the torque ring of the flagellar motor and the molecular basis for rotational switching. *Nature* 466(7309):996-1000.

Lee SY, *et al.* (2001) Crystal structure of activated CheY. Comparison with other activated receiver domains. *J Biol Chem* 276(19):16425-16431.

Lee SY, *et al.* (2001) Crystal structure of an activated response regulator bound to its target. *Nat Struct Biol* 8(1):52-56.

Lertsethtakarn P & Ottemann KM (2010) A remote CheZ orthologue retains phosphatase function. *Mol Microbiol* 77(1):225-235.

Leslie AGW (1992) Joint CCP4 + ESF-EAMCB Newsletter on Protein Crystallography, No. 26.

Li R, *et al.* (2010) CobB regulates Escherichia coli chemotaxis by deacetylating the response regulator CheY. *Mol Microbiol* 76(5):1162-1174.

Liarzi O, *et al.* (2010) Acetylation represses the binding of CheY to its target proteins. *Mol Microbiol* 76(4):932-943.

Lloyd SA & Blair DF (1997) Charged residues of the rotor protein FliG essential for torque generation in the flagellar motor of Escherichia coli. *J Mol Biol* 266(4):733-744.

Lloyd SA, Tang H, Wang X, Billings S, & Blair DF (1996) Torque generation in the flagellar motor of Escherichia coli: evidence of a direct role for FliG but not for FliM or FliN. *J Bacteriol* 178(1):223-231.

Lloyd SA, Whitby FG, Blair DF, & Hill CP (1999) Structure of the C-terminal domain of FliG, a component of the rotor in the bacterial flagellar motor. *Nature* 400(6743):472-475.

Lowder BJ, Duyvesteyn MD, & Blair DF (2005) FliG subunit arrangement in the flagellar rotor probed by targeted cross-linking. *J Bacteriol* 187(16):5640-5647.

Lowenthal AC, *et al.* (2009) Functional analysis of the Helicobacter pylori flagellar switch proteins. *J Bacteriol* 191(23):7147-7156.

Lukat GS, McCleary WR, Stock AM, & Stock JB (1992) Phosphorylation of bacterial response regulator proteins by low molecular weight phospho-donors. *Proc Natl Acad Sci U S A* 89(2):718-722.

Macnab RM & Koshland DE (1972) The gradient-sensing mechanism in bacterial chemotaxis. *Proc Natl Acad Sci U S A* 69(9):2509-2512.

Marshall BJ & Warren JR (1984) Unidentified curved bacilli in the stomach of patients with gastritis and peptic ulceration. *Lancet* 1(8390):1311-1315.

Marykwas DL & Berg HC (1996) A mutational analysis of the interaction between FliG and FliM, two components of the flagellar motor of Escherichia coli. *J Bacteriol* 178(5):1289-1294.

Mathews MA, Tang HL, & Blair DF (1998) Domain analysis of the FliM protein of Escherichia coli. *J Bacteriol* 180(21):5580-5590.

McCarter LL (2001) Polar flagellar motility of the Vibrionaceae. *Microbiol Mol Biol Rev* 65(3):445-462, table of contents.

McCoy AJ, *et al.* (2007) Phaser crystallographic software. *J Appl Crystallogr* 40(Pt 4):658-674.

McCoy AJ, Grosse-Kunstleve RW, Storoni LC, & Read RJ (2005) Likelihood-enhanced fast translation functions. *Acta Crystallogr D Biol Crystallogr* 61(Pt 4):458-464.

McGee DJ, *et al.* (2005) Colonization and inflammation deficiencies in Mongolian gerbils infected by Helicobacter pylori chemotaxis mutants. *Infect Immun* 73(3):1820-1827.

Minamino T, *et al.* (2011) Structural insight into the rotational switching mechanism of the bacterial flagellar motor. *PLoS Biol* 9(5):e1000616.

Minamino T, *et al.* (2009) Roles of the extreme N-terminal region of FliH for efficient localization of the FliH-FliI complex to the bacterial flagellar type III export apparatus. *Mol Microbiol* 74(6):1471-1483.

Mizote T, Yoshiyama H, & Nakazawa T (1997) Urease-independent chemotactic responses of Helicobacter pylori to urea, urease inhibitors, and sodium bicarbonate. *Infect Immun* 65(4):1519-1521.

Nakamura H, *et al.* (1998) Urease plays an important role in the chemotactic motility of Helicobacter pylori in a viscous environment. *Infect Immun* 66(10):4832-4837.

Nakamura S, Kami-ike N, Yokota JP, Minamino T, & Namba K (2010) Evidence for symmetry in the elementary process of bidirectional torque generation by the bacterial flagellar motor. *Proc Natl Acad Sci U S A* 107(41):17616-17620.

Oh JD, *et al.* (2006) The complete genome sequence of a chronic atrophic gastritis Helicobacter pylori strain: evolution during disease progression. *Proc Natl Acad Sci U S A* 103(26):9999-10004.

Ottemann KM & Lowenthal AC (2002) Helicobacter pylori uses motility for initial colonization and to attain robust infection. *Infect Immun* 70(4):1984-1990.

Pallen MJ, Penn CW, & Chaudhuri RR (2005) Bacterial flagellar diversity in the post-genomic era. *Trends Microbiol* 13(4):143-149.

Park SY, *et al.* (2004) Structure and function of an unusual family of protein phosphatases: the bacterial chemotaxis proteins CheC and CheX. *Mol Cell* 16(4):563-574.

Park SY, Lowder B, Bilwes AM, Blair DF, & Crane BR (2006) Structure of FliM provides insight into assembly of the switch complex in the bacterial flagella motor. *Proc Natl Acad Sci U S A* 103(32):11886-11891.

Parkinson JS (1978) Complementation analysis and deletion mapping of Escherichia coli mutants defective in chemotaxis. *J Bacteriol* 135(1):45-53.

Parsonnet J, *et al.* (1991) Helicobacter pylori infection and the risk of gastric carcinoma. *N Engl J Med* 325(16):1127-1131.

Passmore SE, Meas R, & Marykwas DL (2008) Analysis of the FliM/FliG motor protein interaction by two-hybrid mutation suppression analysis. *Microbiology* 154(Pt 3):714-724.

Paul K & Blair DF (2006) Organization of FliN subunits in the flagellar motor of Escherichia coli. *J Bacteriol* 188(7):2502-2511.

Paul K, Gonzalez-Bonet G, Bilwes AM, Crane BR, & Blair D (2011) Architecture of the flagellar rotor. *EMBO J.* 30(14):2962-2971.

Paul K, Harmon JG, & Blair DF (2006) Mutational analysis of the flagellar rotor protein FliN: identification of surfaces important for flagellar assembly and switching. *J Bacteriol* 188(14):5240-5248.

Paul K, Nieto V, Carlquist WC, Blair DF, & Harshey RM (2010) The c-di-GMP binding protein YcgR controls flagellar motor direction and speed to affect chemotaxis by a "backstop brake" mechanism. *Mol Cell* 38(1):128-139.

Pazy Y, *et al.* (2010) Identical phosphatase mechanisms achieved through distinct modes of binding phosphoprotein substrate. *Proc Natl Acad Sci U S A* 107(5):1924-1929.

Pazy Y, *et al.* (2009) Matching biochemical reaction kinetics to the timescales of life: structural determinants that influence the autodephosphorylation rate of response regulator proteins. *J Mol Biol* 392(5):1205-1220.

Pettersen EF, *et al.* (2004) UCSF Chimera--a visualization system for exploratory research and analysis. *J Comput Chem* 25(13):1605-1612.

Pittman MS, Goodwin M, & Kelly DJ (2001) Chemotaxis in the human gastric pathogen Helicobacter pylori: different roles for CheW and the three CheV paralogues, and evidence for CheV2 phosphorylation. *Microbiology* 147(Pt 9):2493-2504.

Rader BA, *et al.* (2011) Helicobacter pylori perceives the quorum-sensing molecule AI-2 as a chemorepellant via the chemoreceptor TlpB. *Microbiology*.

Rao CV, Glekas GD, & Ordal GW (2008) The three adaptation systems of Bacillus subtilis chemotaxis. *Trends Microbiol* 16(10):480-487.

Rao CV & Ordal GW (2009) The molecular basis of excitation and adaptation during chemotactic sensory transduction in bacteria. *Contrib Microbiol* 16:33-64.

Riepl H, Scharf B, Schmitt R, Kalbitzer HR, & Maurer T (2004) Solution structures of the inactive and BeF3-activated response regulator CheY2. *J Mol Biol* 338(2):287-297.

Sachs G, Weeks DL, Melchers K, & Scott DR (2003) The gastric biology of Helicobacter pylori. *Annu Rev Physiol* 65:349-369.

Samatey FA, *et al.* (2001) Structure of the bacterial flagellar protofilament and implications for a switch for supercoiling. *Nature* 410(6826):331-337.

Sarkar MK, Paul K, & Blair D (2010) Chemotaxis signaling protein CheY binds to the rotor protein FliN to control the direction of flagellar rotation in Escherichia coli. *Proc Natl Acad Sci U S A* 107(20):9370-9375.

Sarkar MK, Paul K, & Blair DF (2010) Subunit organization and reversal-associated movements in the flagellar switch of Escherichia coli. *J Biol Chem* 285(1):675-684.

Schreiber S, *et al.* (2004) The spatial orientation of Helicobacter pylori in the gastric mucus. *Proc Natl Acad Sci U S A* 101(14):5024-5029.

Schreiber S & Scheid P (1997) Gastric mucus of the guinea pig: proton carrier and diffusion barrier. *Am J Physiol* 272(1 Pt 1):G63-70.

Schweinitzer T, *et al.* (2008) Functional characterization and mutagenesis of the proposed behavioral sensor TlpD of Helicobacter pylori. *J Bacteriol* 190(9):3244-3255.

Shah DS, *et al.* (2000) Identification of a fourth cheY gene in Rhodobacter sphaeroides and interspecies interaction within the bacterial chemotaxis signal transduction pathway. *Mol Microbiol* 35(1):101-112.

Silversmith RE (2010) Auxiliary phosphatases in two-component signal transduction. *Curr Opin Microbiol* 13(2):177-183.

Silversmith RE, Appleby JL, & Bourret RB (1997) Catalytic mechanism of phosphorylation and dephosphorylation of CheY: kinetic characterization of imidazole phosphates as phosphodonors and the role of acid catalysis. *Biochemistry* 36(48):14965-14974.

Silversmith RE, Smith JG, Guanga GP, Les JT, & Bourret RB (2001) Alteration of a nonconserved active site residue in the chemotaxis response regulator CheY affects phosphorylation and interaction with CheZ. *J Biol Chem* 276(21):18478-18484.

Smith JG, *et al.* (2003) Investigation of the role of electrostatic charge in activation of the Escherichia coli response regulator CheY. *J Bacteriol* 185(21):6385-6391.

Sockett H, Yamaguchi S, Kihara M, Irikura VM, & Macnab RM (1992) Molecular analysis of the flagellar switch protein FliM of Salmonella typhimurium. *J Bacteriol* 174(3):793-806.

Sowa Y, *et al.* (2005) Direct observation of steps in rotation of the bacterial flagellar motor. *Nature* 437(7060):916-919.

Stingl K, Altendorf K, & Bakker EP (2002) Acid survival of Helicobacter pylori: how does urease activity trigger cytoplasmic pH homeostasis? *Trends Microbiol* 10(2):70-74.

Szurmant H, Bunn MW, Cannistraro VJ, & Ordal GW (2003) Bacillus subtilis hydrolyzes CheY-P at the location of its action, the flagellar switch. *J Biol Chem* 278(49):48611-48616.

Szurmant H, Muff TJ, & Ordal GW (2004) Bacillus subtilis CheC and FliY are members of a novel class of CheY-P-hydrolyzing proteins in the chemotactic signal transduction cascade. *J Biol Chem* 279(21):21787-21792.

Szurmant H & Ordal GW (2004) Diversity in chemotaxis mechanisms among the bacteria and archaea. *Microbiol Mol Biol Rev* 68(2):301-319.

Tang H, Billings S, Wang X, Sharp L, & Blair DF (1995) Regulated underexpression and overexpression of the FliN protein of Escherichia coli and evidence for an interaction between FliN and FliM in the flagellar motor. *J Bacteriol* 177(12):3496-3503.

Terashima H, Kojima S, & Homma M (2008) Flagellar motility in bacteria structure and function of flagellar motor. *Int Rev Cell Mol Biol* 270:39-85.

Terry K, Williams SM, Connolly L, & Ottemann KM (2005) Chemotaxis plays multiple roles during Helicobacter pylori animal infection. *Infect Immun* 73(2):803-811.

Thomas DR, Francis NR, Xu C, & DeRosier DJ (2006) The three-dimensional structure of the flagellar rotor from a clockwise-locked mutant of Salmonella enterica serovar Typhimurium. *J Bacteriol* 188(20):7039-7048.

Thomas DR, Morgan DG, & DeRosier DJ (1999) Rotational symmetry of the C ring and a mechanism for the flagellar rotary motor. *Proc Natl Acad Sci U S A* 96(18):10134-10139.

Thomas D, Morgan DG, & DeRosier DJ (2001) Structures of bacterial flagellar motors from two FliF-FliG gene fusion mutants. *J Bacteriol* 183(21):6404-6412.

Thomas SA, Brewster JA, & Bourret RB (2008) Two variable active site residues modulate response regulator phosphoryl group stability. *Mol Microbiol* 69(2):453-465.

Toker AS, Kihara M, & Macnab RM (1996) Deletion analysis of the FliM flagellar switch protein of Salmonella typhimurium. *J Bacteriol* 178(24):7069-7079.

Toker AS & Macnab RM (1997) Distinct regions of bacterial flagellar switch protein FliM interact with FliG, FliN and CheY. *J Mol Biol* 273(3):623-634.

Tomb JF, *et al.* (1997) The complete genome sequence of the gastric pathogen Helicobacter pylori. *Nature* 388(6642):539-547.

Valenzuela M, Cerda O, & Toledo H (2003) Overview on chemotaxis and acid resistance in Helicobacter pylori. *Biol Res* 36(3-4):429-436.

Van Way SM, Millas SG, Lee AH, & Manson MD (2004) Rusty, jammed, and well-oiled hinges: Mutations affecting the interdomain region of FliG, a rotor element of the Escherichia coli flagellar motor. *J Bacteriol* 186(10):3173-3181.

Volz K & Matsumura P (1991) Crystal structure of Escherichia coli CheY refined at 1.7-A resolution. *J Biol Chem* 266(23):15511-15519.

Wadhams GH, Warren AV, Martin AC, & Armitage JP (2003) Targeting of two signal transduction pathways to different regions of the bacterial cell. *Mol Microbiol* 50(3):763-770.

Welch M, Oosawa K, Aizawa S, & Eisenbach M (1993) Phosphorylation-dependent binding of a signal molecule to the flagellar switch of bacteria. *Proc Natl Acad Sci U S A* 90(19):8787-8791.

Williams SM, *et al.* (2007) Helicobacter pylori chemotaxis modulates inflammation and bacterium-gastric epithelium interactions in infected mice. *Infect Immun* 75(8):3747-3757.

Xu Z & Au SW (2005) Mapping residues of SUMO precursors essential in differential maturation by SUMO-specific protease, SENP1. *Biochem J* 386(Pt 2):325-330.

Yan D, *et al.* (1999) Beryllofluoride mimics phosphorylation of NtrC and other bacterial response regulators. *Proc Natl Acad Sci U S A* 96(26):14789-14794.

Yan J, Barak R, Liarzi O, Shainskaya A, & Eisenbach M (2008) In vivo acetylation of CheY, a response regulator in chemotaxis of Escherichia coli. *J Mol Biol* 376(5):1260-1271.

Young HS, Dang H, Lai Y, DeRosier DJ, & Khan S (2003) Variable symmetry in Salmonella typhimurium flagellar motors. *Biophys J* 84(1):571-577.

Yuan J, Fahrner KA, Turner L, & Berg HC (2010) Asymmetry in the clockwise and counterclockwise rotation of the bacterial flagellar motor. *Proc Natl Acad Sci U S A* 107(29):12846-12849.

Zhang ZW, Dorrell N, Wren BW, & Farthingt MJ (2002) Helicobacter pylori adherence to gastric epithelial cells: a role for non-adhesin virulence genes. *J Med Microbiol* 51(6):495-502.

Zhao R, Collins EJ, Bourret RB, & Silversmith RE (2002) Structure and catalytic mechanism of the E. coli chemotaxis phosphatase CheZ. *Nat Struct Biol* 9(8):570-575.

Zhao R, Pathak N, Jaffe H, Reese TS, & Khan S (1996) FliN is a major structural protein of the C-ring in the Salmonella typhimurium flagellar basal body. *J Mol Biol* 261(2):195-208.

Zhou J, Lloyd SA, & Blair DF (1998) Electrostatic interactions between rotor and stator in the bacterial flagellar motor. *Proc Natl Acad Sci U S A* 95(11):6436-6441.

Appendices

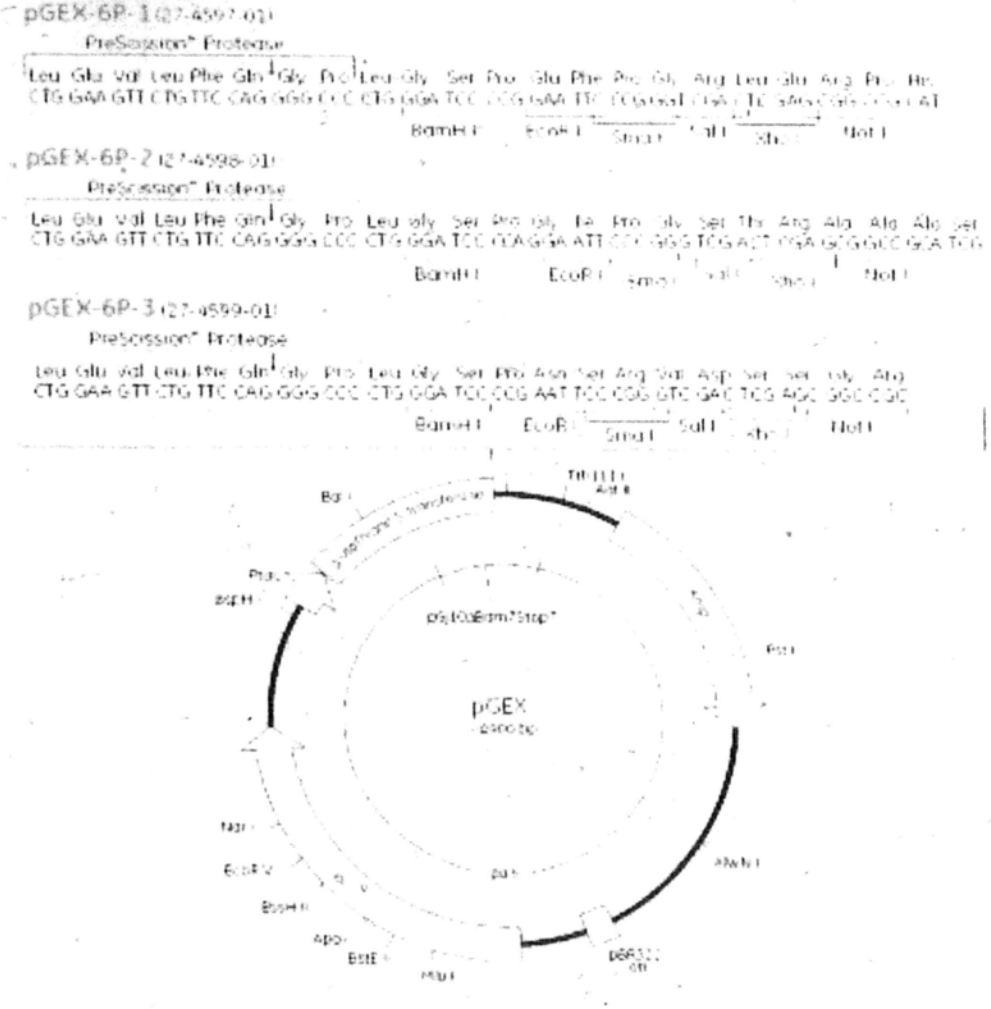

Appendix 1. Vector information. Vector map of pGEX-6p-1

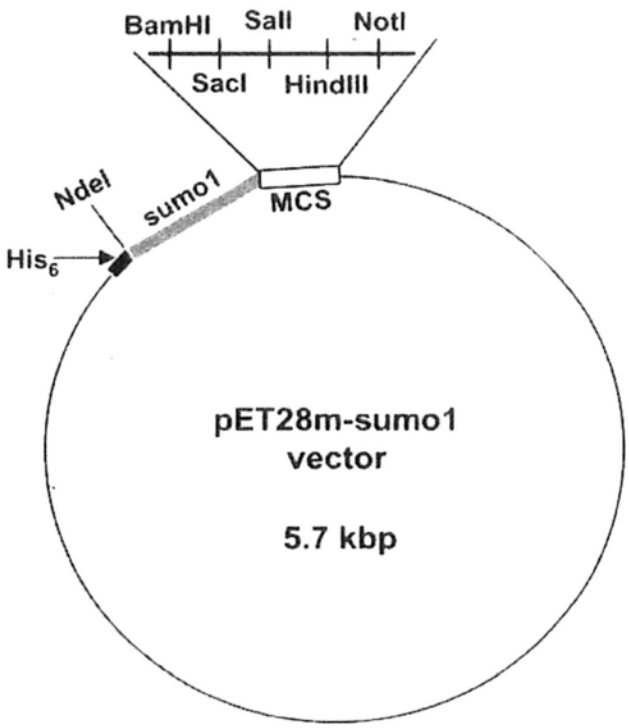

Vector information of pET28m-sumo1. The relative location of his_6-tag, sumo1 and multiple cloning site (MCS) are represented as bar. Commonly used restriction sites in the MCS are highlighted.

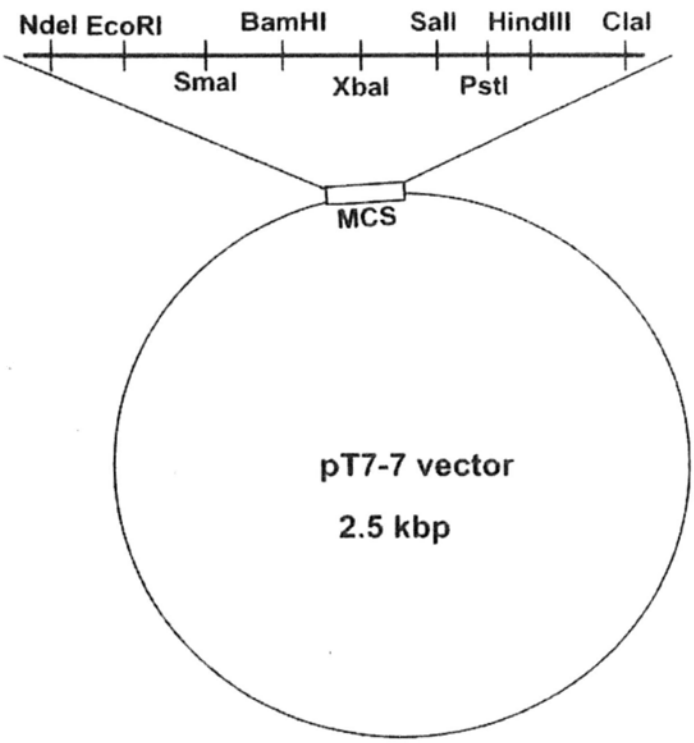

Vector information of pT7-7. Commonly used restriction sites in the MCS are highlighted.

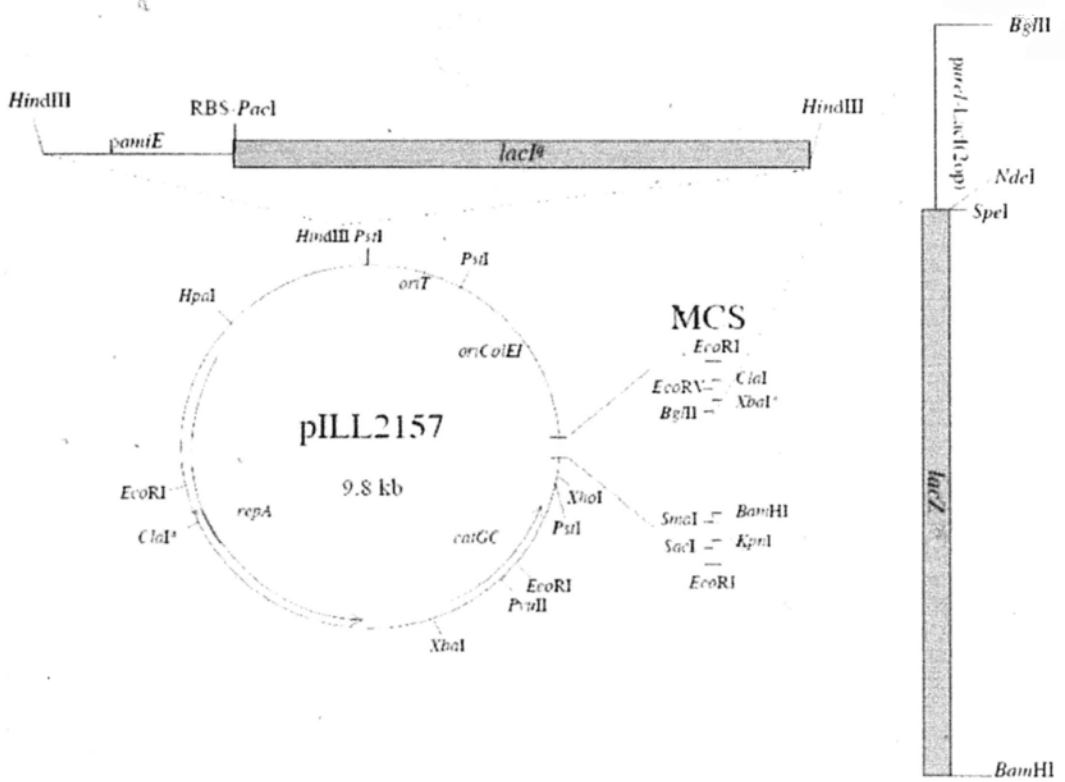

Vector information of pILL2157. * Restriction sites are methylated when purified from *E. coli.* The map is adapted from Boneca IG et al., 2008.

Column	Buffer
CheY1 / mutants / CheV1, 2	
GST	500 mM NaCl, 20 mM Tris pH 7.5, 0.5 mM EDTA, 2 mM DTT, 0.2 mM PMSF, 0.2 mM benzamidine
CLB	150 mM NaCl, 20 mM Tris pH 7.5, 0.5 mM EDTA, 2 mM DTT, 0.2 mM PMSF, 0.2 mM benzamidine
Gel filtration	150 mM NaCl, 20 mM Tris pH 7.5, 2 mM DTT, 0.2 mM PMSF, 0.2 mM benzamidine, 2 mM $MgCl_2$
$FliM_N$-His_8 / CheAP2-His_8	
Nickel-NTA	500 mM NaCl, 20 mM Imidazole pH 8.0, 0.4 mM PMSF, 0.4 mM benzamidine
Elution	500 mM NaCl, 200 mM Imidazole pH 8.0, 0.4 mM PMSF, 0.4 mM benzamidine
Gel filtration	150 mM NaCl, 10 mM HEPES pH 7.3, 0.4 mM PMSF, 0.4 mM benzamidine
CheY2	
Nickel-NTA	500 mM NaCl, 50 mM Tris pH 7.3, 5 mM CHAPS, 20 mM Imidazole, 0.2 mM PMSF, 0.2 mM Benzamidine
CLB	150 mM NaCl, 20 mM Tris pH 7.0, 10 mM Imidazole, 0.2 mM PMSF, 0.2 mM benzamidine
Gel filtration	150 mM NaCl, 50 mM Tris pH 6.8, 20 mM Imidazole, 5 mM CHAPS, 0.2 mM PMSF, 0.2 mM benzamidine
CheV3	
Nickel-NTA	500 mM NaCl, 20 mM HEPES pH 7.5, 20 mM Imidazole, 0.2 mM PMSF, 0.2 mM benzamidine
CLB	150 mM NaCl, 20 mM HEPES, 20 mM Imidazole, pH 7.5, 0.2 mM PMSF, 0.2 mM benzamidine
Gel filtration	150 mM NaCl, 20 mM HEPES pH 7.5, 4 mM DTT, 0.2 mM PMSF, 0.2 mM benzamidine

Appendix 2.1. List of buffer conditions for the purification of chemotaixis proteins. CLB – enzyme cleavage buffer

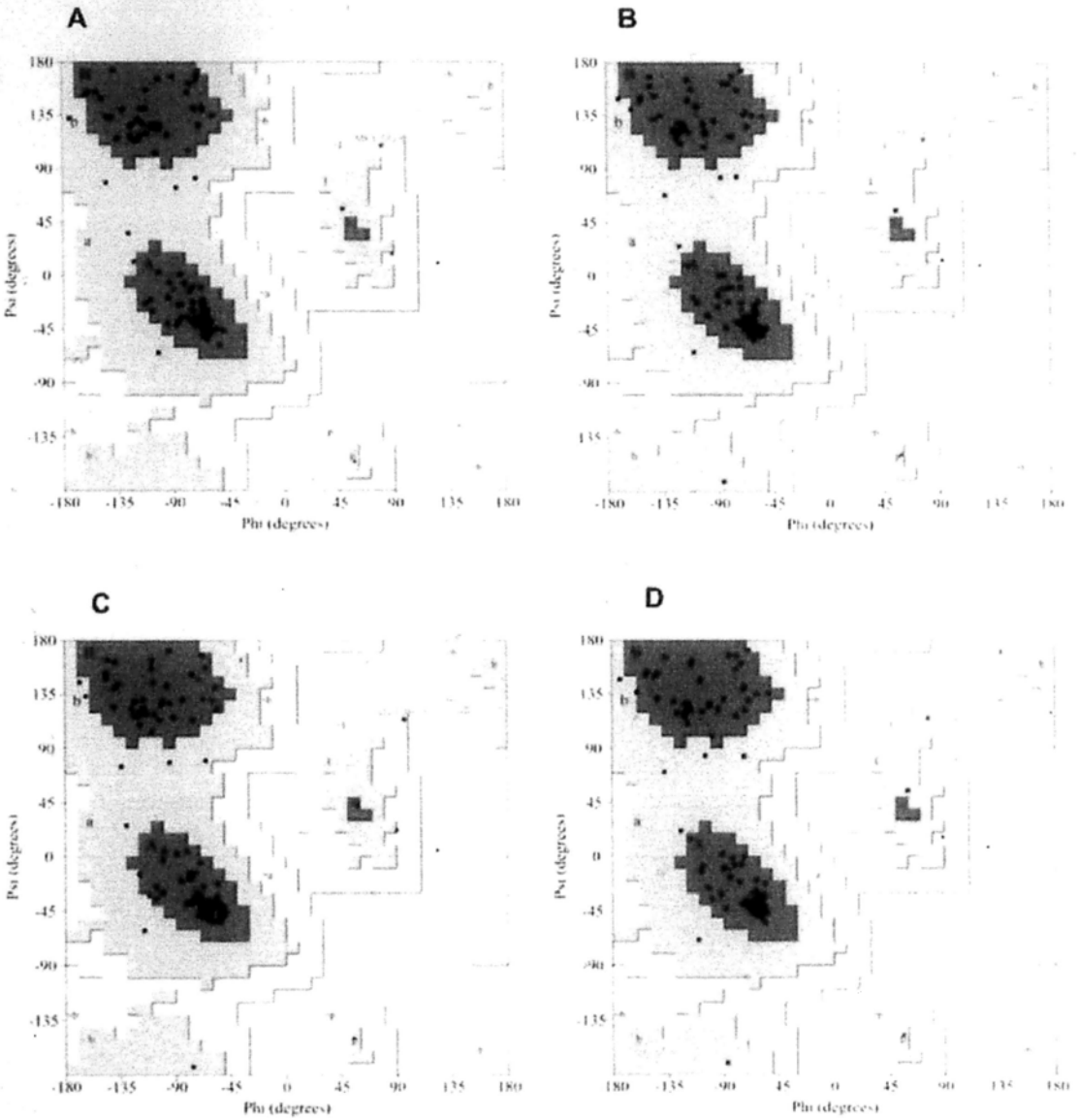

Appendix 2.2. Ramachantran plot of CheY1 structures. **(A)** BeF_3^- bound CheY1. **(B)** SO_4^{2-} bound CheY1. **(C).** CheY1/D53A. **(D).** CheY1/T84A. (PROCHECK). Regions are colored according to: Red: Most favored regions; Yellow: Additional allowed regions; Light yellow: Generously allowed regions; White; Disallowed regions. Glycine is represented as triangle, other residues are represented as square. Met59 labeled in red is in generously allowed region. Gly in white region is within allowed region because of the different Ramachantran restraint on glycine which is not displayed on the Figure.

Column	Buffer
$FliM_M$ / mutants	
GST	500 mM NaCl, 20 mM Tris pH 7.5, 0.5 mM EDTA, 2 mM DTT, 0.4 mM PMSF, 0.4 mM benzamidine
CLB	150 mM NaCl, 20 mM Tris pH 7.5, 0.5 mM EDTA, 2 mM DTT, 0.2 mM PMSF, 0.2 mM benzamidine
Gel filtration	150 mM NaCl, 20 mM Tris pH 7.5, 0.2 mM PMSF, 0.2 mM benzamidine
His_6-sumo1-FliG	
Nickel-NTA	500 mM NaCl, 20 mM Tris pH 8.0, 15 mM Imidazole, 0.4 mM PMSF, 0.4 mM benzamidine
Elution	500 mM NaCl, 20 mM Tris pH 8.0, 300 mM Imidazole, 0.4 mM PMSF, 0.4 mM benzamidine
'CLB	150 mM NaCl, 20 mM Tris pH 7.5, 20 mM Imidazole, 0.2 mM PMSF, 0.2 mM benzamidine
Gel filtration	150 mM NaCl, 20 mM Tris pH 7.5, 0.2 mM PMSF, 0.2 mM benzamidine

Appendix 3.1. Buffer conditions for $FliM_M$ / FliG purification.

[a] Cleavage buffer condition for the removal of His_6-sumo1 tag

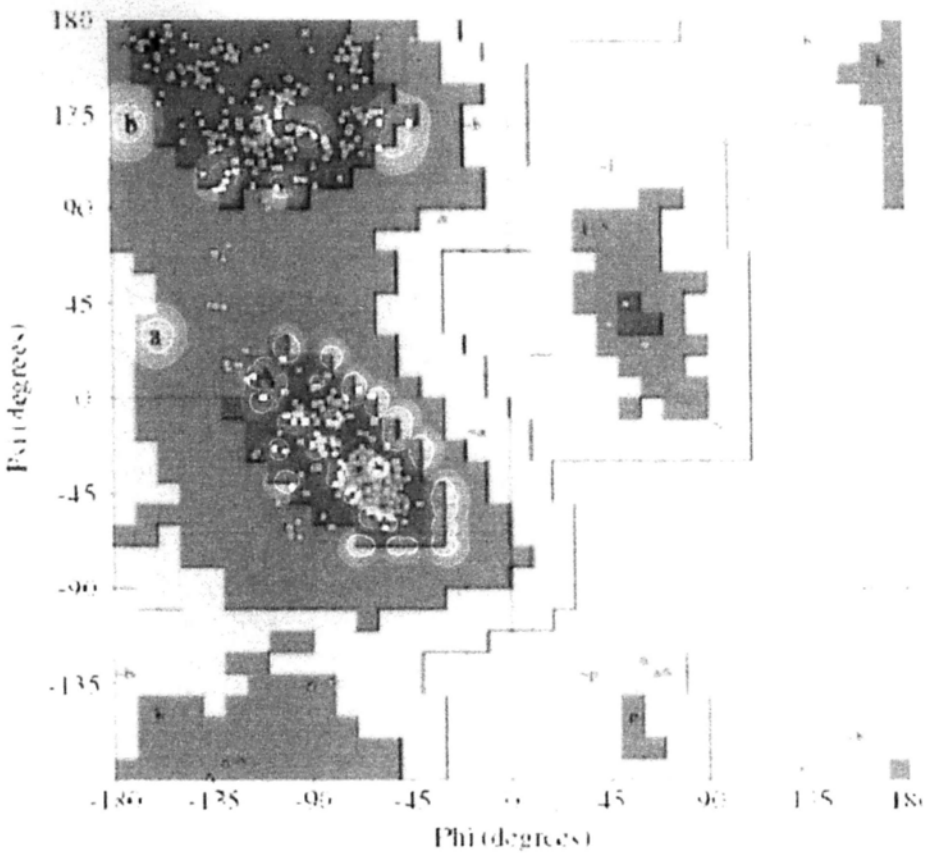

Appendix 3.2. Ramachantran plot of FliM$_M$ structure. Regions are colored according to: Red: Most favored regions; Brown: Additional allowed regions; Light yellow: Generously allowed regions; White; Disallowed regions. Residues are represented according to Appendix 2.2. Glycine residues in the white region are within allowed region.

(A)

Primer Name	Primer Sequence (5' – 3')	Restriction Site
$FliG_{MC}$ – F	catatg**ggatcc**atgcaaaaaaactt gcttatttaggcaaaatcaag	BamHI
$FliG_{MC}$ – F	**gggggggatcc**atgttggaatacgctagagagcttttaaccagg	BamHI
$FliG_N$ – R	catatg**gtcgac**ctacgtttgcaagctttagtgagtttgtccatc	SalI
$FliG_{NM}$ – R	catat**ggtcgac**ctacgatatttcgcctaaattcgccattctaatagag	SalI
EcFliG – F	gggggg**ccatgg**ctagtaacctgacaggcaccgataaaaagc	NcoI
EcFliG – R	ggggggg**cggccgc**tcagacataggtatcctcgccgct	NotI
N204A – F	gaacggcagccgaaattatcgccctgatgaaaactcagcag	
N204A – R	ctgctgagttttcatcagggcgataatttcggctgccgttc	
N204V – F	gaacggcagccgaaattatcgtcctgatgaaaactcagcag	
N204V –R	ctgctgagttttcatcaggacgataatttcggctgccgttc	
N204D – F	gaacggcagccgaaattatcgaccctgatgaaaactcag	
N204D – R	ctgagttttcatcaggtcgataatttcggctgccgttc	
N204H – F	gaacggcagccgaaattatccacctgatgaaaactcag	
N204H – R	ctgagttttcatcaggtggataatttcggctgccgttc	
N238A – F	gagatgttcctgttcgaggctctggtggatgtcgacga	
N238A – R	tcgtcgacatccaccagagcctcgaacaggaacatctc	
M233P – F	gcagaaaatcatcgacgagccgttcctgttcgagaatctg	
M233P – R	cagattctcgaacaggaacggctcgtcgatgattttctgc	
F234P – F	gaaaatcatcgacgagatgcccctgttcgagaatctggtg	
F234P – R	caccagattctcgaacaggggcatctcgtcgatgattttc	
MFPP – F	gcgcagaaaatcatcgacgagccgcccctgttcgagaatctggtgga	
MFPP – R	tccaccagattctcgaacaggggcggctcgtcgatgattttctgcgc	
$FliF_C$ – F	ggggggggatccatggatgaagataaggaagtgaaatccatgtttgaaga	BamHI
$FliF_C$ – R	ggggggcggccgcttaacctttcgcgccgtctgaagag	NotI

(B)

Primer Name	Primer Sequence (5' – 3')
Y88A – F	catcaatacc**ggcggtttggaagccgcta**gagaaactttta
Y88A – R	taaaagctctctag**cggcttccaaaccgccggtat**tgatg
R95A – F	cgctaga**gagcttta**accgcgacttta**ggga**gcgaagaa
R95A – R	ttc**ttcg**ctccctaaagtcg**c**ggttaaaagctctctagcg
E100A – F	caggacttta**ggga**gc**g**cagaagccaaaaaagtga
E100A – R	tcactttttggcttctg**c**gctccctaaagtcctg
D107A – F	agaagccaaaaaagtgat**g**gccaaactcactaaaagcttgc
D107A – R	gcaagcttttagtgagtttggcc**a**tcactttttggcttct
R217C-F	gcggtggctgaaatc**t**ttaactgcctgggccaaaag
R217C-R	cttttggcc**a**ggcagtta**a**agatttcagccaccgc
Q325C-F	ccaaaggaaaatcattgaaatc**g**tgtgtagctt**g**caagaaaaaggcgtgatcc
Q325C-R	ggatcacgc**c**tttttctt**g**caa**g**ctacacacgatttc**a**atgatttcctttgg
E243C-F	caagctcgccggtgcgatcaaatgtatgatgttcacttttgaagac
E243C-R	gtcttcaaaagtgaacatcatacatttgatcgcaccggcgagcttg
R209C-F	agctataaaattgaagtgggtggtttatgcgcggtggctgaaat
R209C-R	atttcagccaccgcgcataaaccacccacttcaattttatagct
S222C-F	ccgcctgggccaaaagtgcgctaaaaccac
S222C-R	gtggttttagcgcacttttggcccaggcgg

Appendix 4.1. Primers used for the cloning of FliG, FliG mutants and FliF. Primers for mutagenesis of *E. coli* FliG and *H. pylori* FliG are summarized in (A) and (B), respectively. Primers sequence for $FliM_N$-His_8 and full length FliG were shown in Table 2.1 and 3.1, respectively.

Column	Buffer
His_6-$FliF_C$ - $FliG_N$	
Ni-NTA	500 mM NaCl, 20 mM Hepes, 20 mM Imidazole, 0.4 mM PMSF, 0.4 mM benzamidine, pH 7.5
Ni - elution	500 mM NaCl, 20 mM Hepes, 200 mM Imidazole, 0.4 mM PMSF, 0.4 mM benzamidine, pH 7.5
GST	500 mM NaCl, 20 mM Hepes pH 7.5, 4 mM DTT, 0.1 mM EDTA, 0.4 mM PMSF, 0.4 mM benzamidine
CLB/ Gel filtration	150 m NaCl, 20 mM Hepes pH. 7.5, 0.1 mM EDTA, 0.2 mM PMSF, 0.2 mM benzamidine
FliG, $FliG_N$, $FliG_{NM}$, FliG mutants	
GST	500 mM NaCl, 20 mM Hepes pH 7.5, 4 mM DTT, 0.1 mM EDTA, 0.4 mM PMSF, 0.4 mM benzamidine
CLB/ Gel Filtration	150 mM NaCl, 20 mM Hepes, 0.1 mM EDTA, 2 mM DTT, 0.4 mM benzamidine, 0.4 mM PMSF, pH 7.5
$FliG_{MC1}$	
Ni-NTA	500 mM NaCl, 20 mM Hepes, 20 mM Imidazole, 0.4 mM PMSF, 0.4 mM benzamidine, pH 7.5
Elution	500 mM NaCl, 20 mM Hepes, 200 mM Imidazole, 0.4 mM PMSF, 0.4 mM benzamidine, pH 7.5
Gel filtration	500 mM NaCl, 10 mM Tris pH 7.5, 0.2 mM PMSF, 0.2 mM benzamidine
$FliG_{MC2}$	
GST	500 mM NaCl, 20 mM Hepes pH 7.5, 4 mM DTT, 0.1 mM EDTA, 0.4 mM PMSF, 0.4 mM benzamidine
CLB/ Gel Filtration	300 mM NaCl, 20 mM Hepes, 0.1 mM EDTA, 2 mM DTT, 0.4 mM benzamidine, 0.4 mM PMSF, 20 mM Imidazole[a], pH 7.5
FliG single or double Cys mutants	
GST	500 mM NaCl, 10 mM Hepes pH 7.3, 0.1 mM EDTA, 4 mM DTT, 0.2 mM PMSF, 0.2 mM benzamidine
CLB/ Gel filtration	150 mM NaCl, 10 mM Hepes pH 7.3, 6 mM DTT, 0.2 mM PMSF, 0.2 mM benzamidine

Appendix 4.2. List of buffer conditions for the purification of FliG and mutants.
CLB – enzyme cleavage buffer
[a] $FliG_{MC2}$ is prone to precipitation when concentrating the sample. Include 20 mM Imidazole improve stability of the protein in solution.

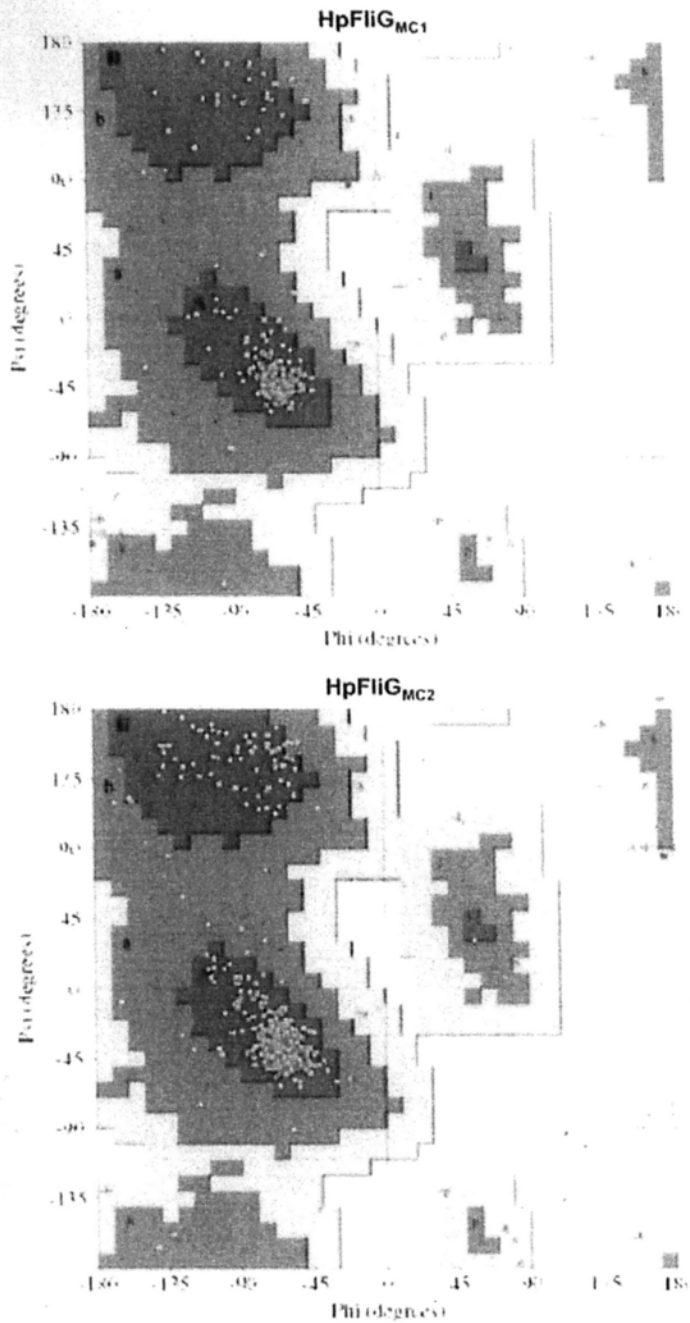

Appendix 4.3. Ramachantran plot of HpFliG$_{MC1}$ and HpFliG$_{MC2}$ structures. Regions are colored according to: Red: Most favored regions; Brown: Additional allowed regions; Light yellow: Generously allowed regions; White; Disallowed regions.

Column	Buffer
FliY/FliN	
GST	500 mM NaCl, 20 mM Hepes pH 7.3, 4 mM DTT, 1 mM EDTA, 0.4 mM PMSF, 0.4 mM benzamidine
CLB/Ni-NTA	150 mM NaCl, 20 mM Hepes pH 7.3, 20 mM Imidazole, 0.2 mM PMSF, 0.2 mM benzamidine
Elution	150 mM NaCl, 20 mM Hepes pH 7.3, 200 mM Imidazole, 0.2 mM PMSF, 0.2 mM benzamidine
Gel filtration	150 mM NaCl, 20 mM Hepes pH 7.3, 2 mM DTT, 0.5 mM EDTA, 0.4 mM PMSF, 0.4 mM benzamidine
GST-FliY/FliN, GST-FliY$_C$/FliN, GST-FliY$_N$	
GST-elution	500 mM NaCl, 20 mM Hepes pH 7.3, 4 mM DTT, 1 mM EDTA, 0.4 mM PMSF, 0.4 mM benzamidine, 20 mM reduced glutathione

Appendix 5.1. List of buffer conditions for the purification of FliY/FliN. CLB enzyme cleavage buffer. The purification conditions for GST-tagged proteins are the same as untagged protein, except that the enzyme cleavage is replaced by GST-elution buffer.